

University of Montana

## ScholarWorks at University of Montana

---

Graduate Student Theses, Dissertations, &  
Professional Papers

Graduate School

---

2012

# AB DIBLOCK COPOLYMER NANOPARTICLES VIA RAFT-MEDIATED POLYMERIZATION AS A PSEUDOSTATIONARY PHASE FOR ELECTROKINETIC CHROMATOGRAPHY

Andre Umansky  
*The University of Montana*

Follow this and additional works at: <https://scholarworks.umt.edu/etd>

**Let us know how access to this document benefits you.**

---

### Recommended Citation

Umansky, Andre, "AB DIBLOCK COPOLYMER NANOPARTICLES VIA RAFT-MEDIATED POLYMERIZATION AS A PSEUDOSTATIONARY PHASE FOR ELECTROKINETIC CHROMATOGRAPHY" (2012). *Graduate Student Theses, Dissertations, & Professional Papers*. 46.  
<https://scholarworks.umt.edu/etd/46>

This Thesis is brought to you for free and open access by the Graduate School at ScholarWorks at University of Montana. It has been accepted for inclusion in Graduate Student Theses, Dissertations, & Professional Papers by an authorized administrator of ScholarWorks at University of Montana. For more information, please contact [scholarworks@mso.umt.edu](mailto:scholarworks@mso.umt.edu).

AB DIBLOCK COPOLYMER NANOPARTICLES VIA RAFT-MEDIATED  
POLYMERIZATION AS A PSEUDOSTATIONARY PHASE FOR ELECTROKINETIC  
CHROMATOGRAPHY

By

ANDRE ANDERYEVICH UMANSKY

Bachelor of Science, University of San Francisco, San Francisco, California, 2008

Thesis

presented in partial fulfillment of the requirements  
for the degree of

Master of Science  
in Analytical Chemistry

The University of Montana  
Missoula, MT

May 2013

Approved by:

Sandy Ross, Dean of The Graduate School  
Graduate School

Christopher Palmer, Chair  
Department of Chemistry and Biochemistry

Michael DeGrandpre  
Department of Chemistry and Biochemistry

Nicholas Natale  
Department of Biomedical & Pharmaceutical Sciences

## Abstract

---

Electrokinetic chromatography (EKC) is a powerful analytical technique where analytes are separated according to their interactions with the pseudostationary and mobile phases within an electric field. Pseudostationary phases (PSPs) are an integral part of EKC and currently there are a limited number of PSPs available. As the fields of medicinal, environmental, and forensics chemistry grow, the necessity for PSPs with varied selectivity and high efficiencies becomes apparent. Until recently, polymeric synthesis of novel PSPs has been difficult due to the lack of control in structure and size distribution. Recent developments in polymeric synthesis, utilizing the Reversible addition-fragmentation chain-transfer polymerization (RAFT) process, have overcome the aforementioned problems.

This study furthers the research of latex nanoparticles as PSPs. 2-Acrylamido-2-methylpropane sulfonic acid (AMPS) was chosen as a novel ionic nanoparticle shell due to its high acidic character. Butyl acrylate was chosen for the hydrophobic core to stay consistent with previous work. Through the RAFT process, nanoparticles were successfully synthesized, demonstrating size control of both the hydrophilic block and hydrophobic block.

The novel PSP performance was characterized in EKC by obtaining its electrophoretic mobility ( $\mu_{ep}$ ) with respect to size and pH. Retention and selectivity were characterized by linear solvation energy relationships (LSER) and compared with currently used PSPs.

## Acknowledgements

---

I would like to thank Chris Palmer for the support he has given, enabling this project to be what it is today. Thank you for all the time, motivation, and encouragement throughout this project.

Thank you Jesse Hyslop for providing a creative environment, where ideas could grow, be discussed, and then be implemented.

Thank you my beautiful wife for putting up with the lights being on at 3AM. Thank you for all your support and love. I couldn't have done it without you. Thank you to our families, without whom, this would have been ten times as hard. Thank you Charlie dog for being the best Aussie ever.

## Table of Contents

---

Abstract .....	ii
Acknowledgements.....	iii
List of abbreviations.....	vi
List of schemes.....	viii
List of tables .....	ix
List of figures .....	x
List of Equations .....	xii
Chapter 1: Introduction and objectives .....	1
1.1 Introduction.....	1
1.2 Electrokinetic Chromatography .....	1
1.3 Free radical polymerization .....	3
1.4 Reversible addition–fragmentation chain-transfer polymerization .....	4
1.5 Objectives of the study.....	5
1.6 Thesis layout .....	6
Chapter 2: Theoretical background .....	7
2.1 Introduction.....	7
2.2 Free radical polymerization .....	8
2.3 Reversible addition–fragmentation chain-transfer polymerization .....	11
2.3.1 Single Block Polymers to AB Diblock Copolymers.....	18
2.4 Capillary electrophoresis.....	20
2.5 Electrokinetic chromatography.....	24
2.5.1 Polymeric PSPs.....	24
2.5.2 Resolution, Efficiency, and Capacity.....	28
2.6 Linear solvation energy relationships and methylene selectivity.....	29
Chapter 3: Synthesis and characterization of RAFT agents and diblock copolymers.....	32
3.1 Introduction.....	32
3.2 Materials .....	33
3.3 Experimental Procedure .....	33
3.3.1 Synthesis of CTA agent.....	33
3.3.2 Synthesis of macro CTA.....	34
3.3.3 Synthesis of diblock copolymers.....	35
3.4 Characterization.....	37
3.4.1 CTA.....	37
3.4.2 Macro-CTA.....	40
3.4.3 Diblock copolymer nanoparticles .....	43

Chapter 4: Performance characterization of nanoparticles in electrokinetic chromatography .....	47
4.1 Introduction.....	47
4.2 Experimental Details.....	47
4.3 Separations of alkyl-phenone derivatives at pH 9.2 .....	48
4.4 Electrophoretic mobility, pH dependence, Size dependence, Migration Range, Methylene Selectivity.....	49
4.5 LSER analysis .....	50
Chapter 5: Results and Discussion.....	52
5.1 Introduction.....	52
5.2 Synthesis of poly (AMPS) macro-CTA .....	52
5.2.1 Neutralization of acrylamides in the synthesis of mCTA .....	52
5.2.2 RAFT control .....	52
5.2.3 NMR analysis and conversion .....	54
5.3 Chain extension of poly(AMPS) macro-CTA with butyl acrylate .....	56
5.3.1 Reaction dependency on pH .....	56
5.3.2 NMR and DLS discussion.....	57
5.4 Methylene Selectivity and CE Current.....	59
5.5 Electrophoretic mobility and efficiency .....	62
5.6 LSER.....	65
5.6.1 Retention.....	65
5.6.2 Selectivity.....	71
Chapter 6: Conclusions and recommendations .....	72
6.1 Conclusions .....	72
6.2 Recommendations for future work .....	72
Bibliography .....	74

## List of abbreviations

$[I_0]$	Initiator Concentration	A	Analyte
$[M_0]$	Monomer Concentration	f	initiator efficiency
$\mu_o$	Electroosmotic mobility	$R_s$	Resolution
$u_a$	Analyte velocity	$\mu_a$	Analyte electrophoretic mobility
AIBN	Azoisobutylnitrile initiator	$t_o$	Elution time for an unretained analyte
CE	Capillary Electrophoresis	V501	4, 4'-Azobis (4-Cyanovaleric Acid) initiator
EKC	Electrokinetic Chromatography	MEKC	Micellar electrokinetic chromatography
$FW_{RAFT}$	Molecular weight of RAFT	PSP	Pseudostationary Phase
HPLC	High-performance liquid chromatography	$FW_m$	Molecular weight of monomer
K	Distribution Coefficient	DLS	Dynamic Light Scattering
$k_B$	Boltzmann Constant	$\mu_{ep}$ or $\mu_{ep,psp}$	Electrophoretic mobility of analyte or PSP
L	Capillary length to detector	u	net velocity
LSEER	Linear solvation energy relationships	PDI	Polydispersity Index
mCTA	macro chain transfer agent	PDI*	DLS Polydispersity Index
$M_i$	Molar mass of polymer species	$N_i$	number of moles (intensity) of polymer species
$M_n$	Number average molar mass	$M_w$	Weight average molar mass
MS	Mass Spectrometer	$u_o$	Electroosmotic flow velocity
MW	Molar weight	UV	Ultraviolet
NMR	Nuclear magnetic resonance	ESI-MS	Electrospray Ionization Mass Spectrometry
$R\cdot$	Radical	$I\cdot$	Initiator Radical
RAFT	Reversible addition-fragmentation chain-transfer	CTA	Chain Transfer Agent
SDS	sodium dodecyl sulfate	$[RAFT_0]$	Initial RAFT Concentration
t	Time	r	Stokes radius
T	Temperature	k	Retention Factor
$t_{psp}$	elution time of a fully retained analyte	EOF	Electro Osmotic Flow
$t_r$	Analyte elution time	$L_t$	Total Capillary length
V	Voltage	x	fractional conversion at time t
$\epsilon$	Relative permittivity	$\zeta$	zeta potential
$\eta$	Viscosity	E	Electric field strength
SPM	Solvation parameter model	N	Plate Number
$u_{pspnet}$	Net PSP velocity	ABS	Absorbance
$\mu_{epnet}$	Net PSP electrophoretic mobility	$D_v$	Distribution by volume
$k_{opt}$	Optimal retention factor	NP	Nanoparticle

<i>MWCO</i>	<i>Molecular weight cutoff</i>	$\alpha_{CH_2}$	<i>Methylene selectivity</i>
<i>DAD</i>	<i>Diode array detector</i>		



## List of schemes

---

Scheme 1: Thermal decomposition of dicumyl peroxide.....	8
Scheme 2: Photolysis of azoisobutylnitrile (AIBN) gives two free radical initiators and nitrogen gas.....	9
Scheme 3: Phenyl initiator attacks and attaches to a double bond on styrene.....	9
Scheme 4: Two pathways of free radical polymerization termination: Combination and disproportionation. ....	10
Scheme 5: Mechanism of RAFT polymerization. [28] "Reprinted with permission from {G. Moad, E. Rizzardo and S. H. Thang, "Living Radical Polymerization by the RAFT Process," Australian Journal of Chemistry, vol. 58, pp. 379-410, 2005.}. Copyright {2013} Australian Journal of Chemistry." .....	16
Scheme 6: A) General reaction process for the creation of a AB diblock copolymer. In illustration the hydrophobic block is added first, followed by the hydrophilic block. [32] B) Micellization and further polymerization with the hydrophobic monomer. [30] The surfactant is the mCTA. Reaction takes place in an aqueous solvent. Initiator molecules consist mostly of R• with a small amount being I•. Schme 6 A and B were "Reprinted with permission from {C. Furgeson, R. Hughes, D. Nguyen, B. Pham, R. Gilbert, A. Serelis, C. Such and B. Hawke, "Ab Initio Emulsion Polymerization by RAFT-Controlled Self-Assembly," Macromolecules, vol. 38, pp. 2191-2204, 2005.}. Copyright {2013} American Chemical Society." And the Dave Weitz group at Harvard University, respectively. ....	20
Scheme 7: Synthetic route to producing 2-{{(butylsulfanyl)carbothioyl}sulfanyl}propanoic acid.....	33
Scheme 8: Synthetic pathway to the mCTA through the RAFT process. ....	35
Scheme 9: Synthetic pathway to the AB diblock nanoparticle through the RAFT process. ...	36

## List of tables

---

Table 1: Four classes of CTAs. ....	13
Table 2: Commercially available CTAs on the left and monomers on top [27]. The “+” indicates a favorable reaction. “Reprinted with permission from Sigma-Aldrich, copyright 2013” .....	14
Table 3: Results of DLS Analysis. The polydispersity index (PDI*) calculated from DLS is different than the PDI discussed earlier. While PDI is based on weight distribution, PDI* is obtained from DLS as a time dependent intensity distribution. A PDI* of <0.1 is considered very monodisperse. A PDI* <0.4 is fairly monodisperse while a PDI* of >0.7 is considered very polydisperse.....	46
Table 4: Electrophoretic properties of AU19B and AU31A in 10mM borate buffer (pH 9.2). 49	49
Table 5: Electrophoretic mobility and migration range dependence on pH. ....	50
Table 6: Determined $k$ and $\log k$ values. Solute descriptors are also reported.....	51
Table 7: System constants for AU31A PSP.....	51
Table 8: AMPS 1 and 2 were synthesized by Sumerlin and analyzed by aqueous size exclusion chromatography. JSH32A was analyzed by ESI-MS. ....	52
Table 9: Theoretical vs. experimental results for mCTA polymerizations presented by Ladaviere (black) and Mori (blue). [46] [47] .....	53
Table 10: Qualitative analysis of nanoparticles dissolved in H <sub>2</sub> O synthesized at different pH. ....	56
Table 11: Results for DLS and NMR analysis of synthesized nanoparticles. The number associated with NMR integration gives the average number of polymerized butyl acrylate monomers.....	58
Table 12: Methylene selectivities.....	59
Table 13: Methylene selectivities table, recreated from Shamsi <i>et.al.</i> , of four homologous series polymeric PSPs. [52] .....	60
Table 14: Comparison between different PSPs and their effects on analysis current. AU19A and AU19A' is the same PSP, the only difference being in the application of post-synthetic dialysis. Poly-SUS is a polymerized micelle-like structure consisting of sodiumundecylenic sulfate. ....	61
Table 15: Performance characteristics for nanoparticles, SDS, and random block polymers. ....	62
Table 16: Electrophoretic mobilities, EOFs, and migration ranges at different pH. Data obtained from results presented in Chapter 4.....	64
Table 17: LSER system constants for AU31A (AMPS-Butyl Acrylate) PSP, Palmer NP (Acrylic Acid-Butyl Acrylate) PSP, SDS, Poly(SUA) (poly(sodium undecylenate)), and Poly(C12Mat/AMPS) (a copolymer of dodecyl methacrylate (15%) and AMPS). SDS values are averages from several studies as reported by Fu and Khaledi. ....	66
Table 18: Normalized system constants obtained from using Equation 29. ....	71

## List of figures

---

Figure 1: Typical molecular weight distributions for a conventional (broad peak) and living radical (narrow peak) polymerization. Peak PDI values obtained from GPC data are 1.74 and 1.04 respectively. [22] "Reprinted with permission from {G. Moad, E. Rizzardo and S. H. Thang, "Living Radical Polymerization by the RAFT Process," Australian Journal of Chemistry, vol. 58, pp. 379-410, 2005.}. Copyright {2013} Australian Journal of Chemistry." .....	11
Figure 2: A general representation of a CTA. ....	12
Figure 3: Major products of the RAFT process decreasing in prevalence from left to right...17	17
Figure 4: GPC data showing a linear relationship between conversion and molecular weight (circles). Polydispersity is exponentially minimized with conversion (squares). [62] "Reprinted with permission from {C. L. McCormick and A. B. Lowe, "Aqueous RAFT Polymerization: Recent Developments in Synthesis of Functional Water-Soluble (Co)polymers with Controlled Structures," <i>Acc. Chem. Res.</i> , vol. 37, pp. 312-325, 2004.}. Copyright {2013} American Chemical Society." .....	17
Figure 5: Basic CE instrument setup. ....	21
Figure 6: a) A zoomed representation of a capillary column in CE. $A^{\text{charge}}$ represents an analyte of a certain charge. Hydrated cations are balancing the negatively charged oxides establishing the EOF. $\mu M^+$ represents the velocity of positively charged ions. $\mu M^-$ represents the velocity of negatively charged ions. The EOF and net migration is towards the cathode. b) Elution order of analytes, positive ions are followed by neutral compounds, followed by negative ions. ....	21
Figure 7: a) Flow profile of a pressure driven flow system. b) Flow profile of an EOF system. ....	22
Figure 8: A cross sectional representation of a capillary column filled with a buffer solution and a PSP. Black interior represents the hydrophobic area of the PSP. Green areas represent the anionic components of the PSP. Analytes A and B partition between the buffer and PSP phases. Analyte B has a partition coefficient less than that of Analyte A thus its net velocity is faster and $t_r$ is smaller. A hypothetical chromatogram illustrates the elution order. ....	25
Figure 9: Resolution as a function of the retention factor. The curves are color coded to the theoretical chromatogram (top), illustrating migration range's effect on resolution.....	29
Figure 10: A) An HPLC chromatogram at 210nm of CTA01 of time vs. ABS. B) Extracted spectra of the main peak at 2.75 min. compared to the ABS spectra reported by Shen and group. ....	39
Figure 11: $^1\text{H}$ NMR spectra and peak assignments for the synthesized CTA in d-chloroform. Each multiplet (labeled at the top) is assigned to the structure at the top left of the figure. For example: M01(m,9) is assigned to the hydrogens of carbon 9.....	40
Figure 12: Mass spectrum of poly(n-AMPS) macro-CTA where the AMPS component has a MW of ~207 and n=number of AMPS/chain. The chromatogram shows a distribution of a RAFT polymerization product with a polydispersity index of 1.03. The major component is the highest intensity peak showing 4-AMPS/chain. ....	41
Figure 13: $^1\text{H}$ NMR spectra reported by Sumerlin and group. [42] "Reprinted with permission from {B. Sumerlin, M. Donovan, Y. Mitsukami, A. Lowe and C. McCormick, "Water-Soluble Polymers. 84. Controlled Polymerization in Aqueous Media of Anionic Acrylamido Monomers via RAFT," <i>Macromolecules</i> , vol. 34, pp. 6561-6564, 2001.}. Copyright {2013} American Chemical Society." .....	42
Figure 14: $^1\text{H}$ NMR spectra of mCTA JSH32A in $\text{D}_2\text{O}$ . Polymerization can be observed by the broad peak shapes of the monomer's hydrogen signals. The AMPS monomer structure is presented to illustrate the vinyl groups present on a free monomer. No vinyl groups are seen in the spectra. ....	43

Figure 15: <sup>1</sup> H NMR spectra of butyl acrylate in d-chloroform. ....	44
Figure 16: <sup>1</sup> H NMR spectra of AU19B in D <sub>2</sub> O after polymerization with butyl acrylate. ....	44
Figure 17: <sup>1</sup> H NMR spectra of AU31A in D <sub>2</sub> O after polymerization with butyl acrylate. ....	45
Figure 18: DLS analysis of AU19B showing a lognormal size distribution by volume.....	46
Figure 19: DLS analysis of AU31A showing a lognormal size distribution by volume.....	46
Figure 20: Separation of acetone (0.2%) and alkyl-phenyl ketones: 1. Acetophenone (3.72ppm), 2. Propiophenone (3.18ppm); 3. Butyrophenone(3.14ppm); 4. Valerophenone(3.31ppm); 5. Hexanophenone(3.32ppm); 6. Heptaphenone(6.30ppm). The separation was performed using a 10mM borate buffer (pH 9.2) and 0.6% AU19B PSP.....	48
Figure 21: Separation of acetone (0.2%) and alkyl-phenyl ketones: peaks as labeled in Figure 20..72ppm), 2. Propiophenone (9.18ppm); 3. Butyrophenone(9.14ppm); 4. Valerophenone(9.31ppm); 5. Hexanophenone(9.32ppm); 6. Heptaphenone(18.30ppm). The separation was performed using a 10mM borate buffer (pH 9.2) and 0.35% AU31A PSP.....	48
Figure 22: Separation of six alkyl-phenone derivatives at pH 7.55.....	50
Figure 23: Separation of six alkyl-phenone derivatives at pH 5.45.....	50
Figure 24: <sup>1</sup> H NMR spectra of mCTA JSH32A in D <sub>2</sub> O. ....	54
Figure 25: <sup>1</sup> H NMR spectra of mCTA JSH42B8 in D <sub>2</sub> O. LH31A2 mCTA before dialysis (BLUE) and after dialysis (GREEN). The green spectrum of dialyzed mCTA is offset to the left to make the figure clearer. ....	55
Figure 26: Plate count for each analyte separated using AU19B as a PSP .....	65
Figure 27: Representative electropherogram for four LSER compounds. Mix # 4 was run under conditions described in chapter 3. 1) Phenyl Acetate. 2) Propiophenone. 3) 4-Nitrotoluene. 4) Iodobenzene. ....	66
Figure 28: A graphical representation of the data presented in Table 17. ....	67
Figure 29: Hydrated interphase region in SDS micelles [61]. Sulfate groups are hydrated through H-bonds. "Reprinted with permission from { R. Buchner, C. Baar, P. Fernandez, S. Shrodle and W. Kunz, "Dielectric spectroscopy of micelle hydration and dynamics in aqueous ionic surfactant solutions," <i>Journal of Molecular Liquids</i> , vol. 118, no. 1-3, pp. 179-187, 2005.}. Copyright {2013} American Chemical Society." .....	68
Figure 30: A 3D representation cutout of an AMPS-Butyl Acrylate nanoparticle. For illustration purposes, only one subunit of the poly AMPS block and poly Butyl Acrylate (BA) block is shown. Note that although the carboxylic acid and butanethiol terminal ends look significant in this image, they only comprise a small portion of the full polymeric NP.....	70

## List of Equations

---

Equation 1: PDI.....	4
Equation 2: Calculation to determine the theoretical molecular weight of the polymer at a certain conversion. The initiator terms are included.....	18
Equation 3: Calculation to determine the theoretical molecular weight of the polymer at a certain conversion. The initiator terms are omitted.....	18
Equation 4: EOF velocity.....	22
Equation 5: Electric field strength.....	23
Equation 6: Electroosmotic mobility.....	23
Equation 7: Charged analyte velocity.....	23
Equation 8: Analyte electrophoretic mobility.....	23
Equation 9: Stokes radius.....	23
Equation 10: Experimental calculation of analyte electrophoretic mobility.....	24
Equation 11: Net analyte velocity.....	24
Equation 12: Electrophoretic velocity of a PSP.....	26
Equation 13: PSP net velocity.....	26
Equation 14: EOF velocity.....	26
Equation 15: PSP net velocity.....	26
Equation 16: Analyte velocity.....	26
Equation 17: EOF electrophoretic.....	26
Equation 18: PSP apparent electrophoretic mobility.....	26
Equation 19: Analyte electrophoretic mobility.....	26
Equation 20: Analyte velocity in EKC.....	27
Equation 21: Retention factor.....	27
Equation 22: Retention factor experimental determination.....	27
Equation 23: Rearrangement of Equation 22.....	28
Equation 24: Determination of the retention factor from electrophoretic mobility.....	28
Equation 25: Master resolution equation for EKC.....	28
Equation 26: The solvation parameter model.....	30
Equation 27: The log of the partition coefficient is related to the selectivity of the PSP through the change in free-energy.....	31
Equation 28: Experimental determination of electrophoretic mobility.....	49
Equation 29: Normalization parameter for LSER system constants.....	71

## Chapter 1: Introduction and objectives

---

### 1.1 Introduction

---

This study addresses the need for new pseudostationary phases (PSPs) for electrokinetic chromatography in order to accommodate the need for analysis of a large number of chemically different analytes. The focus of this study is twofold. First, a novel PSP was synthesized through the Reversible addition–fragmentation chain-transfer polymerization (RAFT) process and characterized. Second, the PSP was used in EKC separations through which its performance was characterized and compared to currently used PSPs.

The RAFT process was chosen for PSP synthesis because of its high control of molecular weight, narrow molecular weight distributions, and the ability to prepare complex macromolecular architectures [1]. The synthesis of the PSP confirmed the advantages of utilizing the RAFT process.

Chapter 1 is a very brief introduction to the methods used in this research. Historical information is presented in order to outline how this group took interest in this research. The main methods and theories, staples to this research, such as capillary electrophoresis, electrokinetic chromatography, and RAFT are presented in this chapter only as an introduction. In-depth discussions follow in Chapter 2

### 1.2 Electrokinetic Chromatography

---

The electrophoresis effect was first observed by a Russian physicist Reuss in 1809 [2], though the theoretical aspects were not formulated until 1897 by Kohlrausch [3]. Introduced in the 1960's by Tiselius and Hjerten, capillary electrophoresis (CE) is an analytical scale technique which utilizes the differences in analyte charge and size to effect separations in a capillary tube [4]. CE, as known today, was first demonstrated, in 1981, on open-tubular fused silica capillaries by Jorgenson and Lukacs [5] [6]. In 1984 the Terabe group reported on a modification of the CE separation technique by including a PSP which allowed separations of charged and neutral compounds [7]. Terabe and group used sodium dodecyl sulfate (SDS) as their PSP, a compound which forms micelles in solutions and thus micellar electrokinetic chromatography

(MEKC) was born. While the technique is described in great detail in Chapter 2, a brief introduction follows:

In this technique, the method of separation is dependent on how the analyte interacts with the chosen anionic PSP and the buffered mobile phase in the presence of an electric field. Due to the anionic character of the PSP, its affinity is towards the anode; away from the detector which is installed at the cathode end of the instrument. The mobile phase flow is established by the presence of cations along the capillary walls and the applied electric field along that capillary, resulting in electroosmotic flow. The mobile phase thus moves towards the detector at or near the cathode. Because of this strong mobile phase flow the net movement of the PSP, although with a different velocity than the mobile phase, is towards the cathode as well. As analytes interact, selectively, with the mobile phase and the PSP (migrating with different velocities) relative transport is established and thus different analytes separate from each other.

The experiments in this work follow the general setup in Terabe's original experiments. The mobile phase is chosen to be basic, although the effect of slightly acidic mobile phases is also investigated. The synthesized PSPs are similar in principle to SDS, containing anionic shells and hydrophobic cores.

Although SDS is an excellent pseudostationary phase there are significant limitations to its performance. Highly retained compounds such as biphenyl have large retention factors and lose resolution in a MEKC separation. The solution is to add an organic solvent as a modifier to the mobile phase to lower the retention factor. SDS, being a micelle, will begin to disassociate in higher organic modifier concentrations losing separation performance.

In 1997 Palmer et al. oligomerized sodium 10-undecylenyl sulfate, a compound analogous to SDS [8]. This micelle-polymer PSP was found to provide selective and efficient separations similar to SDS. Because the new PSP had a polymerized core, its performance was superior to SDS in highly organically modified mobile phases. The issue of tuning PSP selectivity through structural architecture still remained.

The potential of polymeric PSPs made them of great interest to the EKC community and launched a plethora of investigations of how the chemistry of polymers affects selectivity. Many anionic polymeric PSPs like poly(sodium 10-undecylenyl sulfate), sodium-N-undec-10-en-1-oyl

taurate, and sodium-N-undec-10-en-1-oyl aminoethyl-2-phosphate were synthesized and characterized [9]. Random block copolymers utilizing 2-acrylamido-2-methylpropanesulfonic acid (AMPS) and lauryl methacrylamide were synthesized and showed good stability and the potential for different selectivity by introduction of novel functional groups. At this time cyclodextrins, which are readily available to the chemical industry, were also successfully employed in EKC [9].

Many other PSPs, described in Palmer's review article [10], demonstrated a real push to synthesize polymeric PSPs with different selectivity. At that time, success in the utility of random block copolymers as PSPs, and the discovery that (RAFT) polymeric synthesis can be applied to the field of PSP's, has led to the development of spherical nanoparticles as PSPs [10].

The independent development of controlled RAFT polymerization presented opportunities for the synthesis of novel polymeric PSPs. Recently, Palmer and group demonstrated RAFT synthesis and utility of novel latex nanoparticles as PSPs for use in EKC [11] [12]. The group synthesized a nanoparticle with a hydrophobic interior and an ionic exterior. The hydrophobic interior was made up of poly(butyl acrylate). The ionic exterior was composed of poly(acrylic acid), which in a basic buffer provided the electrophoretic mobility ( $\mu_{ep}$ ) necessary for EKC. The novel PSP showed high retention at low concentrations with minimal noise interference with the UV detector. The nanoparticle PSP was also shown to be compatible with mass spectrometric detection, providing a significant advantage over micellar PSPs.

### 1.3 Free radical polymerization

---

To fully grasp the advantage of RAFT a short discussion of free radical polymerization follows. One of the oldest polymerization techniques, free radical polymerization forms polymers by successive additions building blocks to a growing free radical chain. It is still the most versatile method for polymer synthesis due to its compatibility with a wide range of monomers [1]. The process consists of three steps; initiation, propagation, and termination. Because there are numerous chains propagating at once, at an extremely high rate, low polydispersity index (PDI, Equation 1) and specific architectures are difficult to achieve. PDI is given by the ratio of number average molecular weight ( $M_n$ ) and weight average molecular weight ( $M_w$ ).  $N_i$  is the number of molecules of molecular weight  $M_i$ . In a typical GPC plot the peak intensity is



substituted as  $N_i$ . In other words, PDI describes the magnitude of the difference in chain lengths/weights of a particular polymerized sample.

$$PDI = \frac{Mn}{Mw} = \frac{\frac{\sum MiNi}{\sum Ni}}{\frac{\sum Mi^2Ni}{\sum MiNi}}$$

Equation 1: PDI

Eventually all the growing chains terminate as dead polymers and re-initiation to make new architecture becomes impossible. Free radical polymerization with multiple different types of monomers reacting simultaneously results in statistical or random distribution of monomers in the growing chain, rather than polymers with controlled architecture consisting of blocks of monomer. The need for a controlled polymerization scheme, resulting in dormant but not dead chains, becomes apparent.

#### 1.4 Reversible addition–fragmentation chain-transfer polymerization

---

In the 1980's controlled/living radical polymerization was heavily investigated. Nitroxide mediated radical polymerization, a type of controlled/living radical polymerization, gave scientists the ability to control chain length and structure. The process is similar to free radical polymerization as it contains steps such as initiation, propagation, and termination. By using reversible radicals, this technique solves the random termination problem as all chains will propagate until there is no monomer left [1]. Low PDIs can be achieved. The process also results in dormant polymer chains, which can be reinitiated for further polymerization.

In 1998 Rizzardo and group reported on the RAFT process [13]. RAFT is the most robust technique out of the controlled/living group and can be used with a wide range of monomers and reaction conditions [13]. The RAFT technique requires a chain transfer agent (CTA), usually containing a dithiocarbonate or trithiocarbonate group, which mediates the reaction by establishing an equilibrium between growing polymer chains. This ensures that all chains propagate at the same rate giving narrow PDI. The CTA can also be called a RAFT agent. The ability of the CTA agent to reinitiate ensures precise control of polymer architecture. An in-depth discussion follows in Chapter 2.

Major requirements of PSPs, that help to ensure good efficiency and tunable selectivity, are narrow molecular weight distributions of the polymer and specific structure, respectively. The RAFT process has provided the tools to accomplish just that.

### 1.5 Objectives of the study

---

This study aims to further the research conducted by Palmer and Hilder by synthesizing latex nanoparticle PSPs of novel structure, characterizing structure and separation performance of the new materials, and comparing the separation performance and selectivity of the novel PSPs to previous polymeric and micellar PSPs.

The first part of this research project focuses on the synthesis and structural characterization of a novel PSP. Utilizing the RAFT process, AB diblock copolymers consisting of AMPS as the ionic block and butyl acrylate as the hydrophobic block were synthesized. The method of synthesis is a three-step process. The first step is to synthesize the CTA (2- $\{[(\text{butylsulfanyl})\text{carbonothioyl}]\text{sulfanyl}\}$ propanoic acid) due to commercial unavailability of the compound. The second step is a polymerization of the AMPS head groups. The polymerization is initiated with 4, 4'-Azobis(4-Cyanovaleric Acid) (V501). These head groups will later become the ionic shell of the nanoparticle. Because the RAFT process minimizes random radical termination, the end groups still possess the trithiocarbonate functionality having the same polymerization capabilities as the initial CTA. Due to the retained functionality, the differentiation only in polymerized AMPS, the single block polymer is referred to as the macro chain transfer agent (mCTA). In the third step, mCTA is re-initiated with V501 and chain extended with butyl acrylate monomer providing the hydrophobic interior to the nanoparticles.

The second part of this research project focuses on performance characterization of the PSP in EKC separations. Many micellar PSPs have been characterized by defining their  $\mu_{ep}$ , peak capacity, theoretical plates, and solvation characteristics. However, little research has been done to determine the effects of different latex polymer chemistry on separation performance. The newly synthesized PSP will be used to separate an alkyl-phenone mixture providing  $\mu_{ep}$ , peak capacity, and theoretical plates. A study of retention behavior of 39 compounds with varied structure will also be performed utilizing the PSP to obtain linear solvation energy relationships (LSER) characterization of the retention and selectivity. It is sometimes necessary to perform separations in lower pH environments. Performance of the new PSP will be recorded in three different pH environments.

The objectives of the study are as follows:

1. A mCTA polymer consisting of 4 polymerized AMPS monomers will be synthesized. The product will be of 1274 g/mol MW. The effect of using a sulfonate head group as opposed to a carboxylic acid group will be investigated.
2. Using the mCTA, an AB diblock copolymer will be synthesized for use as a PSP. The goal is to achieve synthesis of nanoparticles of about 30 nm. Butyl acrylate will be used for the hydrophobic interior and consist of about 20 polymerized monomers.
3. The polymerized nanoparticles will be used to separate a mixture of 6 alkyl-phenones to obtain information on electrophoretic mobility and methylene selectivity ( $\alpha_{CH_2}$ ).
4. The performance of the PSP will be investigated at lower pHs. The polymerized nanoparticle will be used at three different pHs to separate a mixture of 6 alkyl-phenones.
5. The polymerized nanoparticles will be used in LSER analysis by separating 39 different compounds providing PSP selectivity information.

Synthesis of intermediates and nanoparticles will be verified using appropriate analytical techniques

- High performance liquid chromatography (HPLC) will be used to determine CTA purity.
- $^1H$  nuclear magnetic resonance (NMR) will be used to determine CTA, mCTA, and nanoparticle structure.
- Electrospray ionization mass spectroscopy (ESI-MS) will be used to determine the molecular weight of the mCTA.
- Dynamic Light Scattering (DLS) will be used to determine nanoparticle size.

## 1.6 Thesis layout

---

The thesis consists of six chapters.

### ***Chapter One: Introduction and objectives***

This chapter gives a concise introduction and history to free radical polymerization, RAFT, and EKC. Research objectives are presented.

### ***Chapter Two: Theoretical Background***

Theories behind the RAFT process, CE, and EKC are presented and discussed. EKC with micellar PSP use is reviewed and ideas behind the use of AB diblock copolymer nanoparticles are presented. The theories behind LSER and methylene selectivity are also presented.

### ***Chapter Three: Synthesis and characterization of RAFT agents and diblock copolymers***

Synthesis of CTA, mCTA, and diblock copolymer nanoparticles is described. Specific examples are given. Analytical techniques used to characterize the formed products are discussed. HPLC, NMR, ESI-MS, and DLS data are presented.

### ***Chapter Four: Performance characterization of nanoparticles in electrokinetic chromatography***

Methods of analysis, using the novel PSP in EKC, are presented.

### ***Chapter Five: Results and Discussion***

Results obtained from nanoparticle synthesis and EKC are reported, interpreted, and discussed.

### ***Chapter Six: Conclusions and recommendations.***

Overall conclusions relating to the project are made and recommendations for future research are made.

## **Chapter 2: Theoretical background**

---

### **2.1 Introduction**

---

This chapter will give pertinent theoretical background relevant to this research. The chapter begins with a brief discussion of free radical polymerization in order to give some background to controlled/living free radical polymerization. The theory of controlled/living free radical polymerization, mainly RAFT, will be presented.

A detailed discussion of CE is presented followed by an EKC discussion. The EKC discussion is divided into two parts. The first part will present EKC with use of micelles as a PSP. The second part will deal with the less studied diblock copolymer latex nanoparticles as PSPs. The last part of the chapter will present LSER and the theory behind this characterization.

## 2.2 Free radical polymerization

Free radical polymerization is a process by which polymers can be synthesized. The polymer forms by successive addition of reactive monomers to an active free radical in solution. Free radical polymerization has been, and still is, the choice industrial application for polymer synthesis. In 2001, 40 billion pounds of polymer produced in the United States were produced by free radical polymerization [14].

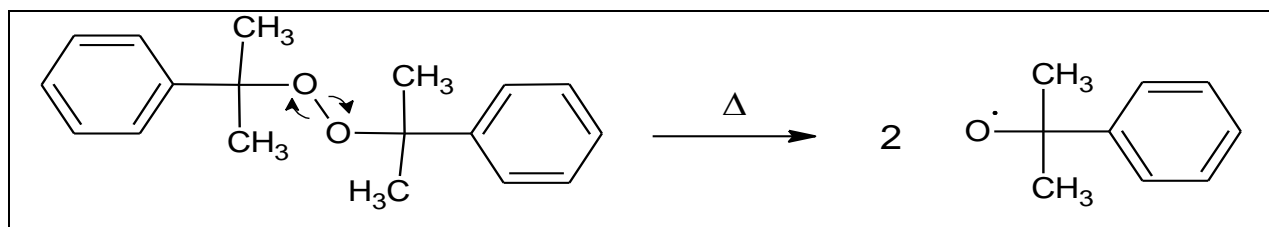
### Reaction Steps:

Free radical polymerization consists of three main reaction steps. These same steps are included in controlled/living free radical polymerization and need to be discussed in order to fully understand RAFT.

#### 1. Initiation

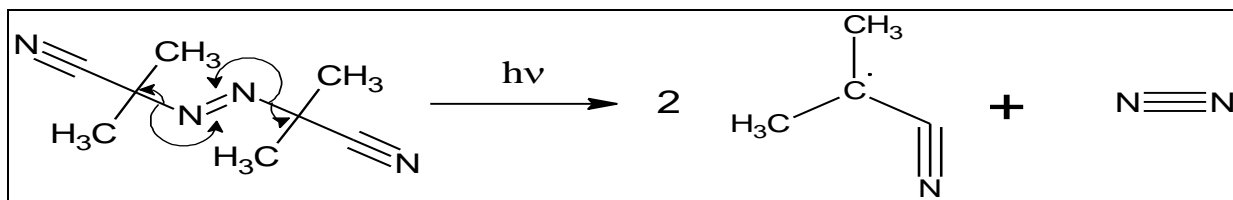
This is the first step in the polymerization process. Suitable monomers containing vinyl or carbon-oxygen double bond groups are radicalized by an initiator molecule. Many initiator molecules are available for polymerization reactions and they can be radicalized in a variety of ways. A couple of examples are given below but many more ways to initiate an initiator exist.

*Thermal decomposition:* Addition of heat to the initiator homolytically cleaves a bond, producing two radicals (Scheme 1). [15]



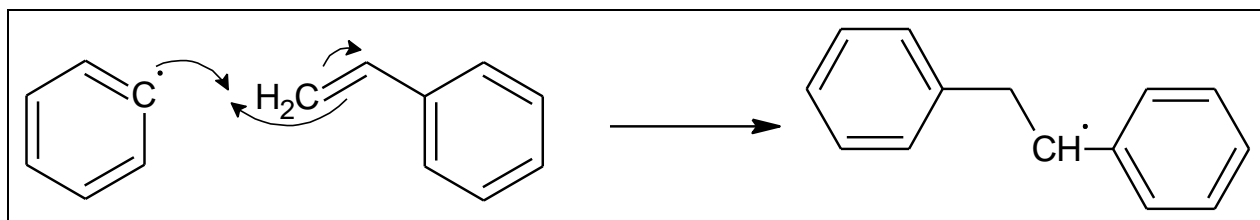
Scheme 1: Thermal decomposition of dicumyl peroxide.

*Photolysis:* Photoinitiation occurs when an electron on a molecule can be excited by photons enabling the radical to be in a lowest triplet excited state (Scheme 2). [16]



**Scheme 2: Photolysis of azoisobutylnitrile (AIBN) gives two free radical initiators and nitrogen gas.**

The second phase of initiation can now begin. This is where the initiator radical attacks and attaches to a monomer molecule, thus activating it. (Scheme 3) [17]



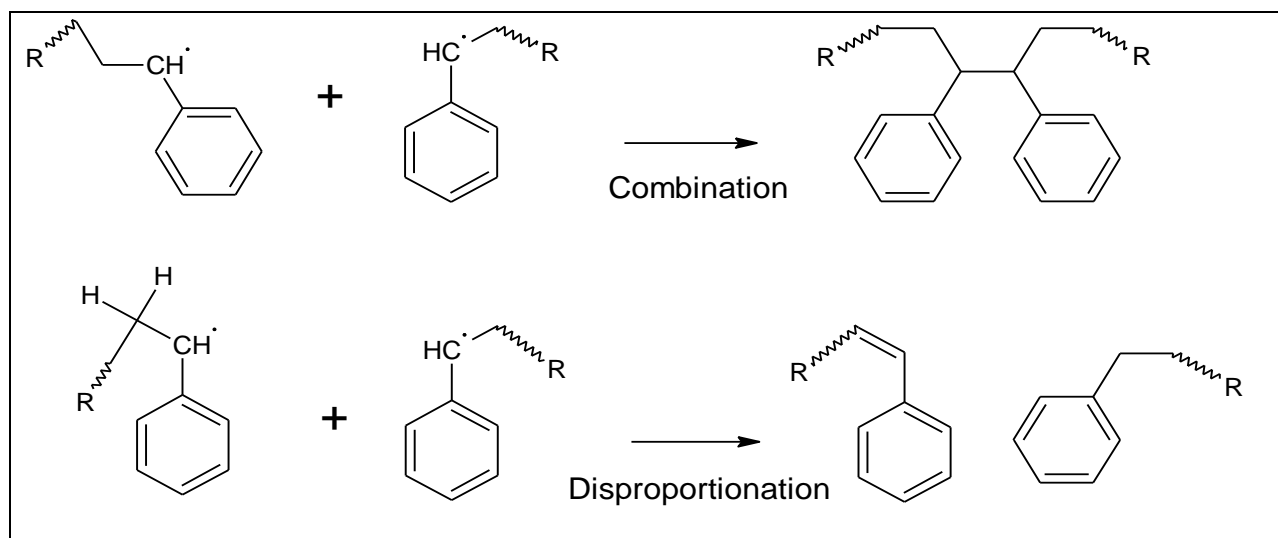
**Scheme 3: Phenyl initiator attacks and attaches to a double bond on styrene**

## 2. Propagation

This is the second step in the polymerization process. The polymer chain grows in this phase. The newly formed activated monomer can attack and attach to another double bond in a monomer, activating it at the same time [17]. The reaction continues this way until all radicals terminate.

## 3. Termination

This is the third and final step in the polymerization process. There are two main pathways a growing polymer chain can terminate. These are combination and disproportionation. The two pathways are illustrated in (Scheme 4).



**Scheme 4: Two pathways of free radical polymerization termination: Combination and disproportionation.**

In the combination termination pathway coupling occurs when two of the growing polymer chains react, leading to a dead polymer. In the disproportionation termination pathway hydrogen is abstracted from one growing polymer chain and transferred to the other giving one saturated and one unsaturated end group [18].

The termination reaction step is the biggest drawback of free radical polymerization. Growing polymer chains are at relatively high concentrations and can find each other with ease, causing termination in some, while others continue to grow. This leads to very high PDI values of greater than 2 [19]. This means that there is a large distribution of polymeric chain size and weight.

High polydispersity is not ideal for polymers to be applied as PSPs. Chromatographers are very concerned that stationary phases or PSPs provide high efficiency separations. One of the main requirements of a good efficient phase is for it to be mono disperse. A mono disperse PSP will have very similar molecules of similar weight and size. This insures that all analytes will interact in the same way with each part of the PSP, and that the PSP will have uniform electrophoretic mobility.

Another drawback in free radical polymerization is the extremely fast propagation rate. It is difficult to quench the reaction at a targeted molecular weight. This leads to loss of size control

in the polymer. As researchers we would like to hold some variables constant while changing others. This becomes difficult when using free radical polymerization.

The last drawback, pertinent to this research, is little control of structure in free radical polymerization. When termination finishes the reaction, all of the polymers are dead and cannot be reinitiated to grow with new monomers. Furthermore, if one initially introduces two different monomers into the reaction, random copolymers will form [20].

Palmer and group reported success using random copolymers as PSPs [21]. However, in part because the ionic and hydrophobic monomers in the polymeric chain randomly alternate, no significant improvements over SDS in hydrophobic interactions, as characterized by methylene selectivity are reported.

The recently introduced method of RAFT addresses the issues mentioned above. RAFT polymerization gives us excellent control over PDI (see Figure 1) and structure, enabling the creation of efficient PSPs.

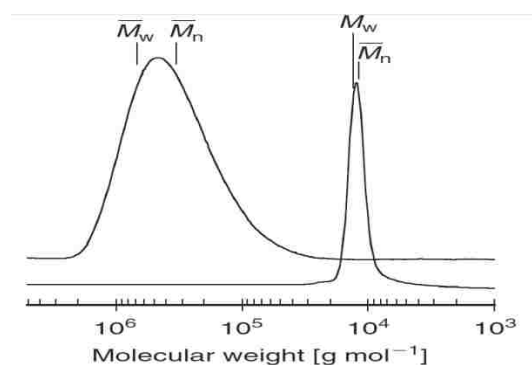


**Figure 1: Typical molecular weight distributions for a conventional (broad peak) and living radical (narrow peak) polymerization. Peak PDI values obtained from GPC data are 1.74 and 1.04 respectively. [22]**  
"Reprinted with permission from {G. Moad, E. Rizzardo and S. H. Thang, "Living Radical Polymerization by the RAFT Process," Australian Journal of Chemistry, vol. 58, pp. 379-410, 2005.}. Copyright {2013} Australian Journal of Chemistry."

### 2.3 Reversible addition–fragmentation chain-transfer polymerization

RAFT is a sub category of controlled/living free radical polymerization. Within the category are also nitroxide mediated polymerization and atom transfer radical polymerization. For this research we have used the RAFT method as our polymerization technique due to the ruggedness of the reaction [13]. In other words, of all the types of controlled/living



polymerizations, RAFT is least susceptible to the negative contaminants such as oxygen and reagent impurities.

First reported by Rizzardo and group, the RAFT process, just like free radical polymerization, contains initiation, propagation, and termination. In addition, the RAFT process utilizes a chain transfer agent (CTA) which mediates the reaction [13]. The following section will give some theoretical background behind the RAFT process.

### Components of RAFT

*Initiators:* Just as in free radical polymerization, RAFT also uses an initiator to start the polymerization process. The mechanisms of initiating the initiator are the same, done by the introduction of heat or photons. Common initiators are AIBN, used in hydrophobic reactions, and V501, used in aqueous reaction media.

*CTA and Monomer:* The CTA gives a polymer its living characteristics. CTAs will differ with respect to different reactions but will always contain a dithiocarbonate moiety. The structure of the RAFT agent is an integral part of the reaction. A general form of the CTA is given in Figure 2.

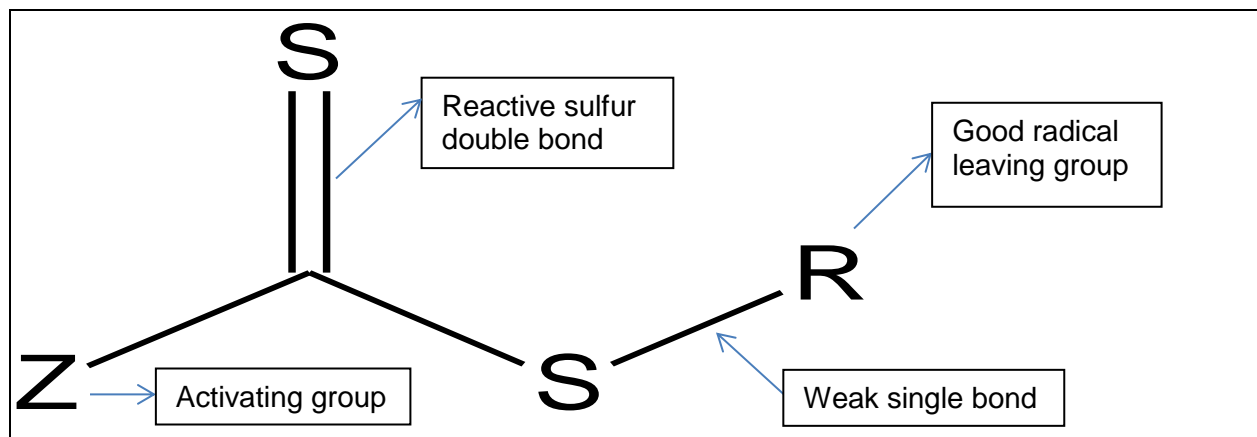


Figure 2: A general representation of a CTA.

Depending on the Z group there exist four main classes of CTAs. These are shown in Table 1.

<i>Class</i>	<i>Activating Group (Z)</i>
Dithioesters [13]	Alkyl or aryl
Trithiocarbonates [23]	Substituted sulfur
Xanthates [24]	Substituted oxygen
Dithiocarbamates [25]	Substituted nitrogen

**Table 1: Four classes of CTAs.**

The Z group controls the C-S double bond reactivity thus influencing the rate of radical addition and fragmentation. Dithioesters, especially benzoates, are prone to hydrolysis as they are more reactive activating groups. Trithiocarbonates, although not as fast, still possess high transfer constants and are reasonably hydrolytically stable in pHs of 6.5 and lower [26]. Xanthates and dithiocarbamates are used with electron-rich monomers. All CTAs must be compatible with the monomer of choice. Table 2, below, shows CTA to monomer compatibility. The current study uses a trithiocarbonate CTA as the polymerization is performed with acrylamides and acrylates.

The R group should also be considered. This group should be directly chosen with regard to the monomer being used. [22] The R group is chosen such that it is a good leaving group. In fact, it must be a more stable radical and a better leaving group than the monomer. The monomer, and Z and R groups on the CTA have to be considered in a RAFT reaction.

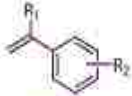
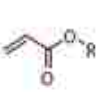
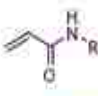
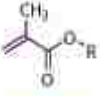
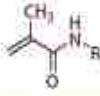
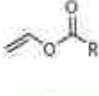
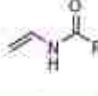
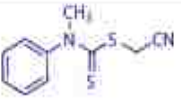
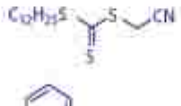
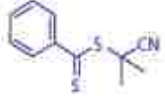
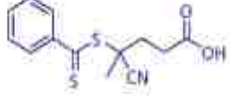
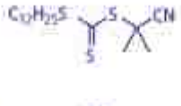
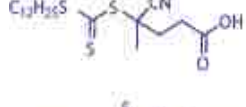
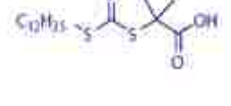
							
	styrenes	acrylates	acrylamides	methacrylates	methacrylamides	vinyl esters	vinyl amides
	—	—	—	—	—	+++	+++
	+++	+++	+++	—	—	—	—
	++	+	—	+++	+++	—	—
	++	+	+	+++	+++	—	—
	+++	++	++	+++	+++	—	—
	+++	++	++	+++	+++	—	—
	+++	+++	+++	+	+	—	—

Table 2: Commercially available CTAs on the left and monomers on top [27]. The “+” indicates a favorable reaction. “Reprinted with permission from Sigma-Aldrich, copyright 2013”

## The RAFT mechanism

The main feature of the RAFT process is the activation/deactivation of growing polymers. Mediated by a CTA, all polymer chains have the same probability of growth. The CTA quickly exchanges polymer chains making sure that there are only a fraction of chains growing at any one time. The use of CTA gives access to size control and narrow PDIs. Unlike free radical addition, there are six steps in the RAFT mechanism. These are initiation, propagation, reversible chain transfer, reinitiation, chain equilibration, and termination [28]. The RAFT mechanism is shown in Scheme 5.

*Initiation:* The reaction is begun in the same way as free radical addition. A relatively low concentration of initiator such as AIBN or V501 decomposes creating  $I^\bullet$  radicals. The initiating radical  $I^\bullet$  adds to monomer M, starting a growing polymeric chain radical of n monomers

denoted as  $P_n^*$ . It should be noted that at this point very few monomers are initiated due to very low concentrations of initiator present in solution. Low concentrations of initiator make sure that the main RAFT mechanism continues through the thiocarbonylthio CTA retaining the “living” character.

*Reversible chain transfer/propagation (pre-equilibrium):* The propagating polymeric radical  $P_n^*$ , initiated by  $I^*$ , attacks the CTA (1) creating an unstable RAFT adduct radical intermediate (2). If the R group was chosen correctly, it disassociates from the CTA as a radical  $R^*$  (3). The need for a good leaving group is illustrated in the pre-equilibrium process as it is reversible, where  $R^*$  can reattach and disassociate the  $P_n^*$ . It is important to note that the number of  $R^*$  produced is directly related to the original concentration of the CTA. This feature is what gives control of chain length. Larger concentrations of CTA, keeping monomer concentration constant, will give shorter polymers.

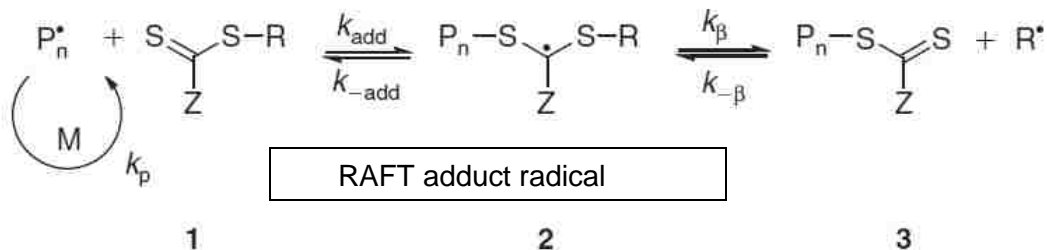
*Reinitiation:* The radicalized R group goes on to initiate more monomer creating a growing polymeric radical  $P_m^*$ .

*Chain equilibration/propagation (main RAFT equilibrium):* This is the most important part of the RAFT process.  $P_m^*$ , an active polymeric chain radical initiated by the  $R^*$  can attack the dormant polymeric CTA (3'). Again this creates an unstable RAFT adduct radical intermediate (4). The RAFT adduct radical intermediate quickly disassociates the previously attached polymeric group as an active radical polymer (3''). The process is reversible, and after the polymer has had a chance to grow it will associate with another polymeric CTA becoming dormant. The extremely fast equilibrium provides equal opportunity for all chains to grow and allows for the production of narrow dispersity polymers [28]. When the reaction is complete or quenched most of the polymers retain the thiocarbonylthio functionality and can be reinitiated for use with a different monomer leading to AB diblock copolymers.

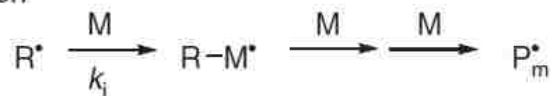
*Initiation*



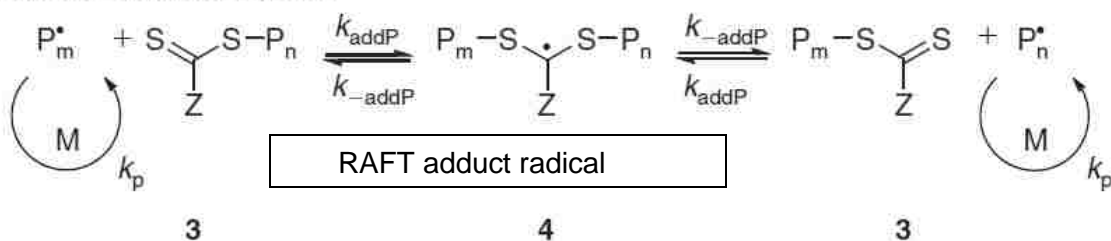
*Reversible chain transfer/propagation (pre-equilibrium)*



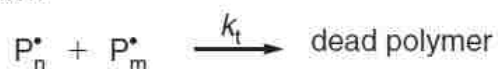
*Reinitiation*



*Chain equilibration/propagation*



*Termination*



**Scheme 5: Mechanism of RAFT polymerization.** [28] "Reprinted with permission from {G. Moad, E. Rizzardo and S. H. Thang, "Living Radical Polymerization by the RAFT Process," Australian Journal of Chemistry, vol. 58, pp. 379-410, 2005.}. Copyright {2013} Australian Journal of Chemistry."

*Termination:* While the major product of RAFT is a living polymer, some termination does take place (Figure 3). Termination occurs in the RAFT process by the same mechanisms as in free radical addition. When a growing polymeric chain, initiated with  $\text{R}^{\bullet}$  ( $\text{P}_m^{\bullet}$ ), attaches to a radical instead of a CTA; a dead polymer is formed ( $\text{R}-\text{M}_m-\text{R}$ ). Due to low concentrations of initiator, the concentration of active radicals remains low during the entire process and dead polymers from two growing  $\text{RP}_m^{\bullet}$  chains combining are relatively rare.

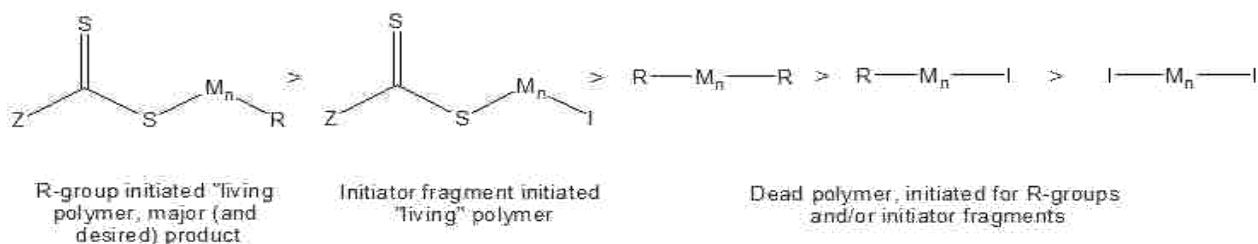


**Figure 3: Major products of the RAFT process decreasing in prevalence from left to right.**

Less likely to form are, again due to low initiator concentrations, dead polymers initiated by the initiator and terminated by R or another initiator fragment (I-M<sub>n</sub>-I). Unlike free radical addition, due to low concentrations of growing chains at any one time, it is difficult for radicals to find each other in solution and terminate polymerization.

### Determination of polymeric molecular weight

As stated before the RAFT process gives unprecedented control over molecular weight. It has been determined that the molecular weight is linear as a function conversion, or polymer growth (Figure 4).

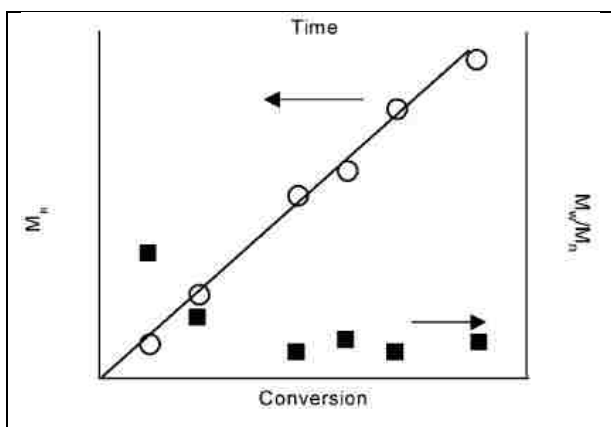


**Figure 4: GPC data showing a linear relationship between conversion and molecular weight (circles). Polydispersity is exponentially minimized with conversion (squares). [62] "Reprinted with permission from {C. L. McCormick and A. B. Lowe, "Aqueous RAFT Polymerization: Recent Developments in Synthesis of Functional Water-Soluble (Co)polymers with Controlled Structures," *Acc. Chem. Res.*, vol. 37, pp. 312-325, 2004.}. Copyright {2013} American Chemical Society."**

Because of this linear relationship, concentrations of monomer, with respect to CTA, needed to obtain a polymer with a required molecular weight can be determined (Equation 2), wherein  $M_{ntheo}$  is the theoretical molecular weight of the polymer,  $FW_{RAFT}$  is the molecular weight of the CTA,  $x$  is the fractional conversion at time  $t$ ,  $[M_0]$  is the initial monomer concentration,  $FW_M$  is

the molecular weight of the monomer,  $[RAFT_0]$  is the initial CTA concentration,  $f$  is the initiator efficiency, and  $k_d$  is the initiator dissociation constant. Because the amount of initiator is a key factor in producing dead chains, the amount of initiator should be kept small relative to the CTA [29]. Because the initiator concentrations are so small, Equation 2 can be simplified by omitting the initiator terms. This gives Equation 3.

$$M_{n_{theo}} = FW_{RAFT} + \frac{x[M_0]FW_M}{[RAFT_0] + 2 * f * [[I_0](1 - e^{-k_d t})]}$$

**Equation 2: Calculation to determine the theoretical molecular weight of the polymer at a certain conversion. The initiator terms are included.**

$$M_{n_{theo}} = FW_{RAFT} + \frac{x[M_0]FW_M}{[RAFT_0]}$$

**Equation 3: Calculation to determine the theoretical molecular weight of the polymer at a certain conversion. The initiator terms are omitted.**

The polymerizations performed in this research will all use Equation 3 to determine monomer and CTA concentrations needed. The initiator concentration is always set to 10 percent of the CTA as this was determined to give the narrowest PDI [22].

### 2.3.1 Single Block Polymers to AB Diblock Copolymers

---

This paragraph describes the general formation of a diblock copolymer. An AB diblock copolymer is a polymer with two distinct subunits composed of different monomers. After the initial RAFT synthesis, producing a single block polymer called a macro chain transfer agent (mCTA), mCTA is created and purified for further use. The mCTA retains the same functionality as the original CTA except it now contains the polymeric A block. Because of its living character, the mCTA can be reinitiated in the same fashion and a new monomer, B block, can be added.

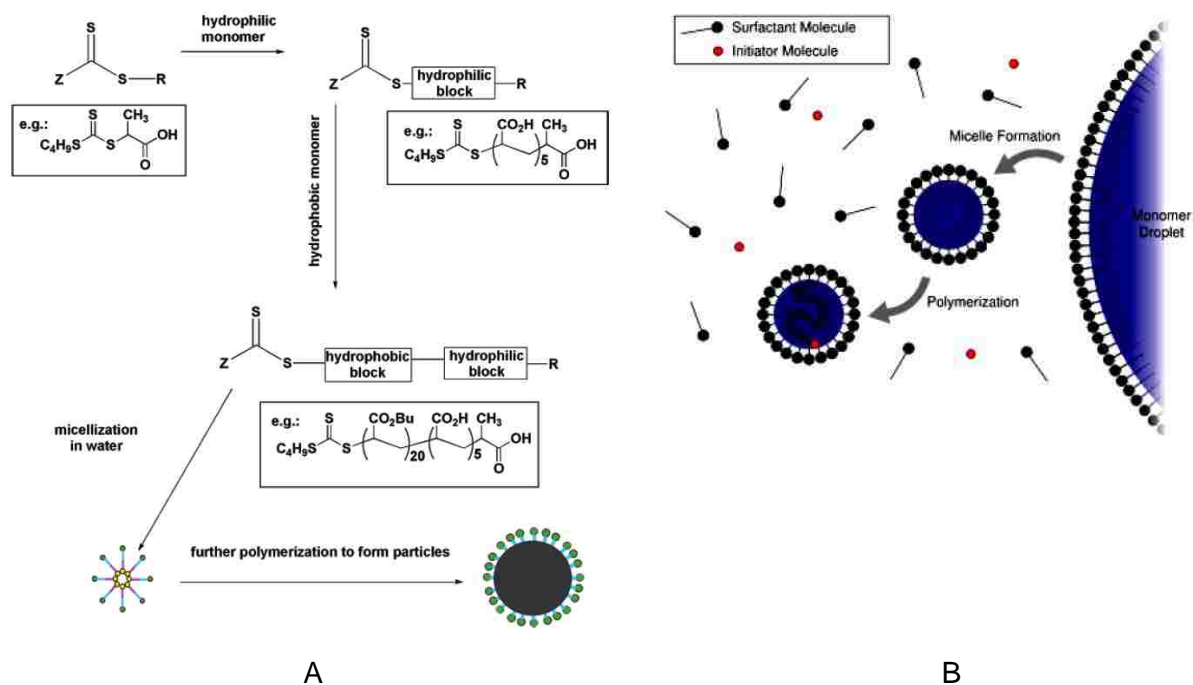
The general reaction process is given in Scheme 6 (A) and is under aqueous solvent conditions. The following describes the path to synthesizing diblock copolymers. In this reaction the hydrophilic monomer is added to the CTA followed by the addition of the hydrophobic monomer. As the hydrophobic block grows it self-assembles into micelles. Further polymerization begins to take place inside the newly formed micelles and a locked-in nanoparticle is formed. In order

for micellization to occur, the pH of the system must be high enough so that the hydrophilic groups are ionized yet low enough that the thiocarbonylthio moiety is not hydrolyzed.

This is further illustrated in Scheme 6 (B). The process described here is macro emulsion polymerization [30]. The hydrophobic monomer is emulsified in the aqueous reaction solvent creating monomer droplets. The surfactant molecule, mCTA, slowly adds some hydrophobic groups until it can self-assemble into micelles. The interior of the micelle swells with the hydrophobic monomer, and RAFT-controlled polymerization proceeds within the micelle.

It is important to note that the smaller the monomer droplets are, the better the activated R groups are distributed through the system; leading to less termination and narrow polydispersity. One way to make sure that the monomer droplets are small is to use a micro emulsion technique. [31] In this technique sonication is added to the reaction breaking up monomer droplets. Another technique which minimizes droplet size was demonstrated by Ferguson *et. al.* The monomer is delivered slowly over time making sure that droplets are small and well emulsified. [32] The research done in this project uses Ferguson's RAFT in emulsion technique to create AB diblock copolymer nanoparticles.





**Scheme 6:** A) General reaction process for the creation of an AB diblock copolymer. In illustration the hydrophobic block is added first, followed by the hydrophilic block. [32] B) Micellization and further polymerization with the hydrophobic monomer. [30] The surfactant is the mCTA. Reaction takes place in an aqueous solvent. Initiator molecules consist mostly of  $R^\bullet$  with a small amount being  $I^\bullet$ . Schme 6 A and B were "Reprinted with permission from {C. Furgeson, R. Hughes, D. Nguyen, B. Pham, R. Gilbert, A. Serelis, C. Such and B. Hawket, "Ab Initio Emulsion Polymerization by RAFT-Controlled Self-Assembly," *Macromolecules*, vol. 38, pp. 2191-2204, 2005.}. Copyright {2013} American Chemical Society." And the Dave Weitz group at Harvard University, respectively.

## 2.4 Capillary electrophoresis

In order to fully describe EKC a brief discussion of basic CE setup and theory will follow. Several advantages make CE a powerful alternative with respect to other analytical separation systems. Rapid analysis and sample preparation times are two. Theoretical plates, or instrument efficiency, are an order of magnitude over that which can be achieved by high performance liquid chromatography (HPLC). CE, utilizing open-tubular glass columns, was introduced in the 1981 for the separation of ions based on their charge and frictional forces and was later modified by Terabe *et. al.* for use with neutral analytes (discussion to follow).

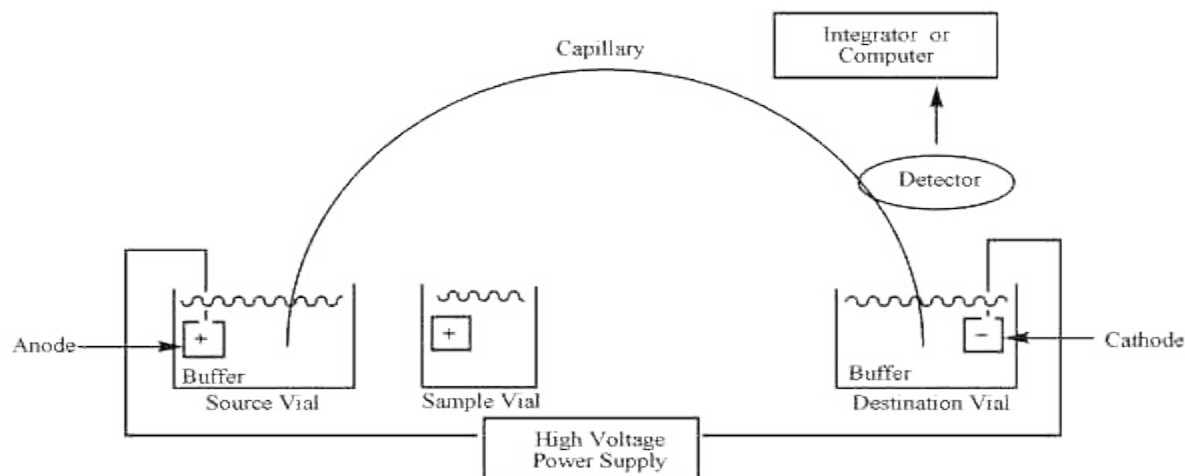


Figure 5: Basic CE instrument setup.

The CE instrument consists of a high voltage power supply, two reservoirs filled with a buffer solution, an anode and cathode submerged into the buffer, a capillary column filled with buffer and submerged into the reservoirs, and a detector (Figure 5). The power supply can deliver voltages across the capillary as high as 30 kV. The buffer solution prevents changes in pH due to oxidation and reduction at the anode or cathode as analysis progresses. The buffer solution also provides electrolytes to set up the electroosmotic flow (EOF), which will be explained. The fused silica capillary column interior walls support ionizable silanols, another component which sets up the EOF. In most cases the detector is a ultra-violet (UV) detector. However, fluorescence and mass spectrometry (MS) detectors are also employed.

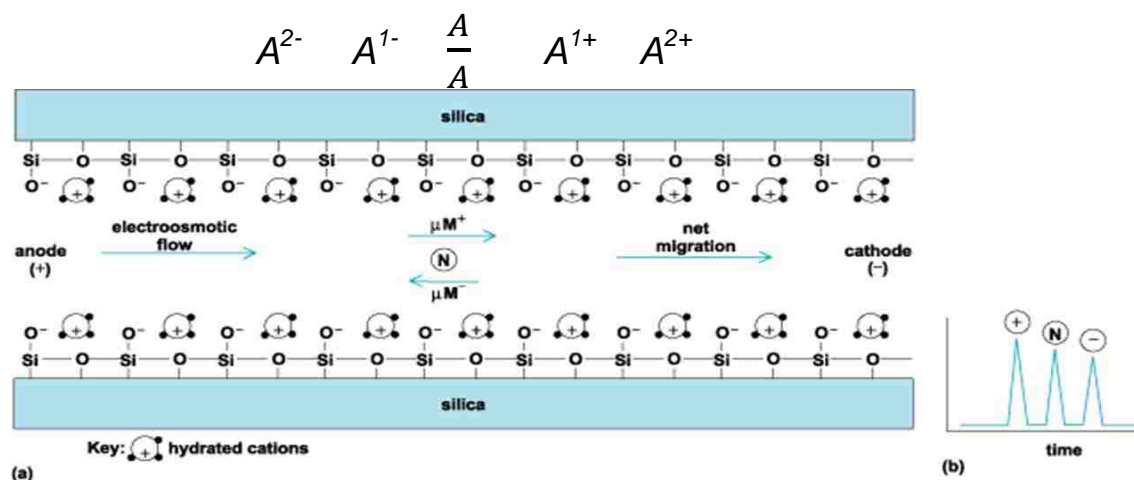
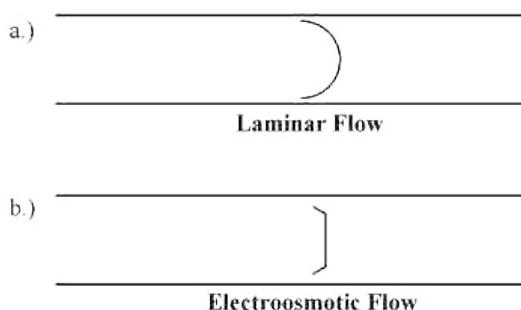


Figure 6: a) A zoomed representation of a capillary column in CE.  $A^{\text{charge}}$  represents an analyte of a certain charge. Hydrated cations are balancing the negatively charged oxides establishing the EOF.  $\mu M^+$  represents the velocity of positively charged ions.  $\mu M^-$  represents the velocity of negatively charged ions. The EOF and net migration is towards the cathode. b) Elution order of analytes, positive ions are followed by neutral compounds, followed by negative ions.

The capillary column is flushed with a base in order to create and regenerate ionizable silanol sites. As an electrolyte fills the column hydrated positive ions create a fixed layer (Figure 6 (a)). On top of the fixed layer another diffuse layer (not shown) of hydrated cations forms. This mobile layer is loosely held by the silanol sites and is free to establish the EOF.

A voltage is applied across the capillary using the power supply and establishing an electric field which moves the cations toward the cathode. This establishes a flat profile EOF. In contrast, pressure driven flows experience a laminar profile which can lead to efficiency loss due to dispersion (Figure 7). Negative ions will have a negative velocity with respect to the EOF (Figure 6 (a)). However, due to the EOF, the net velocity is still positive towards the detector



**Figure 7: a) Flow profile of a pressure driven flow system. b) Flow profile of an EOF system.**

and cathode. Analytes with a larger negative charge ( $A^{2-}$ ) will move slower through the column, separating from ( $A^{-1}$ ). Positively charged analytes will have a positive velocity towards the cathode, with higher charged ( $A^{2+}$ ) moving faster than ( $A^{1+}$ ). In this case the EOF adds to the velocity of the analytes. This method of separation will separate neutral analytes from the ionic analytes but does not separate neutral analytes ( $A$ ) from each other. Neutral analytes move through the capillary with the velocity of the EOF. A simplified electropherogram (Figure 6 (b)) shows a separation of positive, neutral, and negative analytes as they elute with time.

The EOF velocity can be defined as  $u_o$  and is directly dependent on the electric field strength ( $E$ ) and the electroosmotic mobility ( $\mu_o$ ). (Equation 4) The electric field strength can be calculated from the voltage ( $V$ ) and total length of the capillary ( $L_t$ ). (Equation 5)

$$u_o = \mu_o * E$$

**Equation 4: EOF velocity.**

$$E = \frac{V}{L_t}$$

**Equation 5: Electric field strength**

The electroosmotic mobility is defined by the zeta potential ( $\zeta$ ) of the capillary wall times the relative permittivity ( $\epsilon$ ) of the buffer and divided by viscosity of the medium ( $\eta$ ). (Equation 6)

$$\mu_o = \frac{\epsilon * \zeta}{\eta}$$

**Equation 6: Electroosmotic mobility.**

Positive ions migrate towards the cathode and negative ions migrate toward the anode with a certain velocity ( $u_{ep}$ ). The velocity of the analytes is directly dependent on the electric field strength and the electrophoretic mobility of the analyte ( $\mu_{ep}$ ). (Equation 7)

$$u_{ep} = \mu_{ep} * E$$

**Equation 7: Charged analyte velocity**

At a given pH, an analyte will have an electrophoretic mobility dependent on, charge, size, and viscosity of the medium as in Equation 8, where  $Z$  is the net charge of the analyte and  $r$  is the stokes radius. The stokes radius is described by Equation 9, where  $k_B$  is the Boltzmann constant,  $T$  is temperature, and  $D$  is the diffusion coefficient.

$$\mu_{ep} = \frac{Z}{6\pi\eta r}$$

**Equation 8: Analyte electrophoretic mobility**

$$r = \frac{k_B T}{6\pi\eta D}$$

**Equation 9: Stockes radius**

Some of the values in the equations above are difficult to quantify. The determination of analyte electrophoretic mobility is done experimentally. Equation 7 is rearranged solving for  $\mu_{ep}$ . Substituting Equation 7 with Equation 5 and  $u_{ep}$  with  $L/tr$ , Equation 10 is obtained where  $L$  is the distance to the detector and  $t_r$  is the time it takes the analyte to migrate to the detector (retention time) in the absence of any bulk flow.

$$\mu_{ep} = \left(\frac{L}{t_r}\right)\left(\frac{L_t}{V}\right)$$

**Equation 10: Experimental calculation of analyte electrophoretic mobility**

As mentioned before, the net velocity ( $u$ ) of the analyte is also dependent on the velocity of the EOF. Adding the two velocities together gives  $u$ . (Equation 11)

$$u = u_{ep} + u_o = (\mu_{ep} + \mu_o) * E$$

**Equation 11: Net analyte velocity**

Although CE is a powerful technique, it cannot resolve neutral compounds. In neutral compounds  $u_{ep} \rightarrow 0$ . Thus all neutral compounds migrate to the detector with the same velocity of  $u_o$ . A modification of the CE system is required to separate neutral compounds.

## 2.5 Electrokinetic chromatography

---

Electrokinetic chromatography is a modification to the CE system, enabling separation of neutral compounds, with the addition of a PSP. Many different PSPs are employed such as micelles, polymers, micro-droplets, dendrimers, and cyclodextrins [33] [34] [7] [8]. This research focuses on polymeric nanoparticles fashioned after micelles. Micellar and polymeric PSPs are most frequently used in EKC, the latter being employed mainly in academia as they are not yet readily available in commercial settings. It is the focus of this research to extend characterization of polymeric nanoparticles as PSPs.

### 2.5.1 Polymeric PSPs

---

Although micelles and polymeric PSPs differ in some ways, the principles behind the separation of neutral analytes in EKC are the same. Micelles and polymeric PSPs consist of molecules that have ionic and hydrophobic regions. This study uses anionic head groups. Because of the anionic groups, the PSP will have an electrophoretic mobility ( $\mu_{ep}$ ) toward the anode, opposite of the EOF. However, just as with negative ions previously discussed, the net PSP mobility ( $\mu_{pspnet}$ ) is still towards the cathode and the detector. (Figure 8)

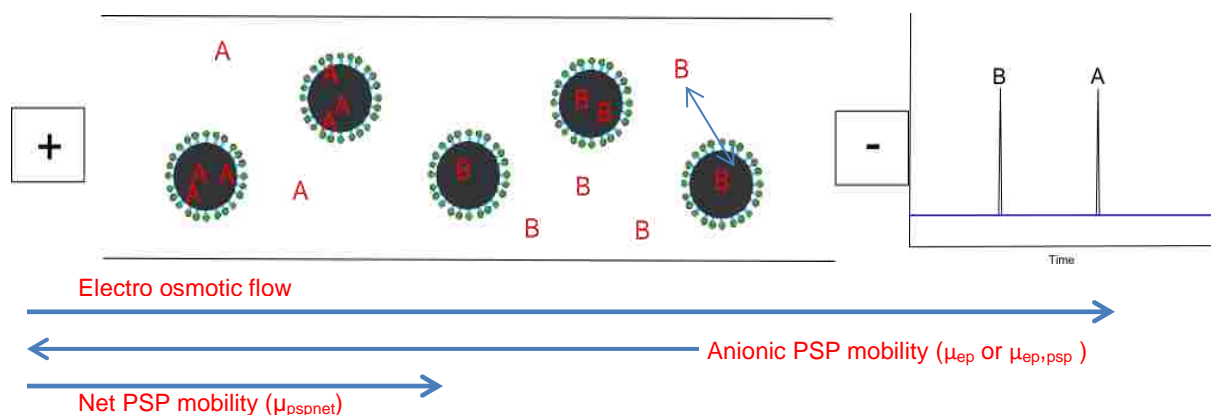


**Figure 8:** A cross sectional representation of a capillary column filled with a buffer solution and a PSP. Black interior represents the hydrophobic area of the PSP. Green areas represent the anionic components of the PSP. Analytes A and B partition between the buffer and PSP phases. Analyte B has a partition coefficient less than that of Analyte A thus its net velocity is faster and  $t_r$  is smaller. A hypothetical chromatogram illustrates the elution order.

Analytes can interact with both the anionic and hydrophobic groups on the PSP. Selective transport of the analytes is achieved by taking advantage of the differing PSP affinity for individual analytes.

Analytes will have different distribution coefficients ( $K$ ) or equilibria between the mobile phase and PSP. In other words, based on the chemical makeup of the analyte, the analyte will spend a certain amount of time associated with the buffer and a certain time associated with the PSP. This is analogous to separations in HPLC. Because velocities differ between the bulk flow and the PSP, analytes will have different elution times based on how much time they associate with the bulk flow and the PSP. Charged analytes' behavior, when using a PSP, is more complex to define as they exhibit their own electrophoretic mobility while interacting with the PSP. [35]

For EKC it is useful to describe the system in terms of the velocities which are determined experimentally. Theoretically determining electrophoretic mobility ( $\mu_{ep}$ ) of the PSP becomes complex, especially with novel PSPs. Effective electrophoretic velocity ( $u_{ep,psp}$ ) (Equation 12) can be obtained by substituting  $\mu_{ep}$  in Equation 7 with  $\mu_{ep,psp}$ . The net velocity of the PSP ( $u_{pspnet}$ ) can be obtained by substituting  $u_{ep}$  in Equation 11 with  $u_{ep,psp}$ . (Equation 13)

These are the same equations used for describing analyte mobility/velocity in CE. In this section, the change in notation is to distinguish that this is an EKC process that utilizes a PSP.

However,  $\mu_{ep}$  and  $\mu_{ep,psp}$  are interchangeable terms, the former being the preferred term for PSP electrophoretic mobility in the absence of any bulk flow. The results given in the following chapters will use the  $\mu_{ep}$  notation for PSP electrophoretic mobility.

$$u_{ep,psp} = \mu_{ep,psp} * E$$

**Equation 12: Electrophoretic velocity of a PSP**

$$u_{pspnet} = u_{ep,psp} + u_o$$

**Equation 13: PSP net velocity**

EOF velocity in EKC can be defined by Equation 14 where  $t_o$  is the elution time of a completely unretained charge-neutral analyte. Because the analyte has no interaction with the PSP, the analyte moves through the capillary with the same velocity as the EOF. Equation 15 gives the experimental value of  $u_{pspnet}$  where  $t_{psp}$  is the elution time of an analyte which is only associated with the PSP. Because the analyte has no interactions with the EOF, it represents the net velocity of the PSP. Equation 16 gives the velocity of the analyte as it migrates through the capillary where  $t_r$  is the elution time of the analyte.

$$u_o = \frac{L}{t_o}$$

**Equation 14: EOF velocity**

$$u_{pspnet} = \frac{L}{t_{psp}}$$

**Equation 15: PSP net velocity**

$$u_a = \frac{L}{t_r}$$

**Equation 16: Analyte velocity**

To experimentally obtain apparent electrophoretic mobility for EOF, PSP ( $\mu_{epnet}$ ), and analyte ( $\mu_a$ ), Equation 10 is used substituting the appropriate  $t$  terms for the EOF and PSP. (Equation 17)(Equation 18)(Equation 19)

$$\mu_o = \left(\frac{L}{t_o}\right)\left(\frac{L_t}{V}\right)$$

**Equation 17: EOF electrophoretic mobility**

$$\mu_{epnet} = \left(\frac{L}{t_{psp}}\right)\left(\frac{L_t}{V}\right)$$

**Equation 18: PSP apparent electrophoretic mobility**

$$\mu_a = \left(\frac{L}{t_r}\right)\left(\frac{L_t}{V}\right)$$

**Equation 19: Analyte electrophoretic mobility**

Analyte velocity is a time weighted average of the time the analyte spends associated with the EOF velocity and the time the analyte spends associated with the PSP velocity (Equation 20). How well the analyte is retained on the PSP is given by the retention factor ( $k$ ). Analyte velocity can also be determined from knowing the retention factor (Equation 20). The retention factor is

also related to the distribution coefficient by the ratio of volumes of the PSP ( $V_{psp}$ ) and mobile phase ( $V_{mob}$ ). (Equation 21)

$$u_a = \frac{t_o}{t_o + t_{psp}} * u_o + \frac{t_{psp}}{t_o + t_{psp}} * u_{pspnet} = \frac{1}{1 + k} * u_o + \frac{k}{1 + k} * u_{pspnet}$$

**Equation 20: Analyte velocity in EKC**

$$k = \frac{V_{psp}}{V_{mob}} K$$

**Equation 21: Retention factor**

The retention factor is an important piece of information because it provides information on the interaction of analytes with the PSP. The natural logarithm of the retention factor is proportional to the free energy involved in the transfer of the analyte from the background electrolyte to the PSP. This is highly useful as it can provide LSER and methylene selectivity information which is also based on free energy relationships. The retention factor for analytes can be obtained by rearranging Equation 20 and substituting Equation 14, Equation 15, and Equation 16 for velocities. [7] This gives Equation 22.

$$k = \frac{t_r - t_o}{t_o \left(1 - \frac{t_r}{t_{psp}}\right)}$$

**Equation 22: Retention factor experimental determination.**

This project characterized the novel PSP through the use of retention factors. However, obtaining  $t_{psp}$  becomes difficult due to the unavoidable use of a fully retained analyte to determine  $t_{psp}$  for each injection, given the inherent CE inconsistency in the migration times of analytes. It is possible to avoid using  $t_{psp}$  to determine  $k$  when  $\mu_{ep,psp}$ ,  $\mu_o$ , and  $\mu_a$  can be experimentally determined. Equation 22 is rearranged into Equation 23. Substituting apparent electrophoretic mobility of analyte, EOF, and PSP, given in Equation 17, Equation 18, and Equation 19, Equation 24 is obtained. Equation 24 will be used in all retention factor calculations in this study, with  $\mu_o$  and  $\mu_a$  being measured for each analyte injection, and  $\mu_{ep,psp}$  being measured independently.



$$k = \frac{\frac{1}{t_o} - \frac{1}{t_r}}{\frac{1}{t_r} - \frac{1}{t_{pssp}}}$$

**Equation 23: Rearrangement of Equation 22**

$$k = \frac{\mu_o - \mu_a}{\mu_a - \mu_{epnet}} = \frac{\mu_o - \mu_a}{\mu_a - (\mu_o + \mu_{ep,pssp})}$$

**Equation 24: Determination of the retention factor from electrophoretic mobility**

## 2.5.2 Resolution, Efficiency, and Capacity

---

In chromatography, resolution ( $R_s$ ) is one of the most important parameters. Resolution describes how well two analyte zones are separated in chromatographic analysis. Resolution depends on efficiency ( $N$ ), selectivity ( $\alpha$ ), and the retention factor. Efficiency is a measure of analyte zone broadening with respect to the distance traveled. Selectivity is given by ratio of retention factors ( $\alpha = k_2/k_1$ ) where  $k_2$  and  $k_1$  are analyte two and analyte one. In EKC, because the PSP is mobile, the resolution equation is modified relative to conventional with a migration range term, which is dependent on the retention factor, which accounts for the mobility of the PSP. (Equation 25) [36]

$$R_s = \frac{\sqrt{N}}{4} \left( \frac{\alpha - 1}{\alpha} \right) \left( \frac{k_2}{k_2 + 1} \right) \left( \frac{1 - \frac{t_o}{t_{pssp}}}{1 + \left( \frac{t_o}{t_{pssp}} \right) k_1} \right)$$

**Equation 25: Master resolution equation for EKC**

In EKC, neutral analytes can only elute within the migration range of the PSP given by  $(t_{pssp}/t_o)$ . This is illustrated in

**Figure 9.** Unlike conventional chromatography where the stationary phase is bonded to the column and  $t_{pssp} \rightarrow \infty$ , EKC suffers from having an inherent limited migration range. The closer the net velocity of the PSP approaches 0 the bigger the migration window. In other words,  $(t_{pssp}/t_o)$  gets large.

The retention factor is also important. In conventional chromatography having a high retention factor always leads to better resolution, the only drawback being long analysis times. In EKC an optimum retention factor is given by  $k_{opt} = \sqrt{(t_{pssp}/t_o)}$ . [36] Bigger retention  $k$  factors lead to loss

of resolution as analytes that are too retained and begin to stack at  $t_{psp}$ . This is illustrated by the downward slope of the curves after  $k_{opt}$  has been achieved.

In summary, EKC requires a large migration range achieved by having a strong PSP  $\mu_{ep}$ , and the best resolution is obtained with an optimum retention factor for the analytes.

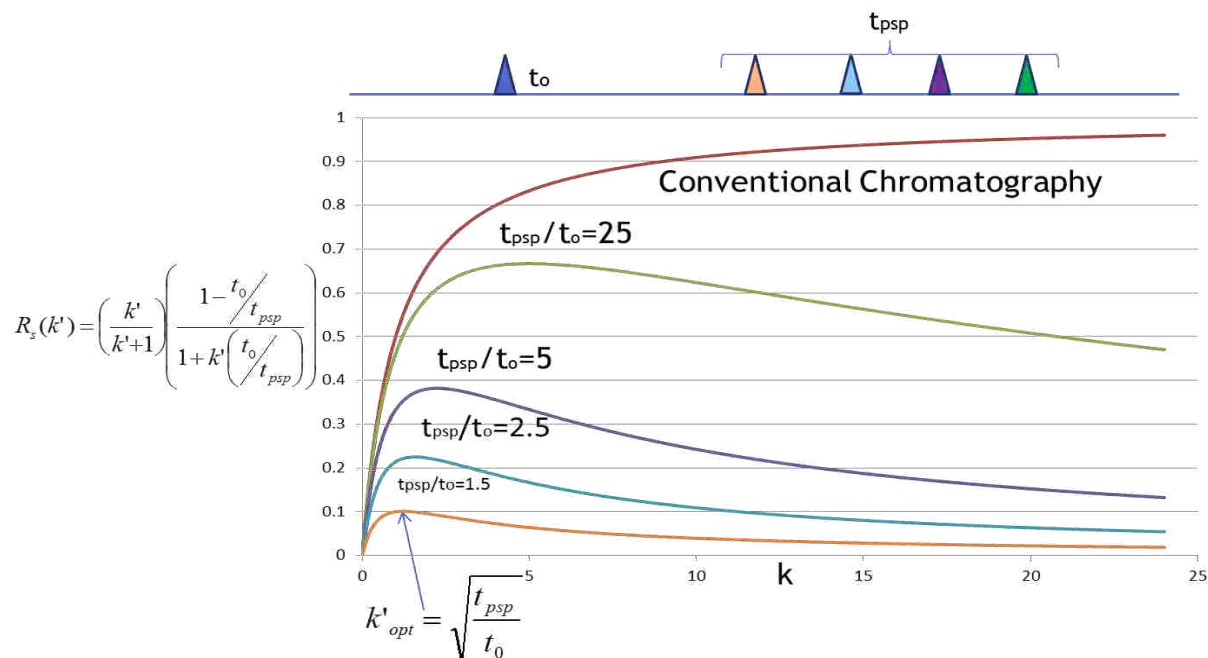


**Figure 9: Resolution as a function of the retention factor. The curves are color coded to the theoretical chromatogram (top), illustrating migration range's effect on resolution.**

The migration range in EKC also limits peak capacity. All analyte peaks elute between  $t_0$  and  $t_{psp}$ . Although the need to attain  $k_{opt}$  and a large migration range does cause some difficulties, it is easily overcome by the ease of switching the PSP thus changing selectivity. It is also common to achieve extremely high plate counts ( $N$ ) such as 200,000 and larger. The added efficiency mostly offsets migration range limitations. In liquid chromatography columns are extremely expensive and take time to switch and condition. In EKC a soluble PSP is added right to the buffer requiring only minutes to equilibrate. The drawback is that not very many PSPs have been characterized thus they do not enjoy widespread industry use.

## 2.6 Linear solvation energy relationships and methylene selectivity

This research utilizes LSER, methylene selectivity, and electrophoretic mobility to characterize the newly synthesized PSP. LSER provides solvation and retention information about the PSP

based on the free energy of solvation of the analytes in the PSP with respect to the bulk phase. Methylene selectivity provides information on retention behavior of the PSP for a homologous series of compounds with differing numbers of methylene units. In other words, information on how retentive the PSP is towards hydrophobic compounds is obtained. Electrophoretic mobility gives insight into the migration range of a PSP and has already been discussed in the previous section.

This research uses the solvation parameter model (SPM) originally suggested by Abraham [37] [38] as opposed to the solvatochromic model proposed by Kamlet-Taft. The advantage of the SPM is that it uses solute descriptors which are all free-energy related. The solute descriptors are characteristic to the analyte and can be obtained by calculation or experimental measurements. The solvation characteristics of a PSP can be defined as its capacity for various intermolecular interactions relative to the background electrolyte. The interactions are described by system constants which include dispersion, induction, cavity formation, permanent dipole, and hydrogen bonding [39]. The system constants describing a PSP solvation and retention properties reflect the difference in solute interactions in the bulk solution and the PSP [40].

The change in free-energy of analyte solvation assumes there are three steps [39]. First, a cavity, identical to the solute volume, is formed in the PSP. The free-energy required in this step is dependent on the forces holding the PSP together and the solute's size [40]. Second, the solute is transferred from the bulk solvent to the cavity and the molecules of the PSP rearrange in a way so that chemical interactions can take place. Finally, the rearranged molecules of the PSP participate in the aforementioned intermolecular interactions with the solute. The process of an analyte transferring into the PSP is defined by properties of both the analyte (solute descriptors) and the PSP (system constants). The product of each type of interaction and the sum of all products describing the system is proportional to the free-energy change of analyte solvation in the PSP relative to the background electrolyte. Equation 26 describes the solvation parameter model where the small letters are system constants ( $v$ ,  $e$ ,  $s$ ,  $a$ ,  $b$ ) and capital letters represent solute descriptors ( $V$ ,  $E$ ,  $S$ ,  $A$ ,  $B$ ).

$$\log SP = c + vV + eE + sS + aA + bB$$

**Equation 26: The solvation parameter model**

$SP$  is some free energy related property [40].  $k$  is directly related to free-energy and so  $SP$  can be substituted with  $k$  (

**Equation 27**). The system constants, describing PSP solvent characteristics, are obtained using multiple linear regression analysis based on measured retention factors for multiple solutes with known descriptors. The  $v$  constant is a measure of the relative ease of forming a cavity for the analyte;  $e$  describes the ability of the PSP to interact with analyte's  $\pi$ - and  $n$ -electron pairs;  $s$  represents the ability of the PSP to interact with the analyte through dipole-dipole and induced dipole processes;  $a$  describes how willing the PSP is to accept a basic interaction from the analyte or hydrogen bond basicity;  $b$  describes how willing the PSP is to participate in an acidic interaction with a basic analyte, or hydrogen bond acidity [40].

$$\log k' = c + vV + eE + sS + aA + bB$$

**Equation 27: The log of the partition coefficient is related to the selectivity of the PSP through the change in free-energy**

The solute descriptors are particular for each analyte.  $V$  is the McGowan characteristic volume or the volume an analyte takes up in solution;  $E$  is the excess molar refraction and describes the analyte's contribution to the change in free-energy from the polarizability of its  $\pi$ - and  $n$ -electron pairs;  $S$  describes the analyte's ability to engage in dipole-dipole and induced-dipole interactions;  $A$  and  $B$  are the analyte's hydrogen bond acidity and hydrogen bond basicity, respectively [39].

There are some general requirements which must be observed when characterizing a PSP with the help of a SPM. The model has to be statistically valid. This requires that a minimum of seven solutes be used [40]. However, with only seven solutes it is statistically impossible to remove any outliers in the analysis. To achieve an exhaustive model about 40 analytes should be analyzed. Furthermore, when selecting the analytes careful attention must be paid to their solute descriptors. If all the analytes chosen for LSER analysis have similar characteristics, it is possible that the model will cross correlate the descriptors giving erroneous system constants. Solute must be chosen so that they cover, as evenly as possible, the descriptor space to be explored [40].

Methylene selectivity is also an important parameter to consider when characterizing a PSP. It refers to the retention behavior of solutes of a homologous series of compounds with different numbers of methylene units [41]. A plot of the logarithm of the retention factor versus the

number of methylene groups in a homologue will yield a linear slope. The slope of the line is the natural logarithm of methylene selectivity and is a measure of the free energy of transfer of one methylene group from the background electrolyte to the PSP [41]. Methylene selectivity predominantly characterizes hydrophobic interactions of analyte with the PSP. A higher methylene selectivity value means that the PSP is able to better separate compounds which interact primarily through Van der Waals forces. Large methylene selectivities also mean that lower concentrations of PSP can be used to achieve good resolution of hydrophobic compounds. This is extremely important since the PSP is mobile and will flow through the detector cell just like the analytes. Less PSP means a better signal to noise ratio and lower current.

## **Chapter 3: Synthesis and characterization of RAFT agents and diblock copolymers**

---

### **3.1 Introduction**

---

This chapter reports on the synthesis techniques and analytical characterization of products. The synthetic route to the AB diblock copolymer nanoparticles was adopted from the work presented by Ferguson *et al.* [32]. The three step process includes the formation of a CTA, followed by the synthesis of a mCTA, and finally the synthesis of the nanoparticle.

The CTA was chosen to have a trithiocarbonate moiety. The Z group was chosen to be a thiol alkane in order to provide the CTA with a hydrophobic character and good C-S double bond activation. The hydrophobic character of the Z group is important to maintain chain character consistency since the third step of the synthesis is an insertion of a hydrophobic block.

mCTA was formulated from the previously described CTA and AMPS. The AMPS acidic monomer is added first because reaction conditions are maintained in aqueous solution throughout all steps of the synthesis. The mCTA is water soluble which makes it ideal for use in the diblock polymerization step.

The final step is the formation of AB diblock nanoparticles. Butyl acrylate was chosen as the hydrophobic block based on the compatibility chart and previous research (Table 2) [11].

The products were characterized by various analytical techniques including HPLC, NMR, ESI-MS, and DLS.

## 3.2 Materials

---

The following materials were used: distilled deionized water (Millipore Milli-Q purification), Sodium Hydroxide (EMD Chemicals), 1-butanethiol (Aldrich, 99%), Acetone (Fisher, HPLC grade), Carbon Disulfide (Aldrich, 99%), 2-bromopropionic acid (Aldrich, 99%), Hexane (Fisher, HPLC grade), Hydrochloric acid (EMD Chemicals), 4, 4'-Azobis (4-Cyanovaleric Acid) (Aldrich, >98%), 2-Acrylamido-2-methylpropane sulfonic acid (Aldrich, 99%), Butyl Acrylate (Aldrich, 99%), Dialysis Tubing (Spectrum Labs).

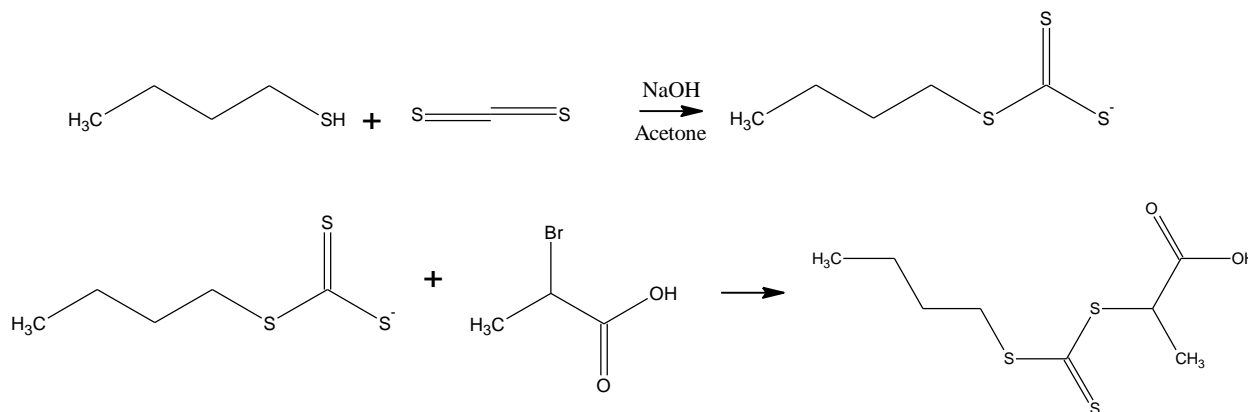
## 3.3 Experimental Procedure

---

### 3.3.1 Synthesis of CTA agent

---

The synthetic pathway is illustrated in Scheme 7. 1-butanethiol is deprotonated with the addition of sodium hydroxide. In the presence of acetone, carbon disulfide will dissolve in solution and react to form an intermediate butyl carbonotrithioate. Addition of 2-bromopropionic acid yields the CTA after clean up and recrystallization.



**Scheme 7: Synthetic route to producing 2-[[[(butylsulfanyl)carbothioyl]sulfanyl]propanoic acid**

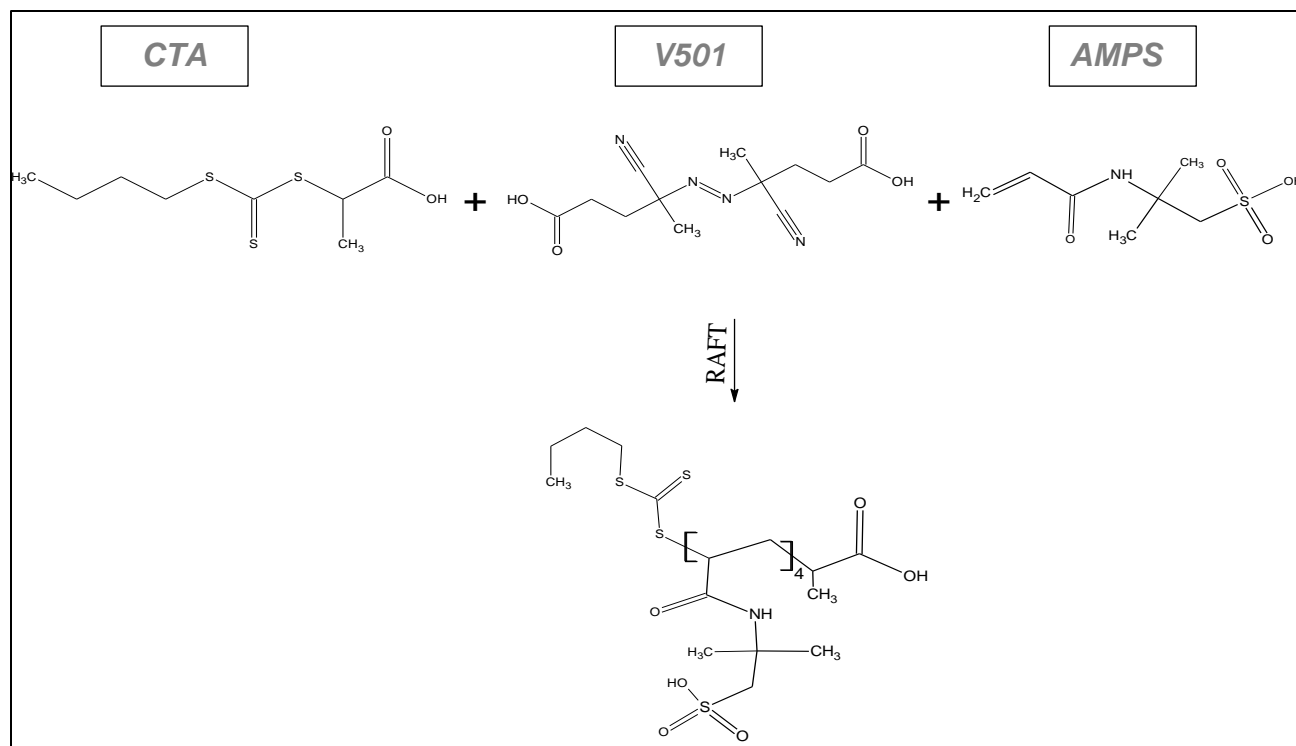
The specific procedure of Scheme 7 is as follows: To 6.0 ml of water 3.2 g (40 mmol) of 50% NaOH solution and 3.6 g (40 mmol) of 1-butanethiol were added. To this solution, 2 ml of Acetone were added. The solution, a clear colorless liquid, was stirred for 0.5 h. The solution was then treated with carbon disulfide (2.7 ml, 45 mmol) and let stir for another 0.5 h. The clear orange solution was then cooled below 10<sup>0</sup>C and 3.7 ml (41 mmol) of 2-bromopropionic acid were added slowly, drop wise, keeping the exothermic reaction under 30<sup>0</sup>C. This was followed

by another addition of NaOH (3.3 g, 41 mmol) maintaining the  $<30^{\circ}\text{C}$  requirement. The reaction was kept in the ice bath until the evolution of heat had ceased. 6 ml of water were added to the solution and which was then brought to room temperature and was left to stir for 24 h. The solution was diluted with 10 ml of  $\text{H}_2\text{O}$  and brought below  $10^{\circ}\text{C}$  utilizing an ice bath. 6 ml of 12M HCL were added drop wise, while stirring, keeping the solution temperature under  $10^{\circ}\text{C}$ . Yellow oil separated from the solution and was extracted with two 10 ml fractions of hexane. The combined hexane fractions were dried using a rotary evaporator (rotovap). The oily substance was then taken to a vacuum oven and further dried under full vacuum at  $30^{\circ}$  for 24 h. The resulting solid was then dissolved in a minimal amount of boiling hexane and placed in a freezer for recrystallization. The recrystallized solid was filtered and washed with cold hexane. The final product was dried in a vacuum oven under full vacuum at  $30^{\circ}$  for 2 h giving an 83.6% yield of CTA. The CTA was labeled CTA01.

### 3.3.2 Synthesis of macro CTA

---

The synthesis of the mCTA employs the previously discussed RAFT method. Utilizing the V501 initiator, previously synthesized CTA, and the AMPS monomer, under aqueous conditions, a mCTA is synthesized. Equation 3 was used to determine the necessary amounts of the CTA for a certain amount of monomer at 100% conversion and a 4 monomer unit AMPS chain length. As mentioned before, the v501 concentration was 1/10 that of the CTA. This is a relatively simple procedure due to the ruggedness of the RAFT process. However, stringent conditions of maintaining an inert atmosphere during the reaction have to be observed. At the end of the reaction a small sample was taken for NMR analysis. The rest of the solution was dialyzed. The use of NaOH to neutralize the acidic character of AMPS as described by Ferguson *et al.* gave unfavorable results in our synthetic attempts. Omission of the neutralization step resulted in a favorable formation of the mCTA with excellent yields. Experimentally it is difficult to achieve a 100% monomer conversion to polymer. For the mCTA to be a viable reagent in the synthesis of the nanoparticle, all AMPS monomer not polymerized must be removed as it can participate in the next reaction randomizing the hydrophobic block. Scheme 8 visually describes the formation of the mCTA.



**Scheme 8: Synthetic pathway to the mCTA through the RAFT process.**

The specific procedure of Scheme 8 is as follows: 4 ml of H<sub>2</sub>O, a magnetic stir bar, 2.0 g of AMPS monomer, 0.575 g of CTA01, and 67.62 mg of V501 initiator were added to a round bottom flask. The flask was capped tightly with a septum, stirred to dissolve all starting materials, and degassed with N<sub>2</sub> for 45 min. After the degassing stage, positive N<sub>2</sub> atmosphere was maintained throughout the reaction. The flask was then submerged into a 60<sup>o</sup>C oil bath and let stir for 12 h. The resulting yellow solution was dialyzed using Spectra/Por dialysis membrane with a 1000 molecular weight cut off (MWCO). The sealed membrane was submerged into 3L of H<sub>2</sub>O and left alone for 24 h. The solution volume was significantly reduced with the aid of a rotovap and the resulting oily solution was transferred to a scintillation vial and frozen. The frozen sample was dried in a freeze drying system forming bright yellow crystals. The yield of the mCTA was found to be 66%. The compound was labeled JSH32A.

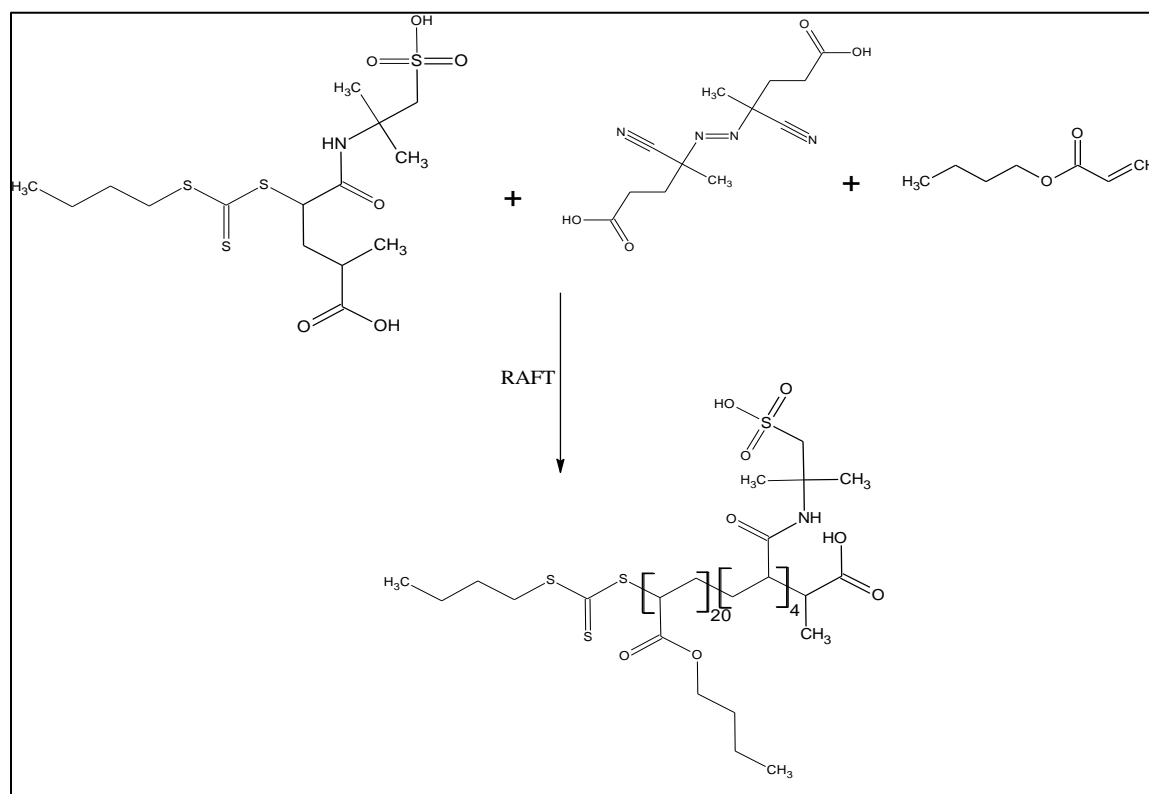
### 3.3.3 Synthesis of diblock copolymers

Because the mCTA is analogous in function to the CTA, the process for making diblock copolymer nanoparticles is somewhat similar to the synthesis of the CTA. Again, careful attention must be paid to the reaction proceeding under inert atmospheric conditions. Utilizing



the mCTA, V501 initiator, and butyl acrylate monomer, an AB diblock copolymer nanoparticle is formed. (Scheme 9)

Equation 3 was used to determine the necessary amounts of the mCTA for a certain amount of monomer at 100% conversion and a 20 unit butyl acrylate monomer chain length. As mentioned in Chapter 2, the acidic groups of the mCTA must be deprotonated for micellization to occur. Sodium hydroxide was added to the reaction mixture. Also, maintaining small monomer droplets was accomplished with a timed addition of the butyl acrylate monomer. At the end of the reaction a small sample is taken for NMR analysis. The rest of the solution is dialyzed to remove most of the sodium hydroxide as it will produce unfavorable current in EKC. Although only negligible concentrations of unpolymerized monomer remain during this step, dialysis does remove any free butyl acrylate monomers.



**Scheme 9: Synthetic pathway to the AB diblock nanoparticle through the RAFT process.**

The specific procedure for Scheme 9 is as follows: 0.825 g of JSH32A mCTA was added to a round bottom flask containing 6.6 ml of H<sub>2</sub>O. The flask was sonicated until all of the mCTA was dissolved. The solution was titrated with NaOH, utilizing an electronic pH meter, until a pH of 6.5 was achieved. 21.68 mg of V501 initiator and a stir bar were added to the flask and

contents sealed with a septum. Using a gas/vacuum manifold, the air inside the flask was exchanged with nitrogen. Nitrogen was then bubbled through the liquid for 45 min. The reaction was then initiated by submerging the flask into a 70°C oil bath, keeping a positive N<sub>2</sub> atmosphere. 2.2 ml of butyl acrylate monomer were added in the following way: with the addition of heat an initial shot of 0.1 ml was added to the reaction mixture. The rest of the butyl acrylate was delivered with a syringe pump at a rate of 1.5 ml/hr. The reaction was left to stir for 24 h. The resulting solution was dialyzed using a dialysis membrane with a MWCO of 2000 in 3L of H<sub>2</sub>O for 24 h. The dialyzed solution was transferred to a scintillation vial, frozen, and dried in a freeze dry system. The compound was labeled AU19B. The second nanoparticle, AU31A, was made following the same procedure, doubling all the reagents and solvents.

### 3.4 Characterization

---

The following subsection gives analytical results using various instruments to show proof of synthesis.

#### 3.4.1 CTA

---

The synthesis of CTA CTA01 was characterized by HPLC with a UV-Vis diode array detector (DAD). HPLC was found to be the best method for performing purity and functionality analysis due to thermal degradation of the CTA on a gas chromatographic system. Purity and structure were then confirmed by <sup>1</sup>H NMR.

##### 3.4.1.1 LC analysis

---

CTA01 was analyzed on an Agilent 1260 HPLC system utilizing an Agilent ZORBAX Eclipse Plus C18 4.4x100mm 3.5-Micron column (P.N. 959961-902). The advantage of performing a separation in addition to collecting absorbance (ABS) is that approximate purity of the sample can be calculated. The ratio of the peak area of the compound of interest to the total peak areas gives an estimate of percent purity. Figure 10 A shows a separation, under the outlined conditions, of CTA01. The broad peak eluting before the first minute was also found in the blank and is thought to be an impurity in the system or the solvent. Because the peak was also recorded in the blank sample it was not used for calculating total peak areas. The separation utilized a 210nm wavelength for detection and purity of CTA01 was determined to be 86.27%.

The use of a DAD enables spectra extraction of individual peaks. Shen and group have reported on the absorbance of trithiocarbonates. [26] The reported maximum absorbance is 306 and 308 nm. The peaks at 1.695 and 5.117 showed zero absorbance at those wavelengths. Figure 10 B shows the extracted absorbance spectra of the major peak at 2.750. The inserted spectrum was reported by Shen and group. The absorbance of CTA01 matches the literature providing proof of the synthesis of a compound with a trithiocarbonate moiety.

A purity of ~86% from absorbance at 210 nm was determined to be acceptable to move forward with mCTA synthesis (although it should be recognized that this is only an estimate of purity). Because the two detected impurities do not contain CTA functionality, they are not likely to participate in the next reaction. As mentioned before, the next step of the synthesis requires dialysis with a 1000 MWCO membrane. Any unreactive impurities left over from the original CTA synthesis will be removed in that step.

Although the HPLC analysis provides information on functionality and purity, it does not contain information of structure. The CTA structure was confirmed by <sup>1</sup>H NMR.

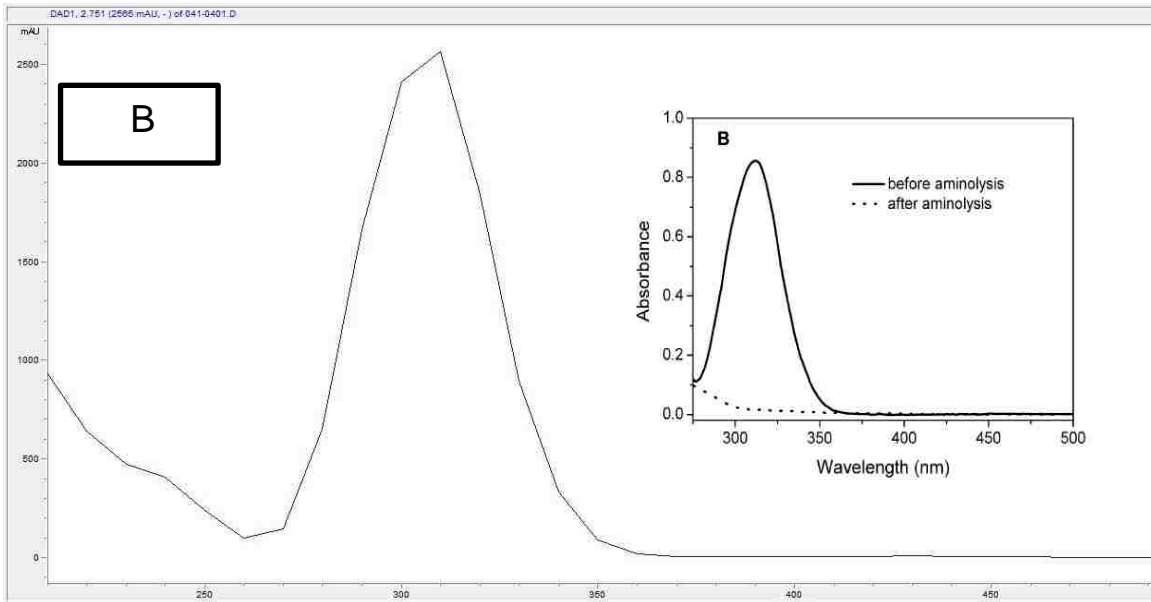
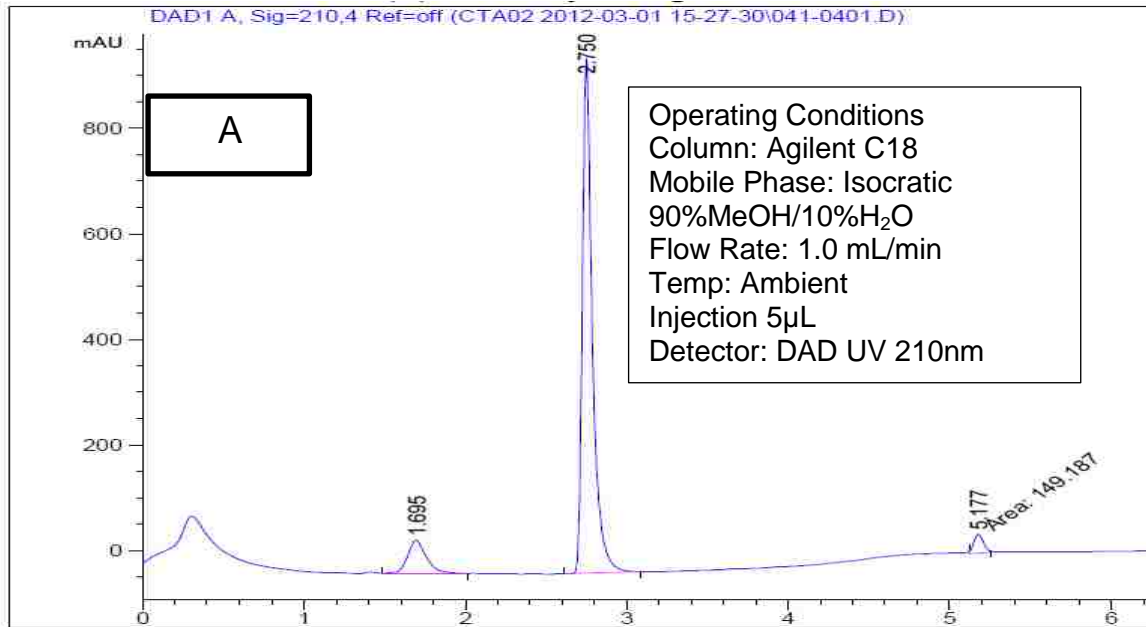


Figure 10: A) An HPLC chromatogram at 210nm of CTA01 of time vs. ABS. B) Extracted spectra of the main peak at 2.75 min. compared to the ABS spectra reported by Shen and group.

### 3.4.1.2 NMR analysis

NMR analysis of the CTA CTA01 was performed using a Varian 500 NMR. The NMR spectrum shown in Figure 11 confirms the synthesis of the CTA. As noted in the HPLC analysis some minor impurities are present.

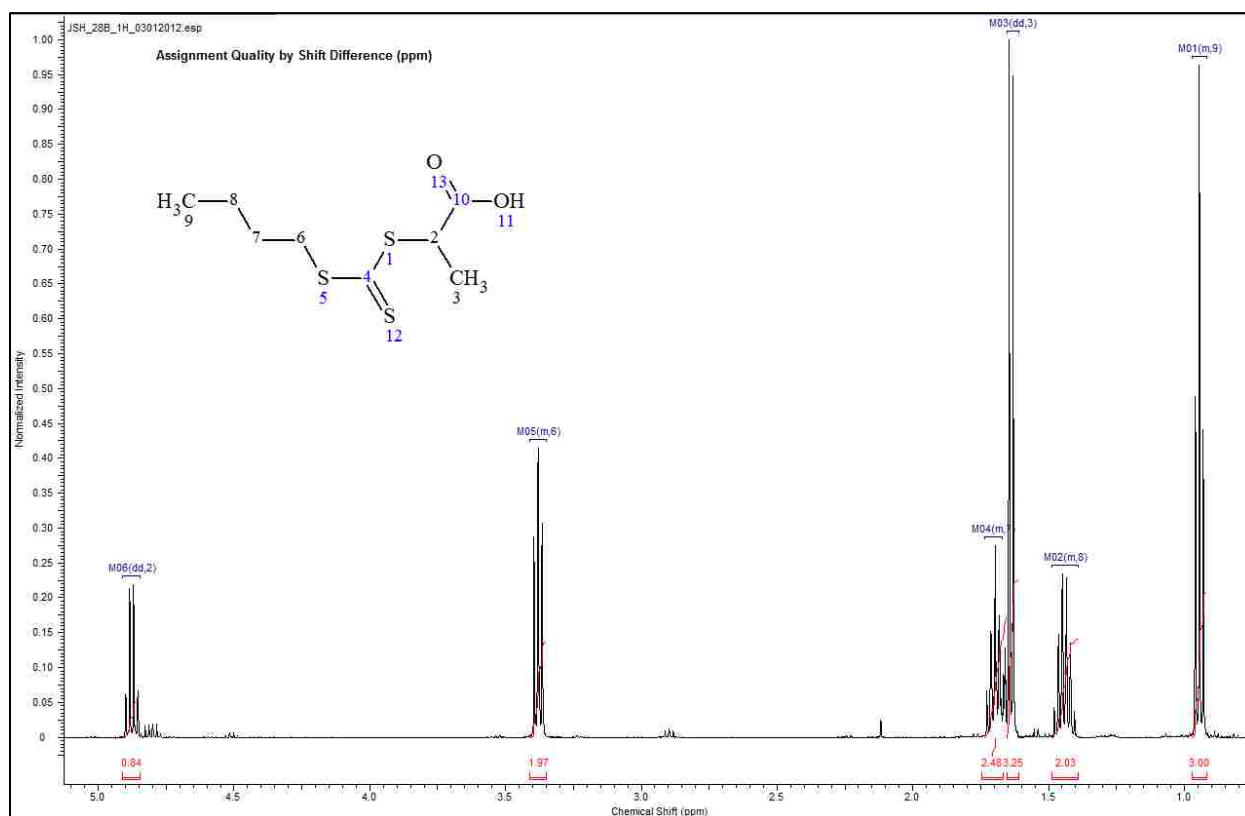


Figure 11: <sup>1</sup>H NMR spectra and peak assignments for the synthesized CTA in d-chloroform. Each multiplet (labeled at the top) is assigned to the structure at the top left of the figure. For example: M01(m,9) is assigned to the hydrogens of carbon 9.

### 3.4.2 Macro-CTA

The synthesis of the mCTA labeled JSH32A was characterized by ESI-MS. While electrospray MS does not give quantitative molecular weight distributions (as distinct from giving the precise molecular weight of each observed species), it is certainly semi-quantitative, for example, in its indications of the relative abundances of tetramers, pentamers, and hexamers of the same species. [32] PDI values and the number of AMPS units polymerized can be obtained from this analysis. NMR was also employed to determine conversion. The NMR spectrum also gives qualitative information on whether polymerization has occurred.

### 3.4.2.1 ESI-MS analysis

ESI-MS analysis was performed by directly injecting a solution of 0.5mg/ml mCTA in 50% $\text{H}_2\text{O}$ /50%MeOH. A very respectable PDI of 1.03 was achieved. The major polymer was determined to be a tetramer of 4 AMPS units. The theoretical MW of a 4 AMPS units CTA polymer, with a negative charge of 1, is 1066.38. The experimental value is 1064.87. Because all of the masses are off by 2 units, the discrepancy is most likely due to instrument calibration. The MW of the AMPS monomer is 207 and

**Figure 12** shows that each chain contains one AMPS unit difference. A strong case can be made that polymerization has occurred.  $^1\text{H}$  NMR further proves polymerization with results presented in the next section.

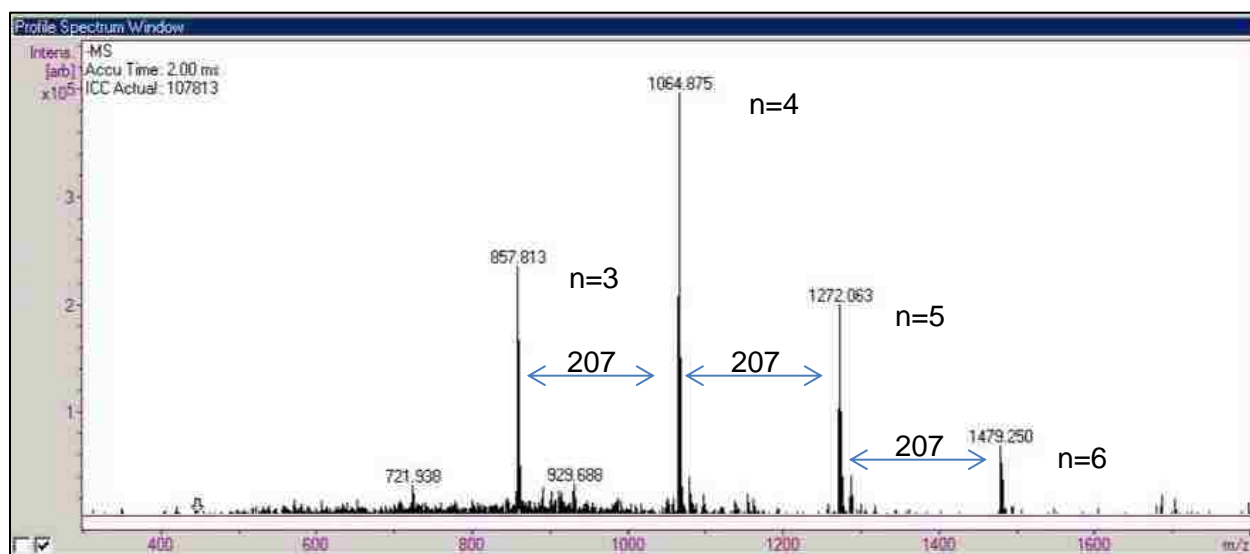


**Figure 12:** Mass spectrum of poly(*n*-AMPS) macro-CTA where the AMPS component has a MW of ~207 and *n*=number of AMPS/chain. The chromatogram shows a distribution of a RAFT polymerization product with a polydispersity index of 1.03. The major component is the highest intensity peak showing 4-AMPS/chain.

### 3.4.2.2 NMR analysis

NMR analysis of the mCTA JSH32A confirms the polymerization and structure of the molecule. Figure 13 is an NMR spectrum of poly(AMPS) as presented by Sumerlin and group. The broad peaks indicate good polymerization of the AMPS. The  $M_w$  reported by Sumerlin was 38,600. This would give close to 186 polymerized AMPS units. The Z and R group signals are suppressed and are not seen in the NMR spectra due to relatively high levels of the polymerized AMPS.

Figure 14 shows the  $^1\text{H}$  NMR spectra of JSH32A. JSH32A is mainly composed of 4 AMPS units as determined by ESI-MS. Because of the relatively small amounts of polymerized AMPS the original CTA protons are not masked. The proton signals from the Z group are clearly seen in the 0.5-1ppm region. The R group proton signals seem to be masked just as in Sumerlin's spectra.

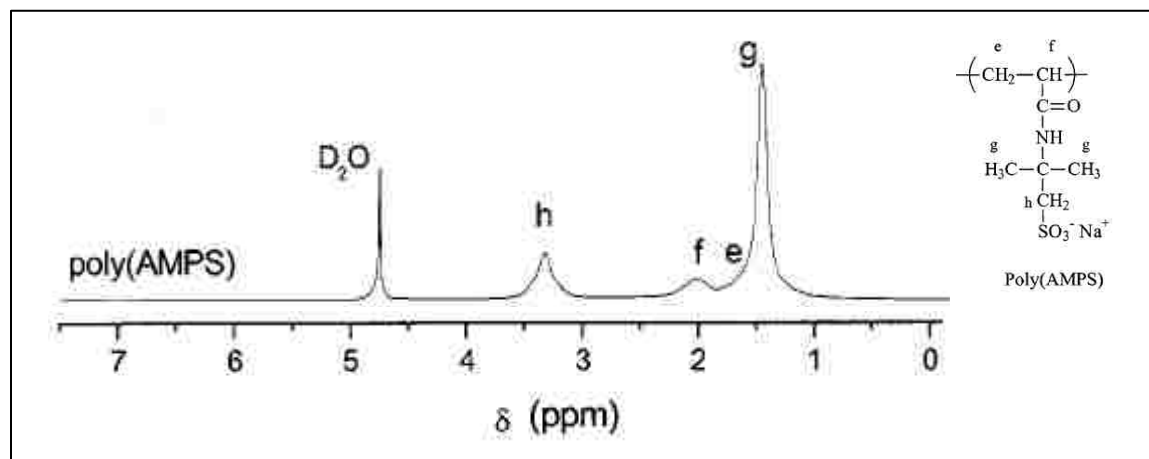


Figure 13:  $^1\text{H}$  NMR spectra reported by Sumerlin and group. [42] "Reprinted with permission from {B. Sumerlin, M. Donovan, Y. Mitsukami, A. Lowe and C. McCormick, "Water-Soluble Polymers. 84. Controlled Polymerization in Aqueous Media of Anionic Acrylamido Monomers via RAFT," *Macromolecules*, vol. 34, pp. 6561-6564, 2001.}. Copyright {2013} American Chemical Society."

Broad peaks (h,f,e,g) show good polymerization of the AMPS monomer. Furthermore, no vinyl groups are seen in the 5.25-6.25 ppm region. This is a clear indicator that polymerization has gone to 100%.

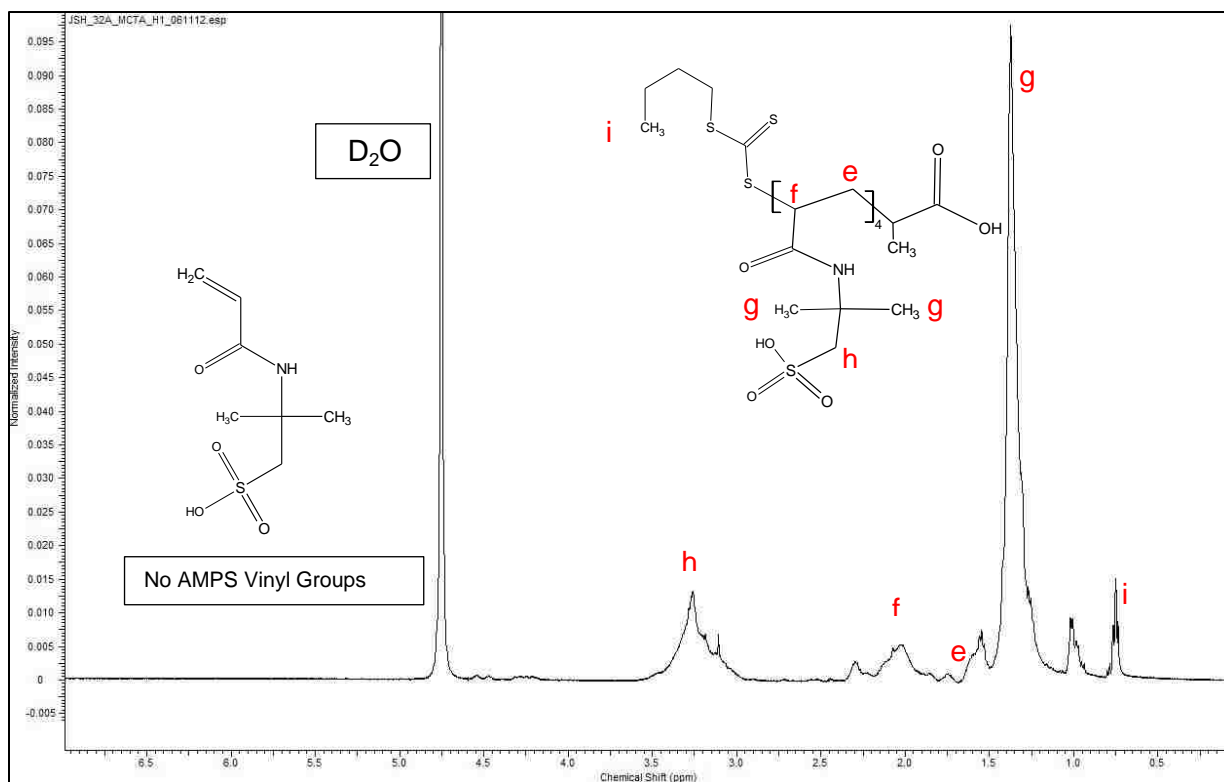


Figure 14:  $^1\text{H}$  NMR spectra of mCTA JSH32A in  $\text{D}_2\text{O}$ . Polymerization can be observed by the broad peak shapes of the monomer's hydrogen signals. The AMPS monomer structure is presented to illustrate the vinyl groups present on a free monomer. No vinyl groups are seen in the spectra.

### 3.4.3 Diblock copolymer nanoparticles

Addition of the hydrophobic block to the mCTA was characterized by  $^1\text{H}$  NMR and DLS. Nanoparticles AU19B and AU31A, synthesized with JSH32A, were characterized. NMR analysis showed good polymerization of the butyl acrylate monomer and retention of the AMPS block. DLS analysis performed on a Malvern Zetasizer instrument provided nanoparticles size which is reported as the Z-average in nanometers.



### 3.4.3.1 NMR analysis

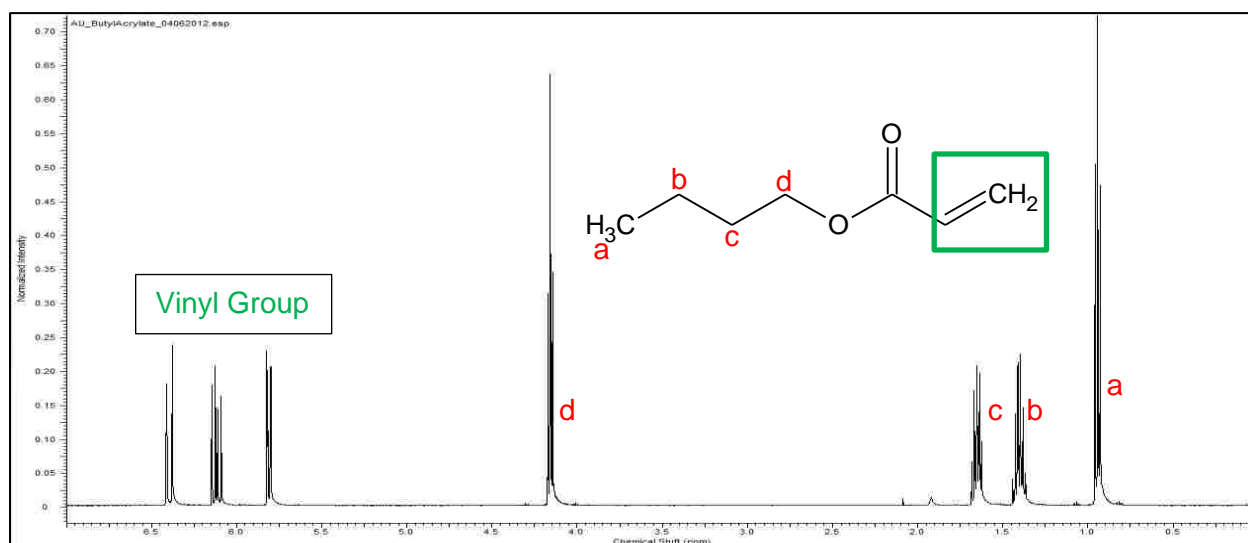


Figure 15:  $^1\text{H}$  NMR spectra of butyl acrylate in  $d\text{-chloroform}$ .

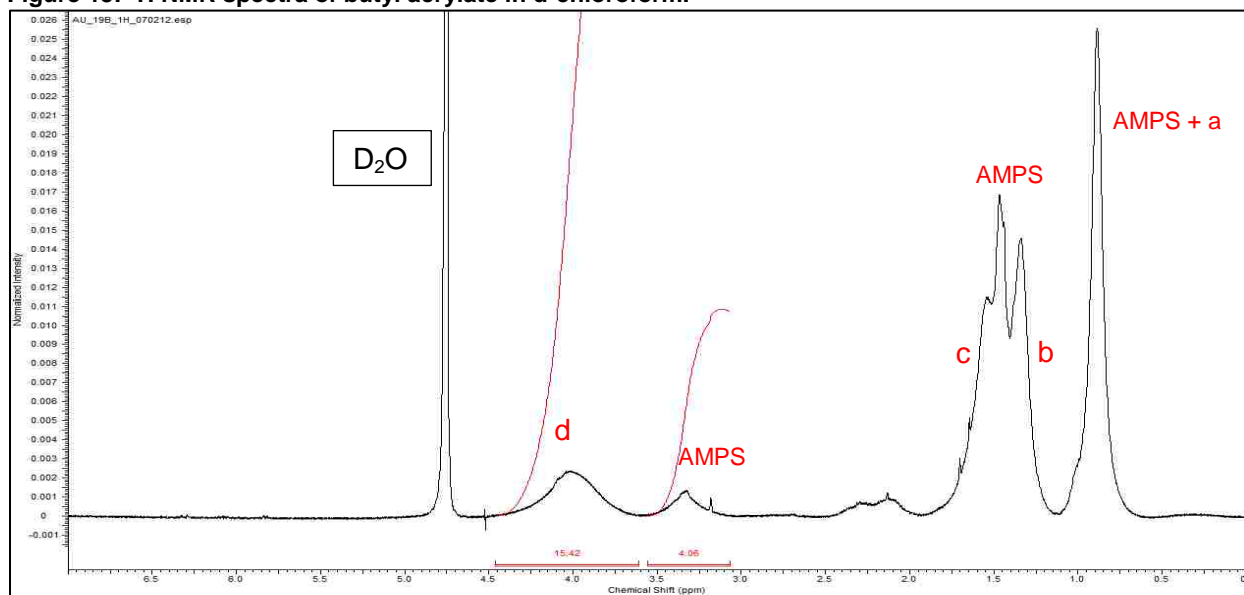


Figure 16:  $^1\text{H}$  NMR spectra of AU19B in  $\text{D}_2\text{O}$  after polymerization with butyl acrylate.

Figure 15 gives an NMR spectrum of a butyl acrylate monomer. The vinyl groups are easily identified in the 5.5-6.5 ppm range. As the polymerization continues the vinyl proton signal disappears indicating polymerization has occurred. Figure 16 shows good polymerization of the hydrophobic block and the retention of the AMPS block. The sharp peaks of the butyl acrylate turn broad after polymerization. The broad AMPS peaks are still present.

The broad peaks and the nature of the nanoparticle, being relatively rigid, make quantitative analysis impossible using NMR. However, integrating the two peaks does give an approximate

estimation of the ratio of the two blocks. From ESI-MS analysis, it was determined that the majority of the chains were a 4 AMPS unit polymer. Setting the AMPS peak to 4 and integrating the d peak on the butyl acrylate gives a ratio of about 4:15 indicating that the average chain contains a 15 unit hydrophobic block.

Figure 17 shows an NMR spectrum of AU31A diblock nanoparticle. As with AU19B good polymerization of the hydrophobic block is confirmed. Retention of the AMPS block is also confirmed.

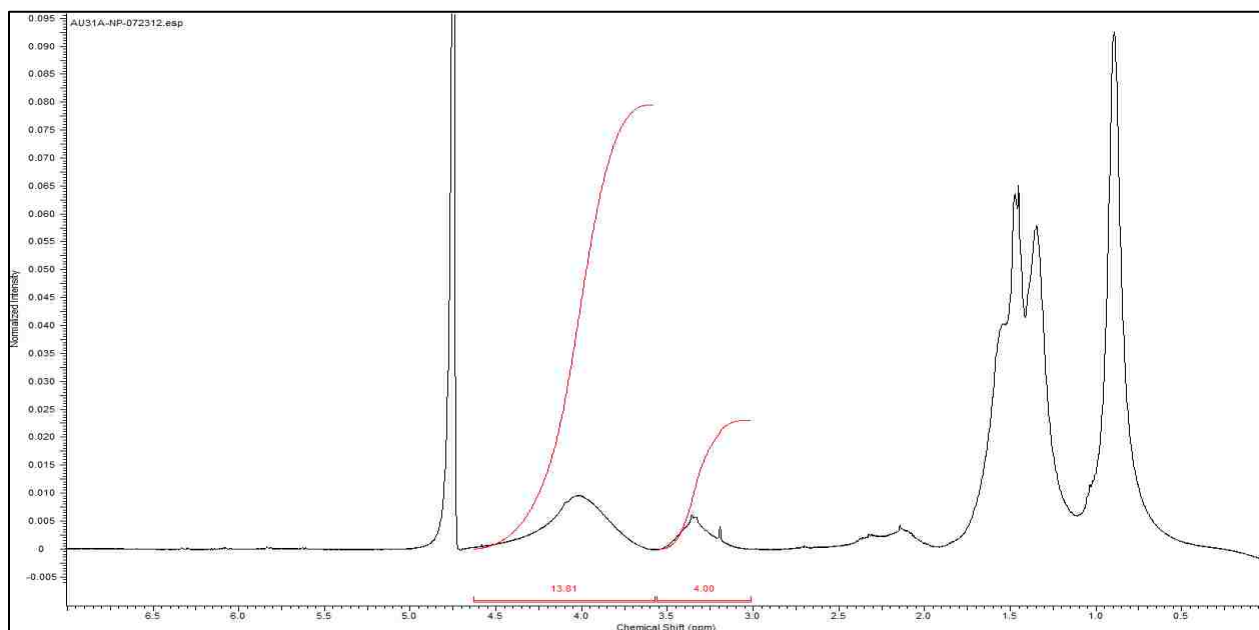


Figure 17: <sup>1</sup>H NMR spectra of AU31A in D<sub>2</sub>O after polymerization with butyl acrylate.

### 3.4.3.2 DLS analysis

DLS analysis was performed to determine the size of the synthesized nanoparticles. DLS analysis results of AU19B and AU31A are shown in Figure 18 and Figure 19. The Z-average, size distribution by volume, and polydispersity index are given in

Table 3. The Z-average size is the intensity weighted harmonic mean size. This means that the Z-average is calculated based on the weighted intensity of the sample. Because larger molecules have more light scattering it is also useful to look at the size distribution by volume ( $D_v$ ). This means that the  $D_v$  is calculated based on the volume weighted distribution.

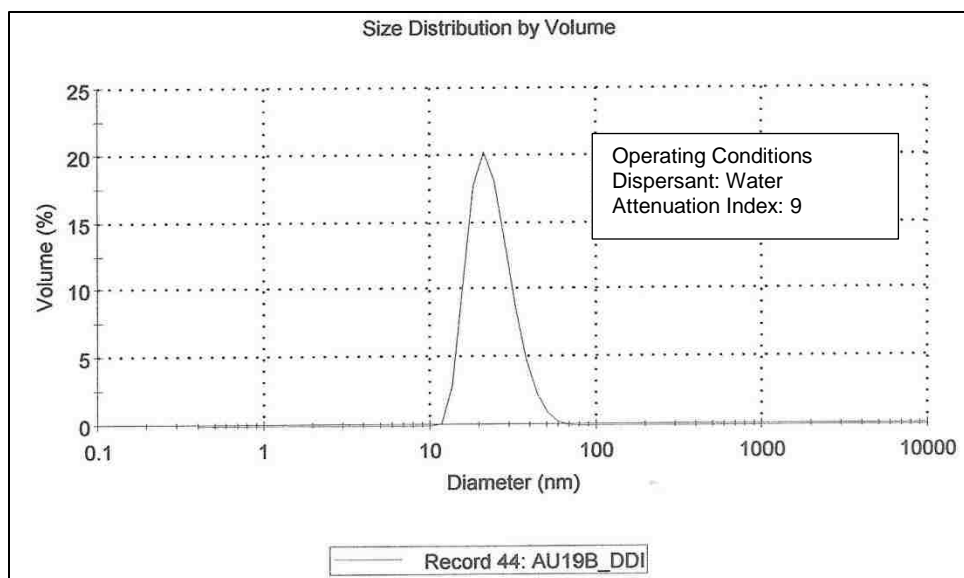


Figure 18: DLS analysis of AU19B showing a lognormal size distribution by volume.

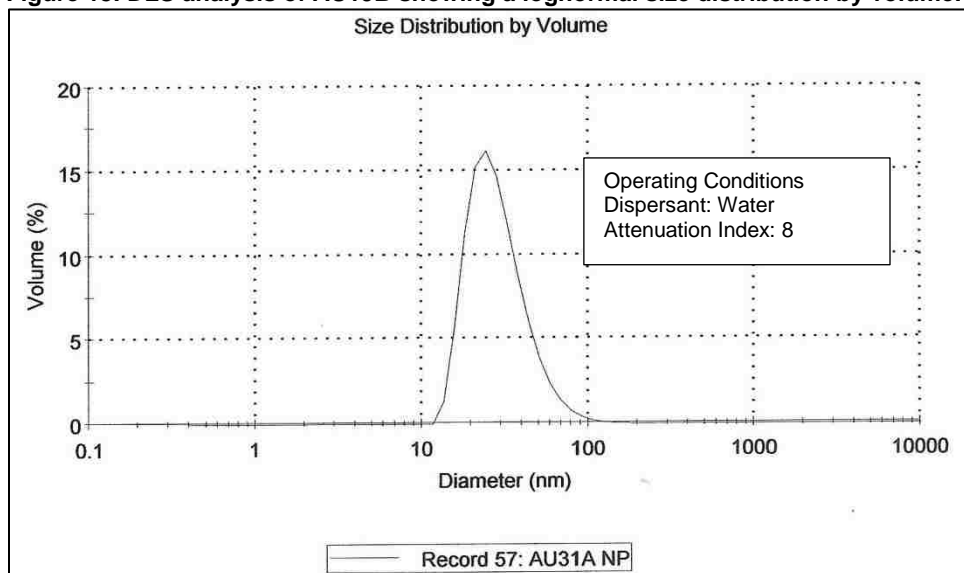


Figure 19: DLS analysis of AU31A showing a lognormal size distribution by volume.

Nanoparticle	Z-average(nm)	Diameter by volume(nm)	Polydispersity Index*
AU19B	28.41	24.1	0.088
AU31A	48.93	29.93	0.345

Table 3: Results of DLS Analysis. The polydispersity index (PDI\*) calculated from DLS is different than the PDI discussed earlier. While PDI is based on weight distribution, PDI\* is obtained from DLS as a time dependent intensity distribution. A PDI\* of <0.1 is considered very monodisperse. A PDI\* <0.4 is fairly monodisperse while a PDI\* of >0.7 is considered very polydisperse

## Chapter 4: Performance characterization of nanoparticles in electrokinetic chromatography

---

### 4.1 Introduction

---

Chapter 4 presents data obtained from the experiments performed. The discussion of the data obtained is presented in Chapter 5.

The PSP performance was characterized by a separation of different analytes on a Hewlett-Packard 3D CE. The electrophoretic mobility of AU19B and AU31A was determined by separating a mixture of alkyl-phenone derivatives in a homologous series. The separation was also performed at three different pHs to show how electrophoretic mobility changes with pH and the effect on the migration range. The two synthesized PSPs were determined to be of different sizes. The effect of size on the electrophoretic mobility was explored. LSER analysis using 39 different analytes was performed to determine PSP retention and selectivity. Finally, a separation of a mixture, containing 22 different analytes, was performed to show the utility of the PSP.

### 4.2 Experimental Details

---

Fused silica capillaries for all experiments were obtained from Polymicro Technologies (Phoenix, AZ) and had an internal diameter of 50  $\mu\text{m}$  and an external diameter of 364  $\mu\text{m}$ . Detection windows of 2mm were made in the capillaries by removing the polyimide coating with the help of a window maker. All capillaries were rinsed in the beginning of the day with 0.1 M sodium hydroxide for 90 min. The capillary was then flushed with nano-pure water for 10 min followed by a flush with the electrolyte/PSP solution for another 10 min. Capillaries were rinsed between injections with the electrolyte/PSP solution. New capillaries were utilized for each new PSP being studied.

All buffers and solutions were prepared in 18 M $\Omega$  distilled deionized water. All buffer solutions were filtered through 0.45 $\mu\text{m}$  filters before use. All buffers were made to 10 millimolar concentrations. The utilized buffers vary for different analyses and are listed in the analytical conditions windows on the chromatograms.

### 4.3 Separations of alkyl-phenone derivatives at pH 9.2

A homologous series of alkyl-phenones was used to initially characterize PSP electrophoretic mobility and performance. Stock solutions, depending on the phenone, were prepared between 300 and 700 ppm in acetone. Sample solutions for EKC analysis were prepared by diluting the stock solutions in run buffer to a final concentration of 3 to 7 ppm (see Figure 20 for exact concentrations). Phenone mixtures were injected using a pressure of 40 mBar for 2 seconds. Additional experimental details for each phenone separation are provided with the figures.

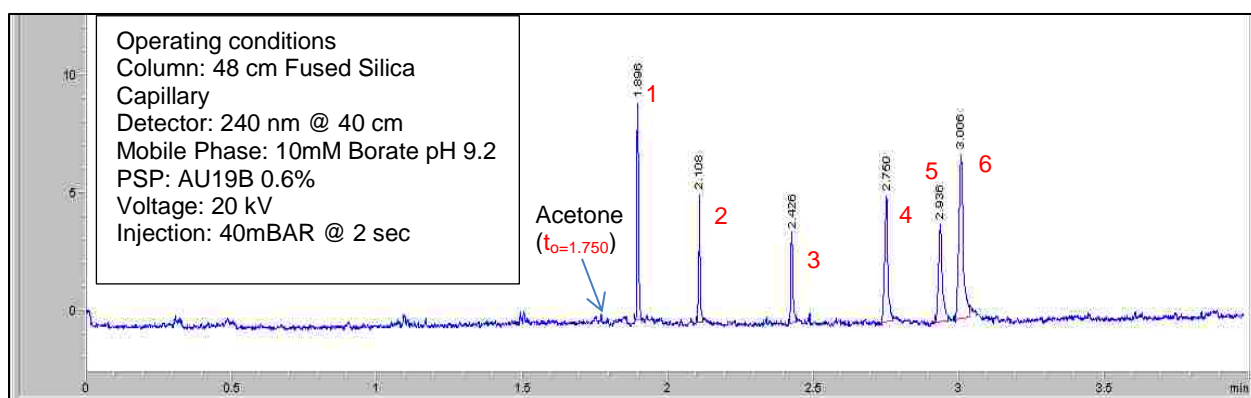


**Figure 20: Separation of acetone (0.2%) and alkyl-phenyl ketones: 1. Acetophenone (3.72ppm), 2. Propiophenone (3.18ppm); 3. Butyrophenone(3.14ppm); 4. Valerophenone(3.31ppm); 5. Hexanophenone(3.32ppm); 6. Heptaphenone(6.30ppm). The separation was performed using a 10mM borate buffer (pH 9.2) and 0.6% AU19B PSP.**

AU19B was used to separate a mixture of alkyl-phenone derivatives and the chromatogram is presented in Figure 20. Acetone was difficult to see at 240 nm. The retention time of the acetone was confirmed by monitoring a 210nm wavelength in addition to the 240 nm wavelength. Due to low concentrations of phenones it was advantageous to monitor at their maximum absorbance of 240 nm. [43]

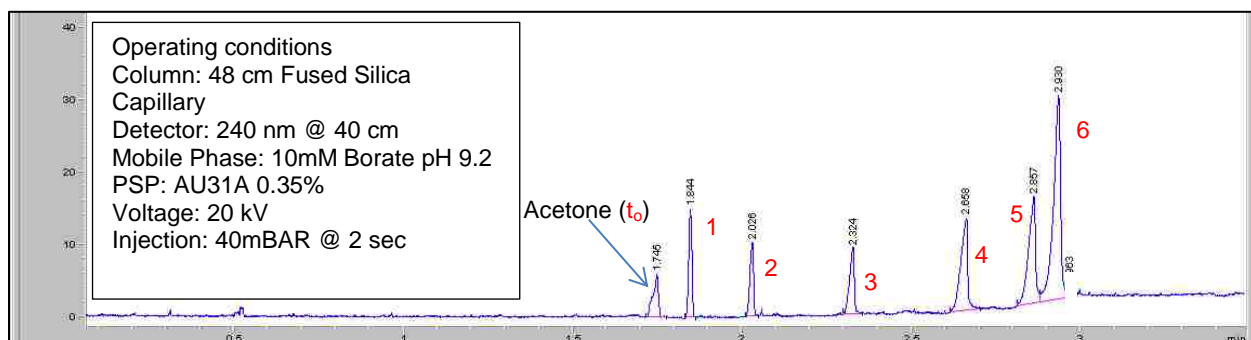


**Figure 21: Separation of acetone (0.2%) and alkyl-phenyl ketones: peaks as labeled in Figure 20..72ppm), 2. Propiophenone (9.18ppm); 3. Butyrophenone(9.14ppm); 4. Valerophenone(9.31ppm); 5. Hexanophenone(9.32ppm); 6. Heptaphenone(18.30ppm). The separation was performed using a 10mM borate buffer (pH 9.2) and 0.35% AU31A PSP.**

AU31A was also used to separate a mixture of alkyl-phenone derivatives. Figure 21 shows the resulting chromatogram.

#### 4.4 Electrophoretic mobility, pH dependence, Size dependence, Migration Range, Methylene Selectivity

---

Electrophoretic mobility is determined by rearranging Equation 12: Electrophoretic velocity of a PSP and substituting electrophoretic mobility for velocity, giving Equation 28. The  $t_{psp}$  was determined using the procedure of Bushey and Jorgenson [44]. Because the separated mixture is a homologous series, the lognormal retention factor for the alkyl phenones should correlate linearly with the number of methylenes. Excel Solver is used to determine a  $t_{psp}$  value that gives a maximum in the correlation coefficient (approaching 1) for a plot of analog phenone  $\log k$  vs methylene number.

$$\mu_{ep} = \mu_o - \mu_{epnet} = \left(\frac{L}{t_o}\right)\left(\frac{L_t}{V}\right) - \left(\frac{L}{t_{psp}}\right)\left(\frac{L_t}{V}\right)$$

**Equation 28: Experimental determination of electrophoretic mobility.**

PSP	$\mu_{ep}$ $10^{-4}(cm^2/V*s)$	Migration Range ( $t_{psp}/t_o$ )	Methylene Selectivity
AU19B (Z-ave = 28.41nm)	-3.893±0.003	1.74	3.048±0.003
AU31A (Z-ave = 48.93nm)	-3.773±0.004	1.70	3.276±0.003

**Table 4: Electrophoretic properties of AU19B and AU31A in 10mM borate buffer (pH 9.2).**

Table 4 summarizes electrophoretic mobility, migration range, and methylene selectivity of the two synthesized PSPs. The electrophoretic properties are compared at a constant pH of 9.2 in 10mM borate buffer. Chapter 5 gives a detailed discussion of these results.

The effect of lowering the pH of the mobile phase, on electrophoretic mobility and migration range, was investigated using AU19B PSP and the six alkyl-phenone derivatives. The representative chromatograms of separations at pH 7.55 in a 10 mM TRIS buffer and at pH 5.45 in a 10 mM phosphate buffer are presented in Figure 22 and Figure 23, respectively. Results are presented in Table 5 and are discussed in detail in Chapter 5.

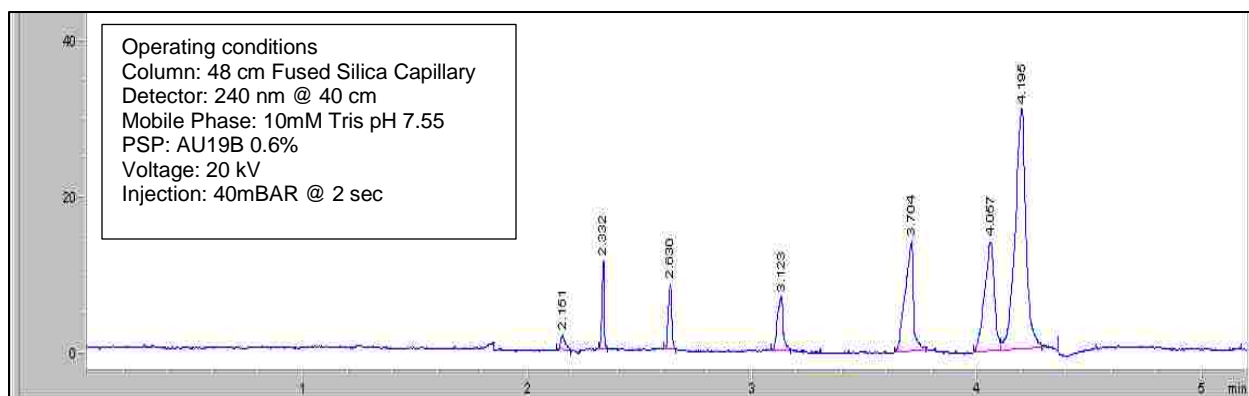


Figure 22: Separation of six alkyl-phenone derivatives at pH 7.55.

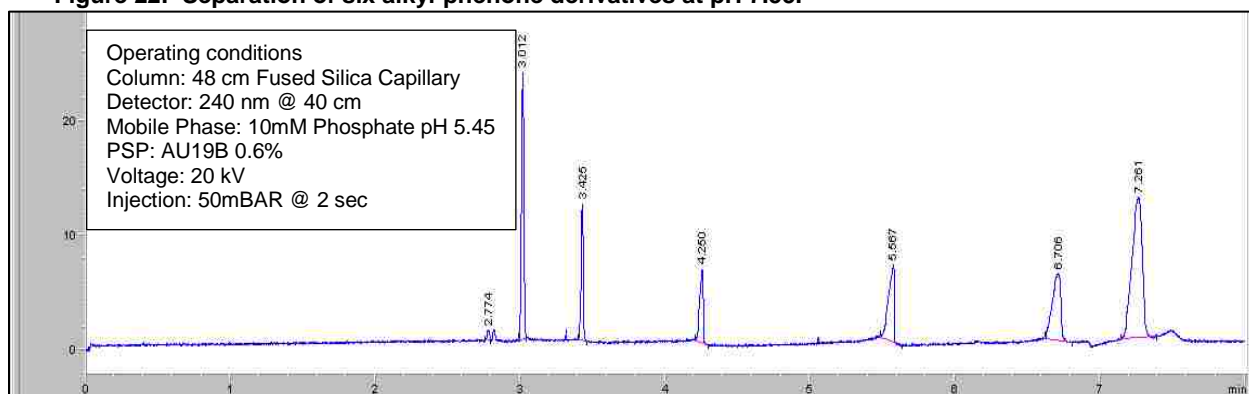


Figure 23: Separation of six alkyl-phenone derivatives at pH 5.45.

AU19B PSP	$\mu_{ep} 10^4 (cm^2/V*s)$	Migration Range ( $t_{psd}/t_o$ )
pH 9.2	-3.893±0.003	1.74
pH 7.55	-3.695±0.003	1.99
pH 5.45	-3.674±0.003	2.75

Table 5: Electrophoretic mobility and migration range dependence on pH.

#### 4.5 LSER analysis

AU31A was characterized by LSER. 39 compounds with varying solute descriptors were separated using the same operating conditions as in Figure 22. Because some of the analytes have very similar  $k$  values and spectra, analysis was done using 3-4 very different analytes at a time for identification purposes.  $k$  values were determined using Equation 24 and are reported in

**Table 6.** Solute descriptors were obtained from Poole. [40] Some analytes do not have significant hydrogen bond acidity (A). These analytes will have a zero value for solute descriptor A. [45] System constants were determined by multiple linear regression analysis using Excel to obtain the constants in

**Equation 27** and are presented in

**Table 7.** The system constants describing PSP retention and selectivity are discussed in detail in Chapter 5.



#	Solute	<i>k</i>	<i>log k</i>	<i>V</i>	<i>S</i>	<i>A</i>	<i>B</i>	<i>E</i>
1	Benzyl Alcohol	2.492E-02	-1.603520599	0.916	0.87	0.33	0.56	0.803
2	Resorcinol	2.707E-02	-1.567466633	0.834	1	1.1	0.58	0.98
3	3-methyl benzyl Alcohol	5.151E-02	-1.288119624	1.057	0.9	0.33	0.59	0.815
4	Phenol	5.906E-02	-1.228698753	0.775	0.89	0.6	0.3	0.805
5	Acetophenone	1.017E-01	-0.992533668	1.014	1.01	0	0.48	0.818
6	Phenyl Acetate	1.023E-01	-0.990312399	1.073	1.13	0	0.54	0.661
7	4-fluorophenol	1.159E-01	-0.936040133	0.793	0.97	0.63	0.23	0.67
8	Benzonitrile	1.398E-01	-0.8543599	0.871	1.11	0	0.33	0.742
9	M-Cresol	1.412E-01	-0.850172813	0.916	0.88	0.57	0.34	0.822
10	p-Cresol	1.485E-01	-0.828262535	0.916	0.87	0.57	0.31	0.82
11	4-nitroaniline	1.861E-01	-0.730358764	0.9904	1.91	0.42	0.38	1.22
12	Nitrobenzene	2.763E-01	-0.558656935	0.891	1.11	0	0.28	0.871
13	Benzene	2.841E-01	-0.546497262	0.716	0.52	0	0.14	0.61
14	Methyl benzoate	3.152E-01	-0.501423587	1.073	0.85	0	0.46	0.733
15	4-Chloroaniline	3.153E-01	-0.501232366	0.939	1.13	0.3	0.31	1.06
16	3,5-Dimethylphenol	3.187E-01	-0.496677486	1.057	0.84	0.57	0.36	0.82
17	Propiophenone	3.311E-01	-0.480030584	1.155	0.95	0	0.51	0.804
18	4-ethylphenol	3.535E-01	-0.451568583	1.057	0.9	0.55	0.36	0.8
19	4-Bromophenol	3.581E-01	-0.445969823	0.95	1.17	0.67	0.2	1.08
20	4-Chlorophenol	4.772E-01	-0.321273673	0.898	1.08	0.67	0.2	0.915
21	4-Chloroacetophenone	5.290E-01	-0.27655878	1.136	1.09	0	0.44	0.955
22	3-Chlorophenol	5.913E-01	-0.228164331	0.898	1.06	0.69	0.15	0.909
23	Indole	6.482E-01	-0.188297879	0.946	1.12	0.44	0.22	1.2
24	Anisole	6.800E-01	-0.167489138	0.916	0.75	0	0.29	0.708
25	4-Nitrotoluene	7.589E-01	-0.119794464	1.032	1.11	0	0.28	0.87
26	3-Bromophenol	7.767E-01	-0.109742416	0.95	1.15	0.7	0.16	1.06
27	Toluene	8.340E-01	-0.078851673	0.857	0.52	0	0.14	0.601
28	Ethylbenzoate	9.121E-01	-0.039979509	1.214	0.85	0	0.46	0.689
29	Methyl-o-toluate	1.045E+00	0.018984915	1.214	0.87	0	0.43	0.772
30	Chlorobenzene	1.624E+00	0.210490074	0.839	0.65	0	0.07	0.718
31	1-Naphthol	2.070E+00	0.315939663	1.1441	1.08	0.61	0.4	1.52
32	p-Xylene	2.459E+00	0.390718532	0.998	0.52	0	0.16	0.613
33	Ethylbenzene	2.466E+00	0.39198169	0.998	0.51	0	0.15	0.613
34	Iodobenzene	4.316E+00	0.63509942	0.975	0.82	0	0.12	1.188
35	4-Chlorotoluene	4.431E+00	0.646540511	0.98	0.67	0	0.07	0.705
36	Naphthalene	6.962E+00	0.842747698	1.085	0.92	0	0.2	1.36
37	Propylbenzene	7.161E+00	0.854947477	1.139	0.5	0	0.15	0.604
38	1-methylnapthalene	1.521E+01	1.182012153	1.226	0.9	0	0.2	1.344
39	Biphenyl	2.363E+01	1.373472332	1.324	0.99	0	0.22	1.36

**Table 6: Determined *k* and *log k* values. Solute descriptors are also reported.**

<i>PSP</i>	<i>V</i>	<i>s</i>	<i>a</i>	<i>b</i>	<i>e</i>
AU31A	3.10	-0.54	-0.32	-3.37	0.74

**Table 7: System constants for AU31A PSP.**

As mentioned in chapter 2, a wide range of solute descriptors must be used to prevent cross-correlation. Using a linear regression, the cross-correlation was determined for each solute descriptor. All correlations are below 0.8 suggesting that the model is statistically valid [40].

## Chapter 5: Results and Discussion

---

### 5.1 Introduction

---

Chapter 4 presented results from synthesis and EKC. This chapter will focus on interpreting those results and comparing them to current and past research. The overall objective of this chapter is to discuss the viability of the synthetic route to novel PSPs by RAFT and the performance of the PSP compared to other PSPs used in industry and academia. In addition, this chapter focuses on the achievement of project goals outlined in chapter one, and discusses questions raised by the results.

### 5.2 Synthesis of poly (AMPS) macro-CTA

---

#### 5.2.1 Neutralization of acrylamides in the synthesis of mCTA

---

Successful synthesis of mCTA was achieved. The use of NaOH to neutralize the acidic groups on the AMPS monomer gave poor results. After numerous attempts no polymerization was observed. This is in contrast to the procedure given by Ferguson. A possible explanation for this effect is the hydrolysis of the trithiocarbonate on the CTA by NaOH. The procedure was modified to omit NaOH addition with good results.

#### 5.2.2 RAFT control

---

As mentioned before the RAFT process distinguishes itself from free radical polymerization by providing polymeric weight control to the chemist. It is important to demonstrate this control over molecular weight, ensuring synthesis viability. One way to show control of polymerization is to compare theoretical weight values with experimental values. In 2001, Sumerlin and group showed that they could control polymerization of acrylamide. Table 8 shows polymerization results AMPS polymers synthesized by Sumerlin et al. and in this study. Sumerlin's syntheses have a percent error in  $M_n$  (expt) vs  $M_n$  (theory) of 7.9 and 10.8 and PDI of 1.29 and 1.16, respectively, confirming relatively good control of the polymerizations.

Sample	Time (min)	Conversion (%)	$M_n$ (theory)	$M_n$ (expt)	$M_w$ (expt)	PDI
AMPS 1 [42]	255	77.1	26,500	24,400	31,500	1.29
AMPS 2 [42]	343	88.0	17,600	19,500	22,600	1.16
JSH32A	1440	100.0	959	1086	1116	1.03

**Table 8:** AMPS 1 and 2 were synthesized by Sumerlin and analyzed by aqueous size exclusion chromatography. JSH32A was analyzed by ESI-MS.

JSH32A, the mCTA synthesized in this work, gives a much better PDI compared to Sumerlin's results. This may be due to relatively low molecular weight polymerizations. After ESI-MS analysis, a 13.2 percent error between the theoretical and experimental  $M_n$  is reported in JSH32A. The relatively small error demonstrates achieved control of the mCTA polymerization. Although this error was acceptable to go forth with the next step of the synthesis, many more polymerizations should be done to determine the possibility of making this error smaller. The experimental  $M_n$  value is larger than expected due to the absence of the  $n=2$  polymer (Figure 12). This is somewhat of a strange occurrence as the RAFT process statistically determines the distribution of poly-AMPS to be symmetric when centered on the major polymer. In other words, if the majority of the product is  $n=4$ , polymers of  $n=6$  and  $n=2$  should also be visible with about the same intensity. More investigation is needed to determine if the absence of the polymer with two units is persistent or due to instrumental/experimental error.

Table 9 presents more data on experimental and theoretical  $M_n$  values obtained by Ladaviere (black) and Mori (blue). Analyzing results presented in Table 8 and Table 9 shows little pattern in experimental vs. theoretical values. Experimental  $M_n$  is expected to be higher than theoretical  $M_n$  at high conversions due to different termination processes that take place with longer reaction times. This however does not always hold true as shown in Table 8 and Table 9. In other words, a long and high conversion synthesis will not necessarily give high experimental  $M_n$  values and other factors can play an important role. The higher than expected  $M_n$  in JSH32A, cannot be simply explained by RAFT termination processes. In our case, we believe that the missing  $n=2$  polymer is skewing the experimental  $M_n$  to a higher value. The process behind this is discussed in the following paragraph.

<i>mCTA (sample)</i>	<i>Conv (%)</i>	<i>M<sub>n</sub>(theo)</i>	<i>M<sub>n</sub> (expt)</i>
Poly acrylic acid (4)	99	1800	1800
Poly acrylic acid (10)	96	3700	3000
Poly acrylic acid (13)	96	3450	2610
(CTA 1)	72	6800	7600
(CTA 2)	99	9300	8000

**Table 9: Theoretical vs. experimental results for mCTA polymerizations presented by Ladaviere (black) and Mori (blue). [46] [47]**

To this group's knowledge all mCTA RAFT polymerizations currently achieved are of relatively high molecular weight. More studies have to be performed on 2-4 unit polymerizations. It is this group's theory that  $n=1$  and  $n=2$  growing chains still possess some of the original R group character, having only been modified by one or two monomers. In other words,  $n=1$  and  $n=2$  could be better leaving groups than  $n=6$  due to chemical or solubility properties of the solution. A better leaving group will have a greater chance to grow, thus we don't detect any  $n=2$  polymer. More experiments should be performed to confirm this hypothesis.

### 5.2.3 NMR analysis and conversion

The use of  $^1\text{H}$  NMR for analyzing the mCTA gives an average number of polymerized monomer and confirms polymerization. In addition to ESI-MS analysis, JSH32A was analyzed by NMR. Figure 24 shows an integrated spectrum of JSH32A. Setting the peak area of the terminal methyl on the Z group to 3 gives a value of 10 to the hydrogens next to the sulfonyl group. Dividing that number by two gives the number of AMPS units contained per polymer. Because NMR analysis is based on averages we do not get detailed information on the distribution of polymers. However the analysis is still useful as it confirms polymerization in terms of broad peaks.

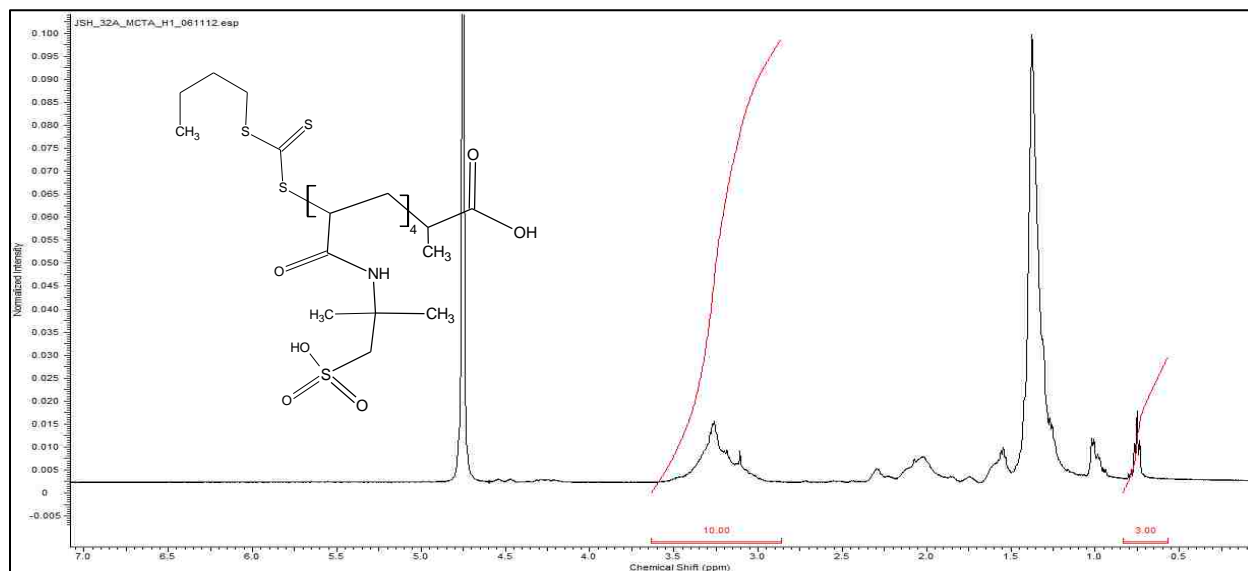
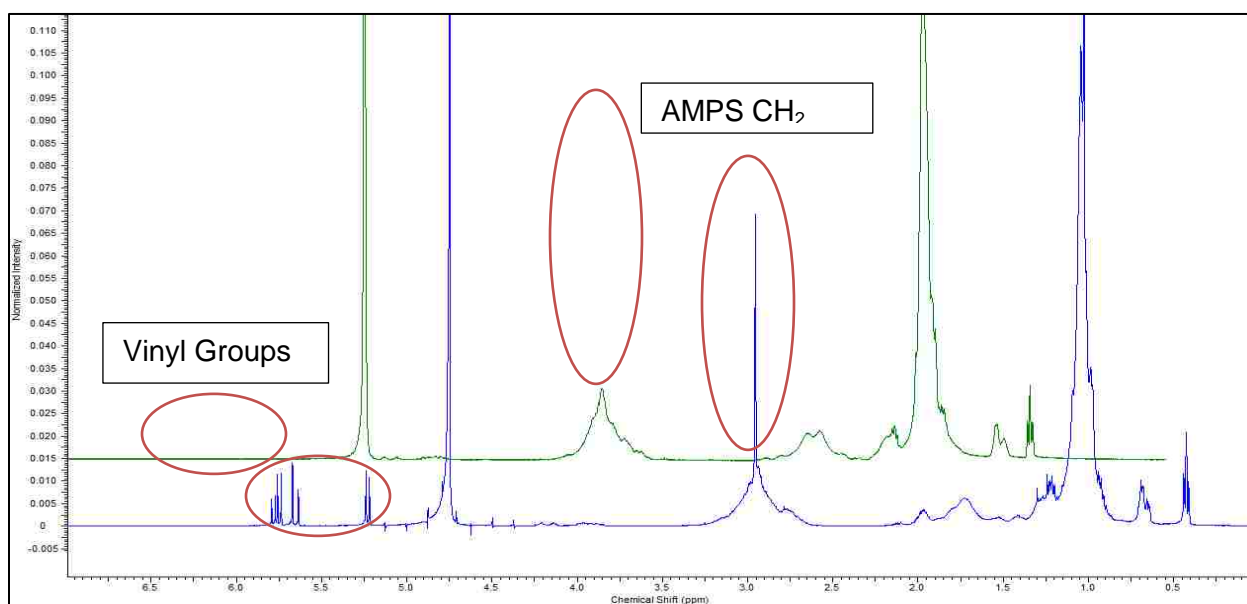


Figure 24:  $^1\text{H}$  NMR spectra of mCTA JSH32A in  $\text{D}_2\text{O}$ .

The spectrum suggests 5 AMPS units per polymer while the ESI-MS analysis shows that 4 AMPS units per polymer is the major polymer. These results are within experimental error for these two techniques. NMR should be used in concert with ESI-MS to analyze mCTAs. The

two techniques in tandem are sufficient to characterize the product, showing structure, polymerization, PDI, and experimental molecular weights.

Unless one encounters an extremely conducive case where the conversion of monomer is 100%, dialysis will be necessary. JSH32A was one of those cases where all of the monomer was converted to polymer and dialysis was not necessary. However, most all other syntheses of the mCTA showed conversions between 90 and 98 percent. An example of a typical mCTA spectrum before dialysis is given in Figure 25. The vinyl group is clearly observed at the higher chemical shift on the left side of the spectrum. The unpolymerized monomer comprises about 18% of the AMPS in solution thus giving an 82% conversion.



**Figure 25:**  $^1\text{H}$  NMR spectra of mCTA JSH42B8 in  $\text{D}_2\text{O}$ . LH31A2 mCTA before dialysis (BLUE) and after dialysis (GREEN). The green spectrum of dialyzed mCTA is offset to the left to make the figure clearer.

The green spectrum in Figure 25 is the same mCTA after dialysis. All the vinyl groups are removed indicating that there is no more free monomer in the system. The sharp AMPS  $\text{CH}_2$  peak is also removed. Dialysis ensures that the next synthesis step forms two distinctive blocks in the diblock-copolymer. Unreacted monomer can still polymerize in the next step randomizing the second block.

One issue arises when the reaction fails to go to 100%. The  $M_{n \text{ expt}}$  will be lower than  $M_{n \text{ theo}}$ , not considering termination processes. When calculating reactant concentrations it is impossible to predict the exact conversion and 100% is generally used. This issue, although important, does not cause major problems since most conversions are >97%. The example in Figure 25 is

exaggerated to show the effectiveness of dialysis. The LH31A2 reaction was quenched early after only 4 hrs. reaction time.

This synthetic route to the mCTA is a viable way of achieving the necessary component for the diblock synthesis. The results show good weight control and PDI.

### 5.3 Chain extension of poly(AMPS) macro-CTA with butyl acrylate

#### 5.3.1 Reaction dependency on pH

Previously presented analyses of AU19B and AU31A show a successful chain extension and nanoparticle formation. As in the mCTA, synthesis pH plays an important part in nanoparticle formation. Due to the omission of the neutralization step in the mCTA formation, the mCTA solution should be neutralized before the diblock reaction is initiated. The Ferguson synthetic pathway assumes that the AMPS groups were neutralized in the mCTA reaction and thus gives no neutralization step for nanoparticle formation. This group struggled identifying the problem with the nanoparticle synthesis because of the omitted step. Although the problem did cause some delay in producing nanoparticles, it also gave some insight into the synthesis.

<i>Nanoparticle (size nm)</i>	<i>pH used in synthesis</i>	<i>30% NP Solution In H<sub>2</sub>O</i>
JSH36A (--)	<2	Rubbery Yellow Solid
AU11B (--)	<2	Rubbery Yellow Solid
AU19B (24.1)	6.5	Somewhat Viscous Yellow Solution
AU31A (29.93)	6.5	Somewhat Viscous Yellow Solution
AU19A (11.4)	8.2	Some Loss of Yellow Color Solution is Non-Viscous (Colloidal)

**Table 10: Qualitative analysis of nanoparticles dissolved in H<sub>2</sub>O synthesized at different pH.**

Table 10 gives a qualitative analysis of synthesized nanoparticles. Varying the reaction pH gives drastically different results. As discussed earlier, a pH of 6.5 was chosen in order to ionize the AMPS groups and minimize hydrolysis of the trithiocarbonate moiety. Nanoparticles synthesized at pH <2 were unusable in EKC due to their poor solubility in water. Nanoparticles synthesized at pH of 6.5 and pH 8.2 performed well in EKC. AU19A exhibited good chromatographic peak shapes but the small size demanded a high PSP concentration

producing a lot of noise in the chromatogram producing some light scattering. The small particle size of AU19A is a result of using too little of the butyl acrylate monomer in the nanoparticle synthesis step. Although all nanoparticles synthesized at a pH of 6.5 performed well in EKC separations, and DLS analysis confirms particle formation, some concern over viscosity still remains. Synthesized latex nanoparticle solutions should not exhibit viscous properties due to their ionic shells.

In the case of the mCTA by McCormick's group, it was shown that synthesis at pH 7 leads to an extremely high PDI signifying loss of raft agent functionality [48]. However, for the diblock synthesis, a pH of ~8 is successfully employed as shown by Sumerlin [49]. The slight loss of the yellow appearance in the current studies at pH 8.2 could signify hydrolysis of the trithiocarbonate moiety, a major concern for this group. Table 10 gives a clear pattern of polymer self-assembly into nanoparticles leading to the following hypothesis. Synthesis at pH 2, 6.5, and 8.2 shows formation of rubber-like polymers (no nanoparticles), viscous solution (some nanoparticles), and colloidal solution (all nanoparticles), respectively. Although further experiments are needed to fully grasp the viscous vs. colloidal nanoparticle properties, current data suggests that optimal conditions for the AMPS-butyl acrylate diblock syntheses would require a solution pH of ~7 to 8.

### 5.3.2 NMR and DLS discussion

---

Synthesized nanoparticles AU19B and AU31A were analyzed by NMR and DLS. Quantitative NMR analysis at the diblock level has proved to be challenging. The broad peaks from the AMPS block and the butyl acrylate block begin to overlap and are very broad due to anisotropic effects. NMR is still useful to obtain an approximate value for the number of polymerized monomers in the hydrophobic block. Because the molecule has now become relatively large the CH<sub>3</sub> on the Z group is masked and we cannot reference hydrogen concentration to that peak. However, good values for the number of polymerized AMPS monomer were obtained by NMR and confirmed by ESI-MS in the mCTA. Thus the broad peak of the AMPS group on the diblock copolymer can be referenced. The degree of polymerization of the butyl acrylate determined by this method is presented in Table 11. Some discrepancy between the degree of polymerization by NMR and the particle diameters by DLS is shown in Table 11.

<i>Nanoparticle</i>	<i>Z-average (nm)</i>	<i>Diameter by volume(nm)</i>	<i>Polydispersity Index*</i>	<i>NMR Integration</i>
AU19B	28.41	24.1	0.088	15.42
AU31A	48.93	29.93	0.345	13.81

**Table 11: Results for DLS and NMR analysis of synthesized nanoparticles. The number associated with NMR integration gives the average number of polymerized butyl acrylate monomers.**

All reagents were kept at the same proportion for the synthesis of AU31A and AU19B. The only difference was in the upscale of the reaction and the lack of degassing the butyl acrylate solution. In NMR analysis the integration values are relatively close as expected. However, analyses by DLS give conflicting results when looking at the z-average data. Insight to the discrepancy can be gained by comparing the number of polymerized butyl acrylate monomers to the nanoparticle size as determined by volume. Taking into account that NMR integration is an approximate technique, when analyzing diblock copolymers, the size by volume and NMR results are in relative agreement. Due to the fact that the Z-average is based on intensity, large particles heavily skew the results although most particles are actually smaller. DLS analysis by volume is based on average concentration showing that most AU31A particles are of about 30nm. NMR is also based on an average concentration. The agreement between the two show that most of the nanoparticles are of expected size.

The Z-average being much higher than the by volume result does show that a higher proportion of large particles were formed in AU31A. This is also confirmed by the relatively large PDI\*, although still in the monodisperse region. Larger than expected polymers and PDI\* are usually due to unwanted termination processes. The omission of the degassing step in the synthesis of AU31A, for the butyl acrylate monomer, may be to blame. PDI\* for AU19B is in the excellent range as related to monodispersity.

Although the PDI\* for AU31A is larger than expected, both synthesized nanoparticles were successfully utilized in EKC. While some minor improvements such as optimal pH and reaction conditions leading to minimal introduction of termination pathways should optimize the synthesis of the diblock, currently synthesized nanoparticles exhibit excellent performance in EKC. The synthetic route from CTA to nanoparticle has been determined as viable.



## 5.4 Methylene Selectivity and CE Current

---

This section begins with a discussion and comparison of methylene selectivities of the synthesized PSPs. As previously discussed, larger PSP methylene selectivities are advantageous as lower PSP concentrations can be used in analysis of neutral compounds, yielding the same separation performance. The section concludes with a discussion of analysis current. High current during EKC analysis is to be avoided. PSP efficiency decreases with rising current due to different temperature zones in the bulk phase. This phenomenon is referred to as Joule heating. This section discusses the necessity for post-synthesis dialysis of the AMPS-butyl acrylate PSP and the advantage of nanoparticle PSPs with respect to current over SDS.

Table 12 gives methylene selectivity results for AU19B and AU31A AMPS-butyl acrylate nanoparticles, Palmer's acrylic acid-butyl acrylate nanoparticles, and SDS micelles. All nanoparticles exhibit much higher methylene selectivity than SDS micelles. These nanoparticles are able to provide extremely strong hydrophobic interactions. Nanoparticle PSPs generally provide much higher methylene selectivities than most polymeric PSPs [8] [50].

<i>PSP</i>	$\alpha_{\text{CH}_2}$ ( <i>Methylene Selectivity</i> )
AU19B (24.1 nm by vol)	3.048±0.003
AU31A (29.93 nm by vol)	3.276±0.003
Palmer NP (63nm Z-ave) [11]	3.25±0.03
Random Block polymers [21]	2.54±0.01
SDS micelles [51]	2.33±0.04

**Table 12: Methylene selectivities**

Acrylic acid-butyl acrylate NPs reported by Palmer and the AMPS-butyl acrylate NPs synthesized in this study are similar and provide excellent methylene selectivity. The Palmer and current NPs contain 5 and 4 polymerized monomer unit ionic shells, respectively [11]. The current NPs, especially AU31A, also exhibit approximately the same methylene selectivity as those synthesized by Palmer. This is odd as AU31A is about 20nm smaller due to its smaller hydrophobic core, and one might expect methylene selectivity to increase with hydrophobic core volume.

Characteristics of the polymeric surfactants	Poly-SAIS surfactant's hydrophobic tail length in carbons			
	C8	C9	C10	C11
$\alpha_{\text{CH}_2}$	1.30( $\pm$ 0.02)	1.39( $\pm$ 0.03)	1.44( $\pm$ 0.02)	1.54( $\pm$ 0.04)

**Table 13: Methylene selectivities table, recreated from Shamsi *et.al.*, of four homologous series polymeric PSPs. [52]**

Methylene selectivity, for polymeric PSPs, increases with larger hydrophobic cores as shown in Table 13. The same applies to nanoparticle PSPs looking at the methylene selectivities of AU19B and AU31A (Table 12). It is reasoned that the ionic shell in the current NPs, having AMPS groups vs. acrylic acid groups in Palmer's NPs, provides the extra hydrophobic interactions. The AMPS monomer has a branched hydrophobic linker region that is absent in acrylic acid. In theory, having the AMPS groups as the shell and increasing the size of the hydrophobic core from 30nm to 60nm, the AMPS-butyl acrylate NPs should provide superior methylene selectivity even when compared to Palmer's NPs.

The experimental procedure in Chapter 3 calls for the dialysis of the mCTA in order to eliminate randomization of the B block in the diblock synthesis. Dialysis of the nanoparticle, as it is the final step, is not necessary from a synthetic point of view. In addition, free monomer was not observed in NMR analysis of the nanoparticles (Figure 16 and Figure 17). However, it has been observed that dialysis of the nanoparticle greatly reduces current when it is applied as a pseudostationary phase.

The NaOH used in the synthesis of the diblock polymer, if not removed, is carried over to the EKC analysis. The carry-over of NaOH increases the analysis current and could alter the pH of background electrolytes. Table 14 gives examples of typical currents observed by this group when applying the newly synthesized PSP to EKC. The last rows give current when using SDS as a PSP.

AU19A PSP was used to perform a separation of the six alkyl-phenone derivatives. AU19A and AU19A' provide a contrast between a PSP without post-synthetic dialysis and a PSP which has undergone dialysis, respectively. An almost 2 fold current drop is the result. It has been determined that post-synthetic dialysis is mandatory to achieve optimal separation conditions.

<i>PSP (concentration)</i>	<i>Dialysis</i>	<i>Buffer</i>	<i>pH</i>	<i>Current (<math>\mu</math>A)</i>
No PSP [blank]	--	10mM Borate	9.2	4.3
AU19A (0.6% (w/v))	no	10mM Borate	9.2	12.0
AU19A' (0.6% (w/v))	yes	10mM Borate	9.2	6.9
AU19B (0.6% (w/v))	yes	10mM Borate	9.2	5.5
AU31A (0.35% (w/v))	yes	10mM Borate	9.2	4.9
SDS (0.50% (w/v))	--	10mM Borate	9.2	30.0
SDS (1.5% (w/v)) [53]	--	12.5mM NaHPO <sub>4</sub> /Na <sub>2</sub> B <sub>4</sub> O <sub>7</sub>	9.2	55.0
Poly-SUS (1.0% (w/v)) [53]	--	12.5mM NaHPO <sub>4</sub> /Na <sub>2</sub> B <sub>4</sub> O <sub>7</sub>	9.2	38.0

**Table 14: Comparison between different PSPs and their effects on analysis current. AU19A and AU19A' is the same PSP, the only difference being in the application of post-synthetic dialysis. Poly-SUS is a polymerized micelle-like structure consisting of sodiumundecylenic sulfate.**

A voltage of 20kV was also applied to a mobile phase containing only borate. This analysis was called the blank. An inherent current to the borate system of 4.3  $\mu$ A was observed. Dialyzed PSPs, AU19A' and AU19B, showed a relatively small increase in the current compared to the blank. As previously discussed larger methylene selectivities give the analyst the ability to use lower PSP concentrations. AU31A exhibits a larger methylene selectivity than AU19B and thus is used at a lower concentration. As expected, a lower concentration of 0.35% (w/v) leads to a significant decrease in current. AU19B increases the base current from the blank by only 0.6  $\mu$ A. In all cases, even with no post-synthesis dialysis, the synthesized AMPS-butyl acrylate PSPs have a much smaller current compared to SDS. This is expected and has been reported by multiple groups. SDS micelles are in equilibrium with free SDS surfactants which cause significant current increase. With respect to current, polymeric PSPs are superior to SDS in EKC.

With the majority of AU31A being of about 30nm size, it is evident that performance can still be increased. Lower limits of AU31A, in terms of PSP concentration, are yet to be explored. Multiple post-synthesis dialyses may also decrease current as more NaOH should be removed. Figure 21, in Chapter 4, shows a separation of alkyl-phenone derivatives using AU31A where  $t_{psp} = 2.98min$  and the last compound elutes at  $2.93min$ .  $R_s$  is much greater than 1.5 for all peaks. It is reasonable to assume that a smaller concentration of AU31A can be used to

effectively separate the same mixture. The decrease in concentration will lead to a lower current potentially providing better separation efficiency.

Chain extension with more butyl acrylate, leading to a larger a PSP, should lead to higher methylene selectivity. Synthesized by Palmer, an acrylic acid/butyl acrylate PSP, under typical operating conditions, was found to have a negligible 0.02  $\mu\text{A}$  current increase. [11] Palmer's PSP, having an average size of 63nm, was used at 0.12% (m/v). Referring back to Table 12 the methylene selectivities for AU31A and Palmer's PSP are almost identical although AU31A is only half the size. Increasing the size of the hydrophobic region of the current NPs to a NP diameter of about 60nm will most likely enable efficient separations with PSP concentrations of <0.1% due to increased methylene selectivity. With these enhancements the AU PSP should not have any noticeable effect on current. The novel AMPS-butyl acrylate PSP, although not yet optimized, already exhibits excellent methylene selectivity and low effect on current.

## 5.5 Electrophoretic mobility and efficiency

Exhibiting excellent selectivity for hydrophobic compounds, AU19B and AU31A also provide competitive electrophoretic mobility. Table 15 gives experimental results for synthesized nanoparticles and comparisons to other PSPs.

<i>PSP</i>	$\mu_{ep} 10^{-4}(\text{cm}^2/\text{V}^*\text{s})$	$\mu_o 10^{-4}(\text{cm}^2/\text{V}^*\text{s})$	<i>Migration Range</i> ( $t_{psp}/t_o$ )	<i>Theoretical plates(ave)</i>
AU19B	-3.893±0.003	9.143	1.74	420,000
AU31A	-3.773±0.004	9.169	1.70	130,000
SDS [21]	-3.97±0.02	--	--	149,000
Palmer NP [11]	-4.06±0.05	7.20	2.25	205,000
Random Block polymers [21]	-3.91±0.03	--	--	232,000

**Table 15: Performance characteristics for nanoparticles, SDS, and random block polymers.**

Migration range is an important factor in EKC. For compounds with certain selectivity and separation efficiency, migration range determines resolution. [54] Thus a larger migration range provides better resolution. However, reporting only migration range to describe PSP performance is not effective. Migration range is determined by the ratio of the elution time of a fully retained compound and a compound not retained at all by the PSP. Excellent migration ranges can be obtained by reducing the EOF at an impractical cost to analysis time. It is also difficult to compare PSPs synthesized by different researchers due to varying EOFs.

A better measurement for characterizing PSP performance, a number that does not vary with EOF, is the electrophoretic mobility ( $\mu_{ep}$ ) of the PSP. Electrophoretic mobilities are presented in Table 15. Although somewhat lower, AU19B and AU31A exhibit fair electrophoretic mobility compared to other PSPs. Because smaller particles experience less drag they should exhibit higher electrophoretic mobility. This is in fact observed when comparing the smaller AU19A to the larger AU31A. However, when comparing Palmer's NP of 63nm, to both smaller AU NPs, electrophoretic results are unexpected. The smaller size of the AU NPs should provide higher electrophoretic mobility, all PSP characteristics being equal. The major difference between Palmer and AU NPs, other than size, is the ionic head group. Palmer's NP utilizes a carboxylic acid head group while the AU NP utilizes a sulfonate head group. The sulfonate head group was chosen because it is easily ionizable even at lower pH. It was also postulated that same or better mobilities could also be achieved at pH greater than 7.5 (normal operating conditions). While the first statement holds true, some decrease in mobility is seen at pH 9.2 when compared to Palmer's NP. The difference in mobility might also be explained by the fact that Palmer's nanoparticles had an acrylic acid degree of polymerization of 5, while the AU nanoparticles have a 20% lower degree of polymerization for AMPS of 4. While further investigation is needed to determine the decrease in mobility, this author believes that the previously discussed viscosity of the NP's may be the culprit. While qualitative viscous properties are only observed in the high concentration stock PSP solutions, there may be quantifiable interactions between NPs during an EKC separation. It is postulated that when two NPs interact, they effectively double in size, creating more drag, and are swept along by the EOF. This could decrease the PSP mobility.

The electrophoretic mobilities given in Table 15 are examples of the top performers in the PSP field. Today, SDS is still defined as a benchmark for  $\mu_{ep}$ . While AU19B and AU31A exhibit a slightly smaller electrophoretic mobility they are still extremely competitive PSPs.

Electrophoretic mobilities were also determined at relatively low pH. With respect to SDS, nanoparticles synthesized by Palmer exhibit better methylene selectivity, efficiency, and can be used with large organic modifier concentrations. However, the use of the carboxylic acid head groups reduces the pH range of the analysis since carboxylic acid will quickly become protonated as the pH drops. As the head group becomes protonated the zeta potential of the particle drops resulting in reduced electrophoretic mobility. This was a main drawback when comparing nanoparticles to SDS. By adding sulfonate head groups, with a low pKa, we have

enabled the NP to function at lower pH without much loss in electrophoretic mobility. Table 16 illustrates experimental results of electrophoretic mobilities of the AU19B PSP at different pH.

<i>PSP (pH)</i>	$\mu_{ep}$ $10^{-4} (cm^2/V*s)$	$\mu_o$ $10^{-4} (cm^2/V*s)$	<i>Migration Range (<math>t_{pso}/t_o</math>)</i>
AU19B (9.20)	-3.893±0.003	9.143	1.74
AU19B (7.55)	-3.679±0.007	7.438	1.98
AU19B (5.45)	-3.648±0.007	5.768	2.72

**Table 16: Electrophoretic mobilities, EOFs, and migration ranges at different pH. Data obtained from results presented in Chapter 4.**

At the lowest studied pH of 5.45 the electrophoretic mobility is reduced by only 6.29%. The results show excellent performance of the AMPS modified NPs at low pH. It is also important to note that the electrophoretic mobility decreases far less than the EOF. Thus the migration range increases, especially at a pH of 5.45. This performance is valuable to analysts who are looking to increase their resolution. Theoretically, with this type of performance, the analysis pH can be pushed even lower if need be. This achievement has put the NP PSP at the same level of performance, in some cases better, as SDS.

In most cases the NPs have a better efficiency, plate count ( $N$ ), than SDS. Both Palmer NPs and random block copolymers exhibit great efficiency. (Table 15) The novel AMPS-butyl acrylate nanoparticles have the potential to greatly surpass SDS and even Palmer's NPs. AU19B exhibits a staggering plate count of almost half a million plates. This gives the ability to perform excellent separations in less time. Although AU31A show a significant decrease in plate count, the issue is synthetic. The PDI\* of the two phases synthesized was previously discussed. AU31A exhibited a somewhat elevated polydispersity. Polydispersity is expected to have negative effects with respect to efficiency. A PSP composed of different size particles provides different separation environments and different mass transfer ratios enabling additional diffusion mechanisms. The plate count in AU31A demonstrated the need for careful synthesis while AU19B demonstrates that incredibly high efficiencies can be attained.

The efficiencies reported in Table 15 are averages of each analyte separated. Theoretically, because analytes that are highly retained, spending most their time in the PSP, have less chance of experiencing diffusion, an increase in efficiency is expected. The number of plates, efficiency, should increase with higher retained compounds. The results presented in Figure 26 and are unexpected.

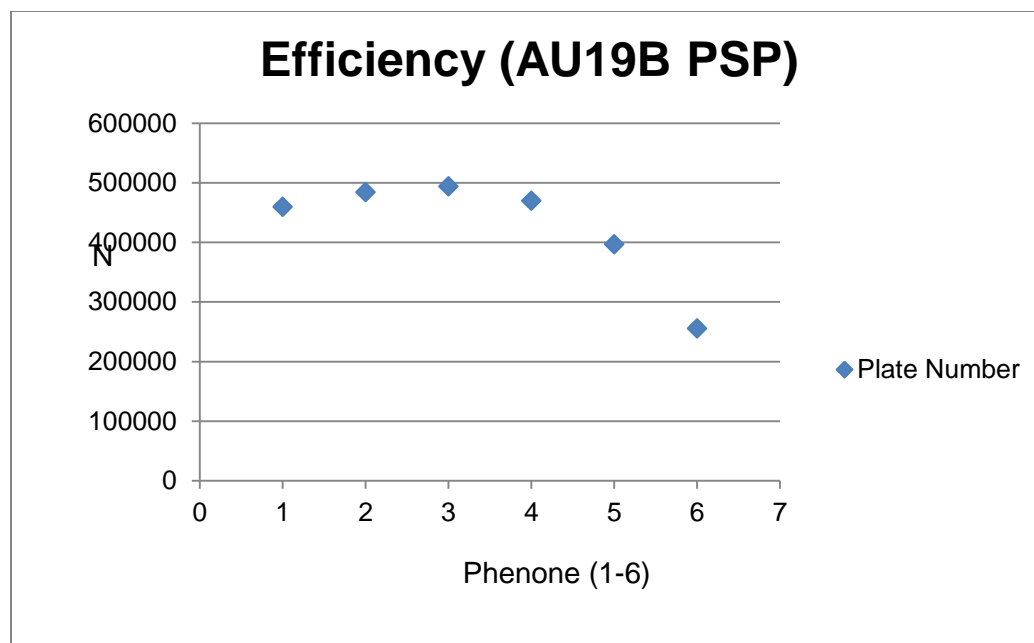


**Figure 26: Plate count for each analyte separated using AU19B as a PSP**

While the first three analytes follow the expected pattern, a decrease in efficiency is illustrated by the last three analytes. A similar pattern was reported by Palmer et al for acrylic acid/butyl acrylate nanoparticles. This phenomenon is not particular to polymeric PSPs as Joe Davis has also shown this trend with SDS micelles. In that case, highly retained hydrophobic compounds are dispersed by Joule heating in the capillary. [55] In the current studies, Joule heating is not expected to be an issue, and it is unclear why the increased dispersion of more highly retained compounds is observed. Although not an optimal situation for the polymeric PSP, SDS suffers from similar drawbacks. Furthermore, the lowest plate count observed in Figure 27, experienced by analyte six, is still higher than the average plate count of SDS.

## 5.6 LSER

---

### 5.6.1 Retention

---

Extensive LSER analysis was applied to AU31A in order to determine and compare the PSP's selectivity. The exact procedure is outlined in Chapter 3. LSER analysis gives further insight into retention behavior of the PSP. A representative electropherogram for four LSER solutes is shown in Figure 27. A total of eleven mixes were employed to determine  $k$  values for 39 compounds. Qualitative analysis of Figure 27 shows excellent efficiency and resolution. Furthermore, issues of peak broadening and peak fronting experienced by Palmer, for highly

retained analytes, have been minimized. While peak number four does exhibit some fronting, it is much less pronounced when the AU PSP is employed.

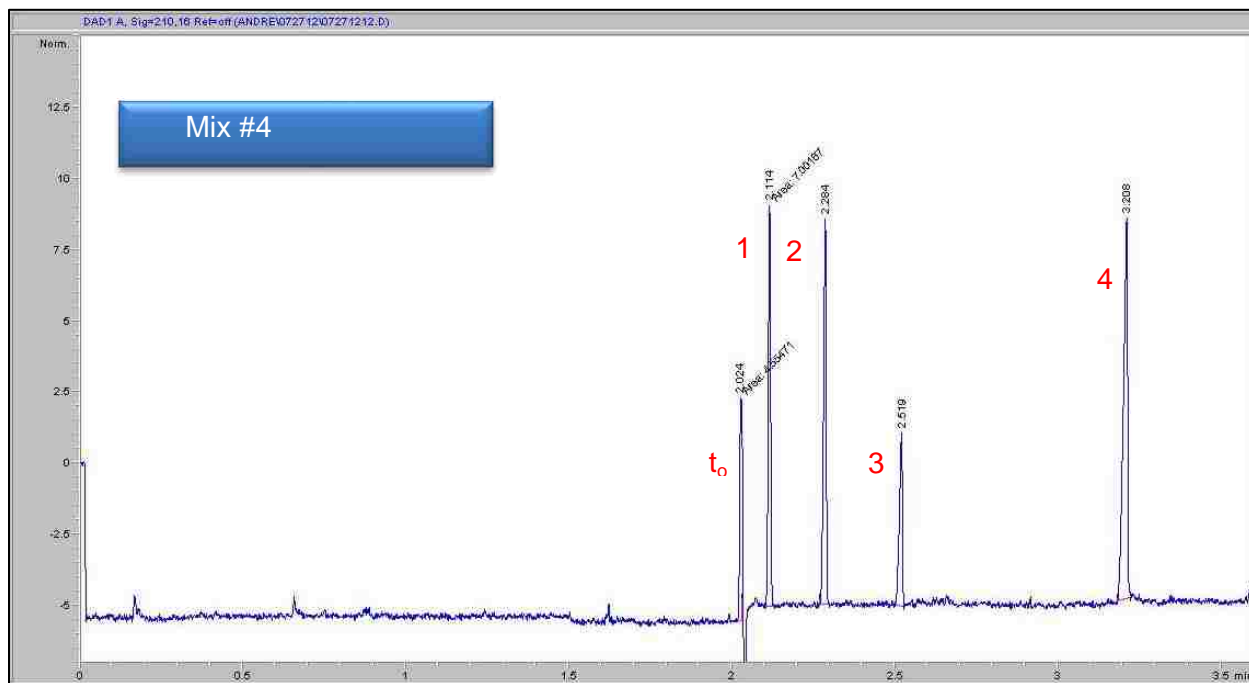


Figure 27: Representative electropherogram for four LSER compounds. Mix # 4 was run under conditions described in chapter 3. 1) Phenyl Acetate. 2) Propiophenone. 3) 4-Nitrotoluene. 4) Iodobenzene.

**Error! Reference source not found.** gives LSER results for PSPs comprised of SDS micelles, polymerized micelle-like Poly(SUA), random block copolymer with AMPS, nanoparticles with acrylic acid, and nanoparticles with AMPS. For ease of comparison the values presented in **Error! Reference source not found.** are graphed in Figure 28. The poly(SUA) was an advancement in PSPs due to its polymerized core. With respect to SDS, the need to reach CMC is eliminated and the PSP is tolerant to organic modifiers. However, the polymerized core

PSP	$\nu$	$e$	$s$	$a$	$b$	$r^2$
AU31A	3.10 (0.22)	0.74 (0.12)	-0.54 (0.13)	-0.32 (0.09)	-3.37 (0.18)	0.97
Palmer NP [12]	3.29 (0.28)	0.61 (0.16)	-0.40 (0.14)	-0.41 (0.11)	-3.94 (0.22)	0.96
SDS [56]	2.86 (0.17)	0.45 (0.10)	-0.52 (0.14)	-0.20 (0.11)	-1.77 (0.14)	NA
Poly(SUA) [12]	2.11 (0.09)	0.26 (0.06)	-0.16 (0.06)	-0.27 (0.11)	-1.05 (0.13)	0.99
Poly(C <sub>12</sub> Mat/AMPS) [12]	3.65 (0.18)	0.44 (0.11)	-0.67 (0.16)	-0.27 (0.08)	-3.70 (0.22)	0.99

of Poly(SUA) provides a ridged-cohesive

Table 17: LSER system constants for AU31A (AMPS-Butyl Acrylate) PSP, Palmer NP (Acrylic Acid-Butyl Acrylate) PSP, SDS, Poly(SUA) (poly(sodium undecylenate)), and Poly(C12Mat/AMPS) (a copolymer of



dodecyl methacrylate (15%) and AMPS). SDS values are averages from several studies as reported by Fu and Khaledi.

core environment as described by its low  $v$  value. This means that it has low retention for larger compounds as it requires more energy to form larger cavities or cavities in general.

The issue of the low  $v$  value in poly(SUA) was overcome by utilizing a random block copolymer Poly(C<sub>12</sub>MA<sub>t</sub>/AMPS). As expected, a high  $v$  value of 3.65 was obtained. However, due to the AMPS group being randomized throughout the backbone; low methylene selectivity is the result. The use of nanoparticles high values for both  $v$  and methylene selectivity. Both nanoparticles exhibit high  $v$  values which rival those of SDS. The high  $v$  value indicates a non-cohesive environment in the hydrophobic core for nanoparticle PSPs. This means that nanoparticles exhibit a relatively low energy barrier to cavity formation.

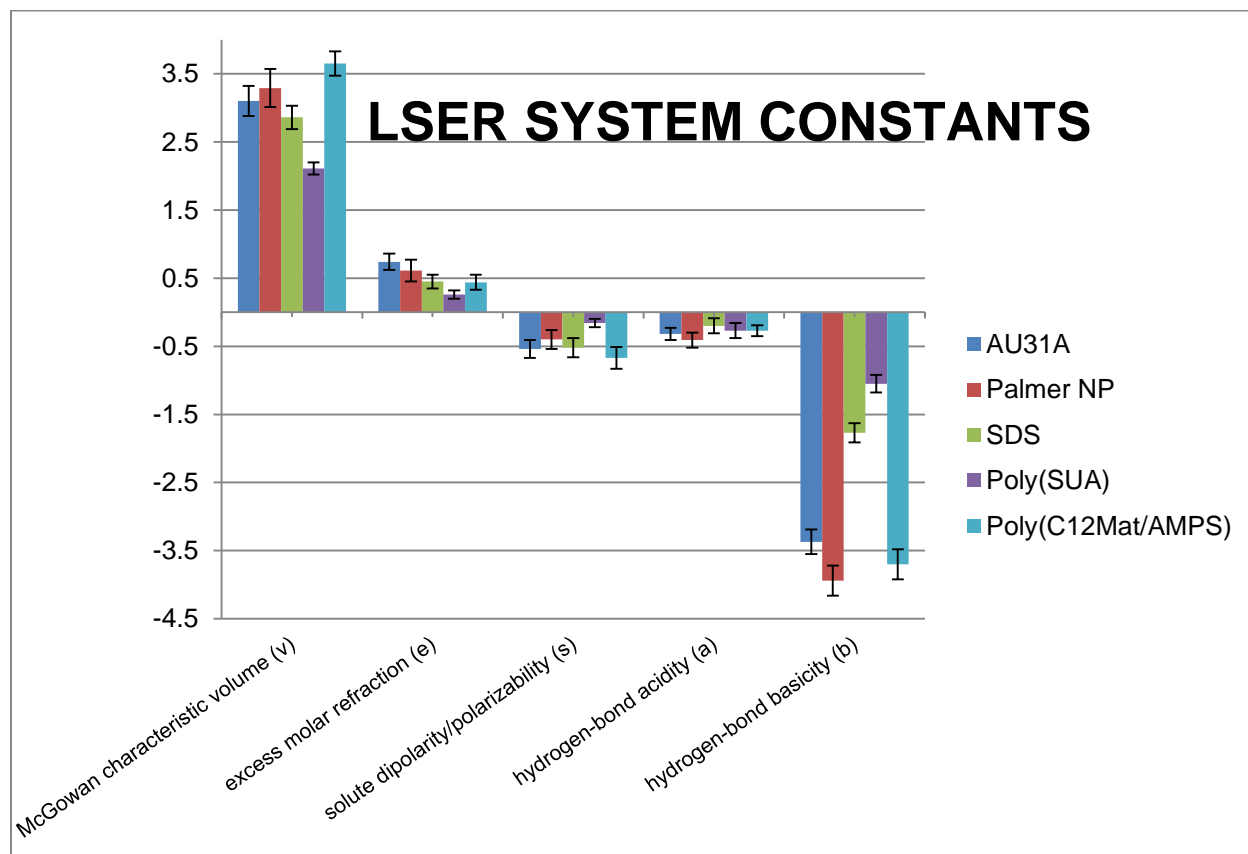


Figure 28: A graphical representation of the data presented in Error! Reference source not found..

The effect of substituting AMPS (AU PSP) for acrylic acid (Palmer PSP) as the ionic shell has little impact on the  $v$  value, indicating that characteristic volume descriptor is only dependent on the hydrophobic core. Because the hydrophobic core for the two nanoparticle PSPs is

composed of poly butyl acrylate, little difference is seen in the  $\nu$  value between the two nanoparticles.

The  $e$  term represents the ability of the PSP to retain an analyte through polarization of with  $n$  and  $\pi$ -type electrons. This term describes both increases in Van der Waals interactions (instantaneous polarization) and dipole-induced dipole interactions, and is thus related to, or a correction to, the  $\nu$  and  $s$  terms in the model [57]. Statistically, except for the poly(SUA) PSP, there is little difference in the  $e$  term for the presented PSPs. Poly(SUA) has a much lower  $e$  term which might be expected based on energetic barriers to forming Van der Waals interactions as implied by the low  $\nu$  term.

The  $s$  term describes the ability of the PSP to retain a polar or permanent dipole analyte. Except for the poly(SUA) PSP, all other PSPs presented have similar values for the  $s$  term. The change negative sign for the  $s$  value indicates that the PSP can provide less interaction for polar analytes than the aqueous background electrolyte used for EKC analysis. Although a negative value, the  $s$  term for the presented PSPs is less negative than expected when considering how well water interacts with polar molecules. For SDS micelles, composed purely of a hydrophobic 12 carbon core, the negative  $s$  value is unreasonably small. For example, when LSER analysis was applied to hexane and octanol the resulting  $s$  values were -1.79 and -1.05, respectively [58]. It has been suggested that the attachment, penetration, content, and orientation of water at the interphase micelle regions can provide a retentive environment for hydrogen bonding analytes [59] [60]. In addition to being able to provide hydrogen bonding, water can provide a favorable environment for polar analytes at the interphase micelle region. (Figure 29)

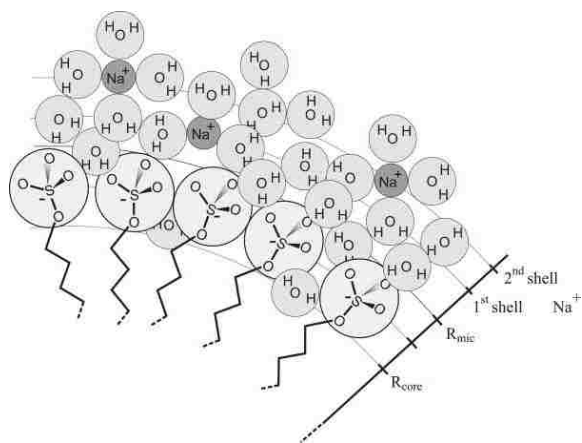


**Figure 29: Hydrated interphase region in SDS micelles [61]. Sulfate groups are hydrated through H-bonds. "Reprinted with permission from { R. Buchner, C. Baar, P. Fernandez, S. Shrodle and W. Kunz, "Dielectric spectroscopy of micelle hydration and dynamics in aqueous ionic surfactant solutions," *Journal of Molecular Liquids*, vol. 118, no. 1-3, pp. 179-187, 2005.}. Copyright {2013} American Chemical Society."**

Water molecules are reduced (but not frozen) in their dynamics [61] due to the highly dynamic structure of the SDS micelle. The relatively small negative  $s$  value for poly(SUA) may be due to polar polymerization initiator groups in the core of the polymerized micelle, or to the highly static environment of poly(SUA). The water molecules spend more time oriented the same way with respect to time. The  $s$  term for nanoparticles, is quite similar to SDS. This fact suggests that the nanoparticles are also hydrated along their shell, and are able to provide limited polar interactions in the interfacial region.

Further evidence for analyte surface interaction due to hydration, at least for SDS, is shown through the  $a$  term of the system constants. The  $a$  term defines the ability of the PSP to interact with analytes through the acceptance of hydrogen bonds. There is no statistical difference in this term for all presented PSPs. However, like the  $s$  term, the  $a$  term is unusually close to zero when considering the molecular structures of the PSPs. The SDS core does not have any ability to accept hydrogen bonds; relating SDS to hexane ( $a=-3.08$ ) the  $a$  term for SDS ( $-0.20$ ) should be more negative. In nanoparticles, whether hydrogen bonding analytes are interacting through the hydrated surface or polymeric core is not clear based solely on the  $a$  term. The cores of the nanoparticles, illustrated in Figure 30, do contain an ester which could accept hydrogen bonds.

The  $b$  term gives further insight into where hydrogen bonding analytes interact on the nanoparticle PSP. The  $b$  term represents the ability of the PSP to interact with analytes through the donation of hydrogen bonds. All presented PSPs show negative values for  $b$ . However, nanoparticles show a much more negative  $b$  than SDS or poly(SUA). Water molecules, when hydrating the PSP, use their hydrogen to interact with the oxygen on the carboxylic acid, sulfonate, or sulfate head group. Thus, hydration mostly contributes to the  $a$  term. However, some hydrogen bond donation is also experienced at PSP water interface, contributing to the  $b$  term; comparing hexane with no hydration and SDS,  $b$  is  $-4.64$  and  $-1.77$ . Palmer NP and AU31A PSP show  $b$  values of  $-3.94$  and  $-3.37$ , respectively. Low  $b$  values for the NP PSPs indicate that ionic shell hydration plays little part in hydrogen bond interactions, and that the relatively high  $a$  value contribution comes from the core ester group.

When comparing Palmer NP and AU31A, a notable difference between the  $b$  terms exists. As illustrated in Figure 30, the AU PSP is composed of the hydrophilic AMPS block. One of the major differences when using AMPS is the amide; not present in Palmer's acrylic acid NP.

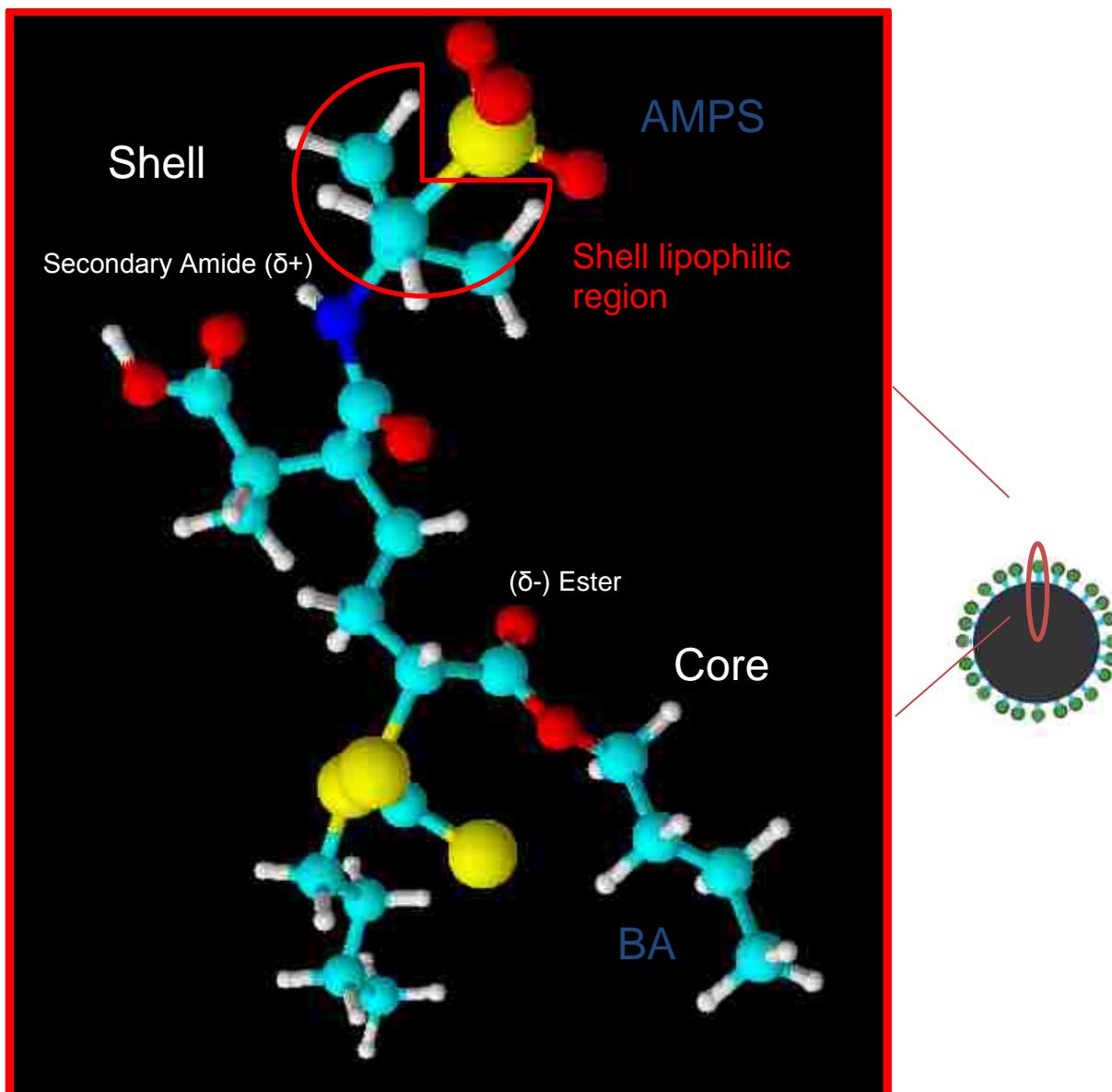


Figure 30: A 3D representation cutout of an AMPS-Butyl Acrylate nanoparticle. For illustration purposes, only one subunit of the poly AMPS block and poly Butyl Acrylate (BA) block is shown. Note that although the carboxylic acid and butanethiol terminal ends look significant in this image, they only comprise a small portion of the full polymeric NP.

The secondary amide provides some ability for the PSP to interact with analytes through hydrogen bond donation characterized by the less negative  $b$  values. The random AMPS copolymer PSP, poly(C12Mat/AMPS), also shows a less negative  $b$  value than the Palmer NP, but its intermediate value between the two nanoparticle chemistries does not provide conclusive support to the present hypothesis. The less negative  $b$  value for the AU PSP, although the difference is small, signifies that a small percentage of analytes may interact with the AMPS

PSP close to or within the ionic shell. It is theorized that the small lipophilic region within the ionic shell could allow access to the amide for neutral analytes which can participate in hydrogen bonding. However, the majority of PSP-analyte interaction still occurs at the core of the NP or at the interface between core and shell regions.

To summarize: Except for permanent dipole analytes, most retention as characterized by the LSER system constants for the AMPS-butyl acrylate PSP occurs at the core of the nanoparticle. The hydration of the nanoparticle's surface only has an effect on polar analyte retention. Due to the inclusion of an amide, some extremely limited ability to donate hydrogen bonding is observed.

### 5.6.2 Selectivity

When discussing selectivity it is often useful to normalize the LSER constants, with the idea being that the larger the relative magnitude of a descriptor in a negative or positive direction, the more important that system constant is to selectivity. For example, if all the system constants were equally doubled, retention would change but selectivity would effectively remain the same, but normalization would make this similar selectivity very apparent. Equation 29 gives the normalization parameter. Results are reported Table 18 where the prime symbol indicates a normalized value.

$$\beta = \sqrt{v^2 + e^2 + s^2 + a^2 + b^2}$$

**Equation 29: Normalization parameter for LSER system constants.**

<i>PSP</i>	$v'$	$e'$	$s'$	$a'$	$b'$
AU31A	0.66	0.16	-0.12	-0.068	-0.72
Palmer NP	0.63	0.12	-0.077	-0.079	-0.76
SDS	0.83	0.13	-0.15	-0.058	-0.51
Poly(SUA)	0.88	0.11	-0.067	-0.11	-0.44
Poly(C <sub>12</sub> MAAt/AMPS)	0.69	0.084	-0.13	-0.051	-0.70

**Table 18: Normalized system constants obtained from Error! Reference source not found. using Equation 29.**

When comparing the normalized coefficients, it is apparent that AU31A, Palmer NP, and Poly(C<sub>12</sub>MAAt/AMPS) all have similar selectivity. This makes sense as their backbone structure is very similar. When considering  $v'$  and  $b'$ , the coefficients with the largest magnitude, it is

apparent that the selectivity for those three PSPs is much different from SDS or poly(SUA). Backbone structure plays an important role in the PSP selectivity. Small differences are also observed between AU31A, Palmer NP, and Poly(C<sub>12</sub>Mat/AMPS), indicating that subtle changes in selectivity may be expected.

## Chapter 6: Conclusions and recommendations

---

### 6.1 Conclusions

---

The research presented shows excellent control of size and structure of novel PSPs through the use of RAFT polymerization. Excellent values for PDI, plate number, electrophoretic mobility, and methylene selectivity were achieved when employing the novel PSP for use in EKC. LSER analysis demonstrated that most analyte interactions are at the core of the nanoparticle. Selectivity is mostly defined through the  $v$  and  $b$  system constants showing a relatively non-cohesive PSP with little ability to donate hydrogen bonds. While somewhat similar to the previously synthesized NP PSP by Palmer, the substitution of AMPS for carboxylic head groups does provide subtle differences in selectivity. While SDS still remains a great option for separation of neutral analytes, this group's research indicates that excellent alternatives in the form of polymeric nanoparticles can be used just as well. Furthermore, the ability to tune polymeric PSP selectivity should prove these NP PSPs superior in niche applications. For many years chemist have had the ability to employ a wide array of stationary phases in HPLC. The door has now been opened, through RAFT polymerization, to develop a wide array of PSPs for use in EKC.

### 6.2 Recommendations for future work

---

The ground work for novel nanoparticle PSPs has been laid down. However, some questions still remain and must be addressed. Systematic experiments should be performed by synthesizing short chained mCTA polymers to determine if the absence of the  $n=2$  hydrophilic group is a constant. The PDI discrepancy between AU19B and AU31A shows a lack of a streamlined synthesis. More syntheses should be performed to standardize the synthetic approach.

High methylene selectivity and  $R_s$  values indicate that the PSP concentration can be much less than this research utilized. Concentration limits should be explored and compared to NP size.

This research mainly focused on standardizing the size of the ionic shell and optimizing the hydrophobic core lengths. Work should be performed to investigate how changing the hydrophilic shell chain length affects separations. This research indicates that a small amount of analyte interactions may be occurring in the proximity of the amide and the small lipophilic region located at the shell of the nanoparticle. Increasing the size of the shell may lead to changes in methylene selectivity,  $\nu$ , and  $b$  values. Taking the polymeric nanoparticle research further can be accomplished by the introduction of chiral cores enabling chiral separations of analytes. The chiral NP PSPs may provide all the excellent separation characteristics demonstrated by the current PSP with the addition of chiral selectivity.

## Bibliography

---

- [1] A. Volker, "Block Copolymers I," *Advances in Polymer Science*, vol. 189, p. 24, 2005.
- [2] F. Reuss, *Mem. Soc. Imperiale Naturalistes de Moscow*, no. 2, p. 327, 1809.
- [3] F. Kohlrausch, "Über Concentrations-Verschiebungen durch Elektrolyse im Innern von Lösungen und Lösungsgemischen," *Ann. Phys. Chem*, vol. 62, pp. 209-293, 1897.
- [4] S. Hjerten, Jerstedt, S. and A. Tiselius, "Electrophoretic "particle sieving" in polyacrylamide gels as applied to ribosomes," *Anal. Biochem*, vol. 11, pp. 211-218, 1965.
- [5] J. Jorgenson and K. Lukacs, "High-resolution separations based on electrophoresis and electroosmosis," *J. Chromatogr.*, vol. 218, pp. 209-216, 1981.
- [6] J. Jorgenson and K. Lukacs, "Zone electrophoresis in open-tubular glass capillaries," *Anal. Chem.*, vol. 53, pp. 1298-1302, 1981.
- [7] S. Terabe, K. Otsuka, K. Ichikawa, A. Tsuchiya and T. Ando, "Electrokinetic Separations with Micellar Solutions and Open-Tubular Capillaries," *Analytical Chemistry*, vol. 56, pp. 113-116, 1984.
- [8] C. Plamer and S. Terabe, "Micelle Polymers as Pseudostationary Phases in MEKC: Chromatographic Performance and Chemical Selectivity," *Analytical Chemistry*, vol. 69, no. 10, pp. 1852-1860, 1997.
- [9] C. Palmer, "Polymeric and polymer-supported pseudostationary phases in micellar electrokinetic chromatography: Performance and selectivity," *Electrophoresis*, vol. 21, pp. 4054-4072, 2000.
- [10] C. Palmer, "Recent progress in the use of ionic polymers as pseudostationary phases for electrokinetic chromatography," *Electrophoresis*, vol. 30, pp. 163-168, 2009.
- [11] C. Palmer, E. Hilder, J. Quirino and P. Haddad, "Electrokinetic Chromatography and Mass Spectrometric Detection Using Latex Nanoparticles as a Pseudostationary Phase," *Analytical Chemistry*, vol. 82, no. 10, pp. 4046-4054, 2010.
- [12] C. Palmer, A. Keeffer, E. Hilder and P. Haddad, "Retention behavior and selectivity of a latex nanoparticle pseudostationary phase for electrokinetic chromatography," *Electrophoresis*, vol. 32, pp. 588-594, 2011.
- [13] G. Moad, E. Rizzardo and S. H. Thang, "Living Free-Radical Polymerization by Reversible Addition-Fragmentation Chain Transfer: The RAFT process," *Macromolecules*, vol. 31, no. 16, pp. 5559-5562, 1998.
- [14] G. Odian, *Principles of Polymerization*, New York: Wiley-Science, 2004.
- [15] G. Allen and J. C. Bevington, *Comprehensive polymer science: the synthesis, characterization, reactions & applications of polymers*, Oxford: Pergamon Press, 1989.
- [16] H. J. Hageman, "Photoinitiators for Free Radical Polymerization," *Progress in Organic Coatings*, vol. 13, no. 2, pp. 123-150, 1985.
- [17] Materials World Modules, "Addition Polymerization," 2009. [Online]. Available: [www.materialsworldmodules.org/resources/polymerization/3-addition.html](http://www.materialsworldmodules.org/resources/polymerization/3-addition.html). [Accessed 16 August 2012].
- [18] M. P. Stevens, *Polymer Chemistry: An Introduction*, New York: Oxford University Press, 1999.
- [19] K. Matyjaszewski and T. P. Davis, *Handbook of Radical Polymerization*, New York: Wiley-Interscience, 2002.
- [20] S. Wei, C. J. Watson and C. P. Palmer, "Sulfonated acrylamide copolymers as pseudo-



- stationary phases in electrokinetic chromatography," *Journal of Chromatography A*, vol. 905, pp. 281-290, 2001.
- [21] C. Palmer, C. Watson and S. Wei, "Sulfonated acrylamide copolymers as pseudo-stationary phases in electrokinetic chromatography," *Journal of Chromatography A*, vol. 905, pp. 281-290, 2001.
- [22] G. Moad, E. Rizzardo and S. H. Thang, "Living Radical Polymerization by the RAFT Process," *Australian Journal of Chemistry*, vol. 58, pp. 379-410, 2005.
- [23] R. T. A. Mayadunne, E. Rizzardo, J. Chiefari, J. Kristina, G. Moad, A. Postma and S. H. Thang, "Living Polymers by the Use of Trithiocarbonates as Reversible Addition-Fragmentation Chain Transfer (RAFT) Agents: ABA Triblock Copolymers by Radical Polymerization in Two Steps," *Macromolecules*, vol. 33, pp. 243-245, 2000.
- [24] R. Francis and A. Ajayaghosh, "Minimization of Homopolymer Formation and Control of Dispersity in Free Radical Induced Graft Polymerization Using Xanthate Derived Macro-photoinitiators," *Macromolecules*, vol. 33, pp. 4699-4704, 2000.
- [25] R. T. A. Mayadunne, E. Rizzardo, J. Chiefari, Y. K. Chong, G. Moad and S. H. Thang, "Living Radical Polymerization with Reversible Addition-Fragmentation Chain Transfer (RAFT Polymerization) Using Dithiocarbamates as Chain Transfer Agents," *Macromolecules*, vol. 32, pp. 6977-6980, 1999.
- [26] W. Shen, Q. Qian, W. Yang, M. Miao, L. Bingshu, Z. Tianshu, C. Aoneng and A. Zesheng, "Hydrazine as a Nucleophile and Antioxidant for Fast Aminolysis of RAFT Polymers in Air," *Macromolecule Rapid Communication*, vol. 31, pp. 1444-1448, 2010.
- [27] Sigma Aldrich, "RAFT polymerization," Sigma Aldrich, 2012. [Online]. Available: [www.sigmaaldrich.com/materials-science/polymer-science/raft-polymerization.html](http://www.sigmaaldrich.com/materials-science/polymer-science/raft-polymerization.html). [Accessed 17 August 2012].
- [28] G. Moad, E. Rizzardo and S. H. Thang, "Living Radical Polymerization by the RAFT process - A second Update," *Australian Journal of Chemistry*, vol. 62, pp. 1402-1472, 2009.
- [29] G. Moad, J. Chiefari, Y. K. Chong, J. Kristina, T. A. Mayadunne, A. Postma, E. Rizzardo and S. H. Thang, "Living free radical polymerization with reversible addition - fragmentation chain transfer (the life of RAFT)," *Polymer International*, vol. 49, pp. 993-1001, 2000.
- [30] J.-W. Kim, "Techniques for Synthesizing Polymer Particles," Harvard, Boston, 2007.
- [31] K. Landfester, "Polyreactions in Miniemulsions," *Macromolecules Rapid Communications*, vol. 22, pp. 897-936, 2001.
- [32] C. Furgeson, R. Hughes, D. Nguyen, B. Pham, R. Gilbert, A. Serelis, C. Such and B. Hawke, "Ab Initio Emulsion Polymerization by RAFT-Controlled Self-Assembly," *Macromolecules*, vol. 38, pp. 2191-2204, 2005.
- [33] G. M. Janini, G. M. Muschik and H. J. Issaq, "Electrokinetic chromatography in suppressed electroosmotic flow environment: use of charged cyclodextrin for the separation of enantiomers and geometric isomers," *Electrophoresis*, vol. 17, no. 10, pp. 1575-83, 1996.
- [34] G. Muijselaar, A. Claessens and A. Cramers, "Dendrimers as Pseudo-Stationary Phases in Electrokinetic Chromatography," *Journal of High Resolution Chromatography*, vol. 18, pp. 121-123, 1995.
- [35] R. Cunico, K. Goodin and T. Wehr, *Basic HPLC and CE of Biomolecules*, Richmond: Bay Bioanalytical Laboratory, 1998.
- [36] S. Terabe, "Capillary Separation: Micellar Electrokinetic Chromatography," *Annual Review of Analytical Chemistry*, vol. 2, pp. 99-120, 2009.
- [37] Abraham, M.H.; Powitzer, P.; Murray, J.S., *Quantitative Treatments of Solute/Solvent*

- Interactions*, Amsterdam, Elsevier, 1994, pp. 83-130.
- [38] M. Abraham, "Scales of solute hydrogen-bonding: their construction and application to physicochemical and biochemical processes," *Chemical Society Reviews*, vol. 22, 1993, pp. 73-83.
- [39] C. Poole, *The Essence of Chromatography*, Amsterdam: Elsevier Science, 2003.
- [40] C. Poole, "Selectivity Characterization of Pseudostationary Phases Using the Solvation Parameter Model," in *Electrokinetic Chromatography*, West Sussex, Wiley & Sons Ltd, 2006, pp. 55-78.
- [41] E. Katz, R. Eksteen, P. Schoenmakers and N. Miller, *Handbook of HPLC*, New York: Marcel Dekker, Inc., 1998.
- [42] B. Sumerlin, M. Donovan, Y. Mitsukami, A. Lowe and C. McCormick, "Water-Soluble Polymers. 84. Controlled Polymerization in Aqueous Media of Anionic Acrylamido Monomers via RAFT," *Macromolecules*, vol. 34, pp. 6561-6564, 2001.
- [43] L. D. S. Yadav, *Organic Spectroscopy*, New Delhi: Anamaya Publishers, 2005.
- [44] M. A. J. J. Bushey, "Separation of dansylated methylamine and dansylated methyl-d3-amine by micellar electrokinetic capillary chromatography with methanol-modified mobile phase," *Analytical Chemistry*, vol. 61, no. 5, pp. 491-493, 1989.
- [45] F. Poole, K. Poole and M. Abraham, "Recommendations for the determination of selectivity in micellar electrokinetic chromatography," *Journal of Chromatography A*, vol. 798, pp. 207-222, 1998.
- [46] C. Ladaviere, M. Llauro, J. Egraz, J. Suau, N. Doerr and J. Loiseau, "Synthesis and Characterization of Poly(acrylic acid) Produced by RAFT Polymerization. Application as a Very Efficient Dispersant of CaCO<sub>3</sub>, Kaolin, and TiO<sub>2</sub>," *Macromolecules*, vol. 36, pp. 3066-3077, 2003.
- [47] H. Mori, I. Kato, M. Matsuyama and T. Endo, "RAFT Polymerization of Acrylamides Containing Proline and Hydroxyproline Moiety: Controlled Synthesis of Water-Soluble and Thermoresponsive Polymers," *Macromolecules*, vol. 41, pp. 5604-5615, 2008.
- [48] C. McCormick, A. Lowe, B. Sumerlin and D. Thomas, "Conditions for Facile, Controlled RAFT Polymerization of Acrylamide in Water," *Macromolecules*, vol. 36, pp. 1436-1439, 2003.
- [49] B. Sumerlin, A. Lowe, B. Thomas and C. McCormick, "Aqueous Solution Properties of pH-Responsive AB Diblock Acrylamido Copolymers Synthesized via Aqueous RAFT," *Macromolecules*, vol. 36, pp. 5982-5987, 2003.
- [50] C. Palmer, C. Watson and W. Shi, "Sulfonated acrylamide copolymers as pseudo-stationary phases in electrokinetic chromatography," *Journal of Chromatography A*, vol. 905, pp. 281-290, 2001.
- [51] S. Rizvi, J. Zheng, R. Apkarian, S. Dublin and S. Shamsi, "Polymeric Sulfated Amino Acid Surfactants: A Class of Versatile Chiral Selectors for Micellar Electrokinetic Chromatography (MEKC) and MEKC-MS," *Anal. Chem.*, vol. 79, pp. 879-898, 2006.
- [52] S. Shamsi and C. Akbay, "Polymeric sulfated surfactants with varied hydrocarbon tail: I. Synthesis, Characterization, and application in micellar electrokinetic chromatography," *Electrophoresis*, vol. 25, pp. 622-634, 2004.
- [53] I. Warner, C. Akbay and S. Shamsi, "Polymeric Anionic Surfactant for Electrokinetic Chromatography: Separation of 16 Priority Polycyclic Aromatic Hydrocarbon Pollutants," *Analytical Chemistry*, vol. 70, pp. 3078-3083, 1998.
- [54] J. Foley, *Analytical Chemistry*, "Optimization of micellar electrokinetic chromatography,"

vol. 62, p. 1302, 1990.

- [55] J. Davis, T. Seals and L. Yu, "Reexamination of Dependence of Plate Number on SDS Concentration in Micellar Electrokinetic Chromatography," *Analytical Chemistry*, vol. 68, pp. 4270-4280, 1996.
- [56] C.P. Palmer and H.M. McNair, " Novel pseudostationary phase for micellar electrokinetic capillary chromatography," *J. Microcol.*, vol. 4, pp. 509-514, 1992.
- [57] C. West and E. Lesellier, "Characterisation of stationary phases in supercritical fluid chromatography with the solvation parameter model V. Elaboration of a reduced set of test solutes for rapid evaluation," *Journal of Chromatography A*, vol. 1169, pp. 205-219, 2007.
- [58] G. Maurer, K. Quitzsch, W. Hauthal, S. Ritter, J. Durr and J. Schulte, "Partition Coefficients for Environmentally Important Multifunctional Organic Compounds in Hexane + Water," *J. Chem. Eng. Data*, vol. 43, pp. 69-73, 1998.
- [59] C.-Y. Kuo and S. Wu, "Micellar electrokinetic chromatography for simultaneous determination of six corticosteroids in commercial pharmaceuticals," *Journal of Separation Science*, vol. 28, pp. 144-148, 2005.
- [60] P. Mukerjee and J. Ko, *Journal of Physical Chemistry*, "Solubilization of ethyl o-, m-, and p-aminobenzoates in micelles of different charge types: interfacial adsorption and orientation effects," vol. 96, pp. 6090-6094, 1992.
- [61] R. Buchner, C. Baar, P. Fernandez, S. Shrodle and W. Kunz, "Dielectric spectroscopy of micelle hydration and dynamics in aqueous ionic surfactant solutions," *Journal of Molecular Liquids*, vol. 118, no. 1-3, pp. 179-187, 2005.
- [62] C. L. McCormick and A. B. Lowe, "Aqueous RAFT Polymerization: Recent Developments in Synthesis of Functional Water-Soluble (Co)polymers with Controlled Structures," *Acc. Chem. Res.*, vol. 37, pp. 312-325, 2004.